NASA Contractor Report 3605

Mean Velocities and Reynolds Stresses in a Juncture Flow

H. McMahon, J. Hubbartt,
and L. Kubendran

GRANT NAG1-40
AUGUST 1982

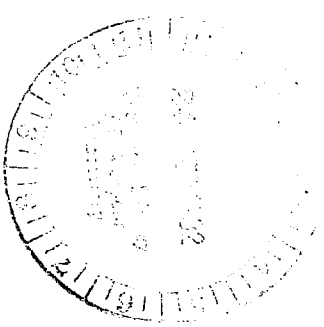

NASA

NASA Contractor Report 3605

Mean Velocities and Reynolds Stresses in a Juncture Flow

H. McMahon, J. Hubbartt,
and L. Kubendran
Georgia Institute of Technology
Atlanta, Georgia

Prepared for
Langley Research Center
under Grant NAG1-40

National Aeronautics
and Space Administration

**Scientific and Technical
Information Branch**

1982

Use of trade names or names of manufacturers in this report does not constitute an official endorsement of such products or manufacturers, either expressed or implied, by the National Aeronautics and Space Administration.

SUMMARY

Values of three mean velocity components and six turbulence stresses measured in a juncture flow are presented and discussed.

The juncture flow is generated by a constant thickness body, having an elliptical leading edge, which is mounted perpendicular to a large flat plate along which a turbulent boundary layer is growing. The measurements were carried out at two streamwise stations in the juncture and were made using two single-sensor hot-wire probes.

The secondary flow in the juncture results in a considerable distortion in the mean velocity profiles. The secondary flow also transports turbulence in the juncture flow and has a large effect on the turbulence stresses.

From visual inspection of the results, there is considerable evidence of similarity between the turbulent shear stresses and the mean-flow strain rates. There is some evidence of similarity between the variations in the turbulent stress components. These points should be investigated further.

INTRODUCTION

Turbulent viscous flow in a streamwise juncture or corner is characterized by the existence of mean velocity components in a plane perpendicular to the main flow direction which are called secondary flows.

One type of secondary flow (called the "second kind") is observed in the corners of straight non-circular ducts and in the corners formed by two semi-infinite flat plates with coincident leading edges. This type of secondary flow is generated by Reynolds stress gradients in planes normal to the main flow direction and is a purely viscous interference problem with no leading edge effects present. Several investigators (e.g. refs. 1, 2, 3, 4, 5) have studied such secondary flows both experimentally and analytically.

Another type of secondary flow (called the "first kind") comes about when a shear layer is skewed about an axis parallel to the plane of the mean shear, resulting in the generation of mean streamwise vorticity. Such secondary flows are observed in the corners of curved ducts and in corners formed by bodies protruding from a wall.

The juncture flow considered here is the flow in a corner formed by a body of constant thickness mounted at right angles to a flat plate. A turbulent boundary layer is developing along the flat plate, so that the latter type of secondary flow ("first kind") is present. Thus, the vortex lines within the oncoming boundary layer, which are initially straight and aligned perpendicular to the main flow and parallel to the flat plate, are skewed and stretched due to the three-dimensional curvature of the streamlines as the flow goes around the body (fig. 1). This results in streamwise vorticity being produced in the juncture.

In addition to the skewing of the boundary layer, the blockage effect when a body protrudes from a surface introduces another factor into the juncture flow. The oncoming boundary layer on the surface of the flat plate experiences steep adverse pressure gradients as it nears the leading edge of the body. As a result, the boundary layer separates ahead of the leading edge, and a vortex sheet rolls up and trails downstream in the juncture (fig. 1). This vortex is actually the dominant feature of a juncture flow of this type.

The coupled effects of the skewing of the oncoming two-dimensional shear flow and the separation of the boundary layer, with subsequent vortex roll-up, lead to a complex secondary flow. The resulting shear flow in the juncture is a three-dimensional turbulent flow containing significant velocity components normal to the main flow direction. Such secondary flows give rise to significant problems in aircraft design and wind tunnel testing.

Secondary flows caused by coupled viscous and blockage interference occur in the junctures of wing-fuselages, wing-pylons, and wing-winglets. An understanding of such secondary flows is important in optimizing aircraft performance as well as in assessing the role which the juncture plays as regards the wake flow on the surfaces downstream of the wing or pylon trailing edge. In the two-dimensional wind tunnel testing of airfoils, the ends of the airfoil are immersed in sidewall or end-plate boundary layers. The resulting secondary flow in the junctures can have a significant effect, particularly on airfoil drag measurements (e.g. ref. 6).

Juncture flows involving both boundary layer skewing and separation have been studied previously (e.g. refs. 7, 8, 9, 10), but turbulence measurements have been lacking and the available analyses do not treat the details of the turbulent secondary

flow. Recently, Shabaka and Bradshaw (refs. 11, 12) have published an extensive collection of mean flow and turbulence data taken in an idealized wing-body juncture. The present work differs from that reported by Shabaka (refs. 11, 12) in the following ways. The elliptical leading edge used in Shabaka's tests was very slender (6:1 ellipse) while that studied here was relatively blunt (1.5:1 ellipse). Also, the present tests were performed in a large-scale open jet to eliminate wind tunnel wall effects. In contrast, Shabaka used the test section of a small wind tunnel, and the wall boundary layers, which filled about 80% of the flow area at the exit of the working section, induced favorable pressure gradients. Furthermore, Shabaka used both a single wire and a cross-wire probe with the probe support located in the shear flow. The measurements reported herein were made using only single sensors supported on needles which projected into the boundary layer from the flat-plate surface. Thus, there was no possibility of probe support interference nor of mutual interference between two crossed wires. Finally, Shabaka obtained instantaneous voltages which were used to calculate instantaneous velocities that were then averaged to yield mean velocities and velocity correlations. In the present tests, mean voltages were obtained and then used to evalutate the mean velocities and velocity correlations (turbulence stresses).

The juncture flow investigated here was generated by a constant-thickness body ("wing"), having an elliptical leading edge, which was mounted perpendicular to a large flat plate ("fuselage") along which a turbulent boundary layer was developing (fig. 2). Three mean velocity components and six turbulence stresses have been measured in this juncture flow at two streamwise stations using hot-wire anemometer techniques. The primary objective of this experimental study was to secure detailed mean flow and turbulence data to aid in the development of numerical analyses for juncture flows by methods similar to those reported in reference 4. The data should be useful for formulating and also for evaluating numerical analyses of the juncture flow problem.

SYMBOLS

a	Coefficients of polynomial approximation (eq. 32)
A-F	Constants used in data reduction, defined in equations 10-15
e_ℓ	AC component of E

E	Nonlinear output voltage of constant-temperature anemometer
E_{ℓ}	Linearized output voltage of hot-wire anemometer
E_o	Output voltage of hot-wire anemometer at zero velocity
h	Binormal velocity coefficient (eq. 2)
k	Tangential velocity coefficient (eq. 2)
ℓ_{ij}	Cosine of angle between x'_i and x_j coordinate axes
Re_{δ}	Reynolds number based on boundary layer thickness
s,y,n	Hot-wire coordinate system (figs. 7 and 12)
S	Constant of proportionality (eq. 4)
T_{ij},T'_{ij}	Second order tensor components (velocity correlations) used in coordinate transformations (eqs. 37 and 38)
u	Instantaneous fluctuating velocity
u'	Root-mean-square fluctuating velocity, i.e., $u' = \sqrt{\overline{u^2}}$
U	Local mean or time-averaged velocity
U_{BN}	Binormal velocity component, normal both to U_N and U_T (eq. 2)
U_{eff}	Effective cooling velocity (eq. 1)
U_N	Velocity component normal to hot wire in plane of wire-support needles (eq. 2)
U_T	Velocity component tangent to the hot wire (eq. 2)
V_i,V'_i	Velocity components used in coordinate transformations (eqs. 34 and 35)
V_{∞}	Undisturbed freestream velocity
x,y,z	Laboratory coordinate system (fig. 7)
x_i,x'_i	Cartesian coordinate axes used in coordinate transformations
$\alpha, \Theta, \lambda, \psi$	Angles expressing hot-wire orientation (fig. 7)

Subscripts:

i,j,p,q	Indices for coordinate, velocity, and tensor components (1, 2, 3)
n	Component in n direction
s	Component in s direction
x	Component in x direction
y	Component in y direction
z	Component in z direction
α, ψ	Indicates that quantity is evaluated with wire angles α and ψ (eqs. 24-31)

Superscript:

—	Time average or mean

EQUIPMENT

The wind tunnel model, and much of the equipment and instrumentation used in this experiment, was identical to that employed by Oguz (ref. 10). The reader is referred to reference 10 for discussions of the model and actuator details.

Wind Tunnel

All tests were carried out in the Georgia Tech Low Speed Wind Tunnel. This wind tunnel is of the open return type with a test section 1.07 x 1.09 x 6.10 m (42 x 43 x 240 in.). The freestream turbulence intensity u'_∞ / V_∞ near the exit of the test section was measured during the course of the experiments to be 0.5%.

Body and Flat Plate

The body, which was mounted perpendicular to the flat plate and aligned with the wind tunnel axis within $\pm$ 0.5° (figs. 2 and 3), had a constant thickness of 57.9 mm (2.28 in.), a height of 609.6 mm (24 in.), and a length of 1.22 m (48 in.). The leading edge of the body was a 1.5:1 ellipse with a strip of distributed roughness 6.35 mm (0.25 in.) wide beginning 25.4 mm (1.0 in.) downstream of the leading edge. The roughness was achieved by using glass beads having an average diameter of 0.25 mm (0.01 in.).

In order to have easy access to the measuring probes and actuators, and especially to allow movement of the probes over a considerable distance in the streamwise and transverse directions, the flat plate and body were mounted in the free jet at the exit of the open return wind tunnel (figs. 2 and 3). Previous measurements (ref. 13) had determined the boundaries of the free jet and had established that the quality of the jet flow was acceptable. The flat plate was mounted on support legs and positioned 216 mm (8.5 in.) above the wind tunnel floor at the tunnel exit. An extension of the plate, which served as a boundary layer development section, protruded 572 mm (22.5 in.) upstream into the wind tunnel and was fitted with a trip wire 0.965 mm (0.038 in.) in diameter located 101.6 mm (4.0 in.) downstream of the leading edge. A preliminary evaluation (ref. 10) showed that there was no separation at the leading edge of the flat plate extension.

The flat plate was designed with interchangeable segments (fig. 2) so that the particular segment containing the probe and actuator (fig. 4) could be located at selected streamwise stations. Whenever the segments of the plate were re-arranged, the flow surface was checked with a dial gage and shimmed so that the step at any joint was at most $\pm$ 0.127 mm (0.005 in.). This may be compared to the nominal boundary layer thickness in the measurement region of 25.4 mm (1.0 in.). All joints were sealed with modeling clay.

Hot Wires

The juncture flow region of interest comprised a rectangle approximately 25.4 mm (1.0 in.) high normal to the flat plate and 76.2 mm (3.0 in.) wide as measured from the body surface. Various methods for supporting the hot-wire needles were considered. It was felt that a probe with its axis perpendicular to either the flat plate or to the body surface would lead to possible interference problems. A probe in the juncture with its axis aligned in the nominal streamwise direction would introduce an unknown probe interference and might also affect the roll-up of the vortex in the juncture. Accordingly, in order to minimize probe interference effects, the hot wires were supported on needles projecting through the surface of the flat plate. This arrangement had the added advantage of placing the probe actuator below the plate and hence out of the flow field.

The hot wire with the wire parallel to the flat plate (i.e., with support needles of equal length) is shown in figure 5(a) and is termed the "horizontal wire." The needles were 3.18 mm (0.125 in.) apart and were made of gold-plated stainless steel 0.58 mm (0.023 in.) in diameter. The access holes through which the needles pass were 1.32 mm (0.052 in.) in diameter. The probe was designed so that the needles could extend through the access holes to a maximum height of approximately 35.6 mm (1.40 in.). The surface plug containing the access holes rotated with the probe. The hot-wire was 0.0038 mm (0.00015 in.) in diameter and was made from platinum-coated tungsten with an etched sensor portion in the center which was 1.27 mm (0.050 in.) long. The needles were ground down to about 0.25 mm (0.01 in.) in diameter over a length of about 1.27 mm (0.05 in.) at the tips before the wire was soldered in place. There is a small velocity increment (less than 3% of the oncoming velocity) at the sensor portion of the wire as the flow accelerates due to the blockage of the two cylindrical needles. This interference effect was accounted for by carrying out both the hot-wire calibration and

the hot-wire measurements with the same orientation of the needles relative to the oncoming flow. The calibration was accomplished by extending the needles upward until the wire was at the outer edge of the boundary layer and then performing the calibration in this flow of known (measured) velocity. Measurements using the horizontal wire were performed from the edge of the viscous layer down to 0.51 mm (0.020 in.) above the surface of the flat plate.

Since the data analysis method used here required the use of a second wire orientation at an angle to the flat plate, it was necessary to use a second hot-wire probe with needles of unequal length (fig. 5(b)), termed the "slant wire." This wire was the same type and diameter as the horizontal wire and was 4.50 mm (0.177 in.) long. The sensor portion was concentric with the axis of rotation of the probe within $\pm$ 0.152 mm ($\pm$ 0.006 in.). In order that the wire not be in the wake of the longer needle in certain wire orientations, the longer needle was offset by a distance of 5.10 mm (0.20 in.) as shown in figure 5 (b). The wire orientation angle, α, was intended to be 45° but was measured with an optical comparator to be $47.3^{\circ} \pm 0.05^{\circ}$. The sensor portion of the slant wire could be set at a maximum height of y = 27.9 mm (1.10 in.) above the plate surface and at a minimum height of y = 2.29 mm (0.090 in.).

Both probes were checked for vibration at various values of wire height, angular orientation, and velocity by outputting the anemometer signal through a Fourier Analyzer and examining the resulting energy spectra. It was concluded that probe vibration was negligible over the range of velocities and probe orientations required. Further, the spectra from the slant wire gave no indication of any downstream wake effect at the wire due to the longer upstream needle.

Actuators

The segment of the flat plate which contained the hot-wire probe consisted of a slide and slide bed (fig. 4). The probe was held in an actuator which hung below the slide and moved with the slide.

The streamwise (x) location of the survey station was changed by manually interchanging suitable segments of the plate. The linear movement of the hot wire in directions perpendicular to the plate (y) and normal to the body surface (z) was accomplished by using stepper motors which turned lead screws (figs.6 and 3 (b)). The

stepper motors were under computer control, and both linear motions were monitored visually on read-out counters. Absolute position in both y and z was checked periodically. Considering all sources of error, it is estimated that the y location of either hot wire during a survey was accurate to within $\pm$ 0.051 mm ($\pm$ 0.002 in.), while the z location was accurate to within $\pm$ 0.10 mm ($\pm$ 0.004 in.).

In addition to linear motion, the hot wire probes also had to be rotated about their axes in order to acquire the necessary data. This rotary motion was obtained by directly coupling the probes to a third stepper motor having a step increment of $\pm$ 0.90°. Rotary motion was monitored with a counter and checked for absolute accuracy at the end of each run by means of a fixed rotary limit switch. Preliminary tests confirmed that the stepping error in the motor was non-cumulative and considerably less than $\pm$ 0.50°. Since the determination of the angle of yaw, θ, between the x-axis and the s-axis (fig. 7) involved both a measurement to establish the main flow direction (i.e., the x axis) and one to find the local flow angle (i.e., the s axis), the final uncertainty in θ is estimated to be $\pm$ 1.0°.

Sensor Locaters

Measurements with both the horizontal and slant wires were required at a common point in space in order to determine all of the required mean flow and turbulence quantities at that point. In addition, the local flow direction angle, θ, found with the horizontal wire formed the basis for the orientation of the measurement coordinates system for the slant wire. Because the two wires were used sequentially, it was important that the location of the sensor portions of each wire be referenced to a precisely known datum in y, z, and θ. This was done by fabricating a sighting tube approximately 259 mm (10.2 in.) long and 38 mm (1.50 in.) in diameter. One end of the tube was fitted with 7-power magnifying optics, such as found in a machinist's pocket optical comparator, while the other end was covered with a disc containing a small sight hole. This sighting tube was mounted horizontally in a machined aluminum block containing two dowel pins that mated with two holes precisely located in the slide bed. By looking through the sight-hole and along the tube axis, a horizontal reticle line on the optics could be observed. The precise height of this reticle above the slide bed was established by using a height gage. The sensor portion of the wire could be viewed through the sighting tube with the aid of the magnifier, and the wire was moved

vertically in increments of 0.0254 mm (0.001 in.), using the actuator, until the sensor and the reticle line were coincident. Hence, a known sensor location in y was established. The vertical motion counter then was set to zero, and the probe was run down to a vertical-travel limit switch in order to establish the limit switch location for future use. This same technique, utilizing a second sighting tube mounted vertically, was employed to establish the location of the sensor portions of the two wires in the z direction and in rotation. By using these two sighting tubes, it is estimated that the sensor portions of the two hot wires could be located at a given common point to within $\pm$ 0.0254 mm ($\pm$ 0.001 in.) in y and z, and to within less than $\pm$ 0.5° in angle.

INSTRUMENTATION

Freestream Velocity. - The velocity of the wind tunnel flow was monitored by a visual read-out of dynamic pressure. This pressure was measured with a pitot-static probe mounted just outside the boundary layer at the streamwise measurement station of interest (fig. 3(b)). The probe was connected to a Barocel electronic manometer and read with a digital voltmeter. The tunnel flow velocity was maintained constant within $\pm$ 0.5% during the runs, and was in error by less than $\pm$ 0.5%.

The same pitot-static probe and read-out were used for the velocity calibrations of the hot wires. In this case, the wires were located adjacent to the pressure probe at the edge of the boundary layer and at z = 152 mm (6.0 in.), where the flow is effectively two-dimensional.

Hot-Wire Anemometer. - The hot-wire probes were connected to a TSI Model 1050 anemometer, and the output of the anemometer was then processed through a TSI Model 1052 Polynomial Linearizer.

Local Mean Velocity. - The linearized output of the hot-wire anemometer was fed to an HP 2401C integrating digital voltmeter, and the integrating time on the voltmeter front panel was set to 1.0 s. Consecutive calls to the voltmeter were made and the output was arithmetically averaged to yield the mean D. C. voltage over some specified averaging time.

Turbulence Measurements. - The A.C. component of the hot-wire signal was measured using an HP Model 3400A true RMS meter and read with the HP 2401C digital voltmeter. Consecutive readings integrated over 1.0 s were arithmetically averaged to yield the required RMS data.

Data Handling. - All data were acquired under computer control using an HP 2115A computer at the wind tunnel site. Both the DC and RMS hot-wire signals from the digital voltmeter were output on paper tape. This paper tape then was read onto magnetic tape, and the data processed on an HP 21MXE computer to be output on a line printer or graphics printer as required.

TEST CONDITIONS AND METHOD

All of the tests were carried out at a nominal freestream velocity of 15.24 m/s (50 ft./s) corresponding to a Reynolds number of 984,000/m (300,000/ft.). The leading edge of the body was located 254 mm (10.0 in.) downstream of the wind tunnel exit plane where the turbulent boundary layer on the flat plate in the absence of the body was approximately 22.9 mm (0.9 in.) thick, corresponding to a ratio of body thickness to boundary layer thickness of 2.53.

The first measurement station in the juncture was located 165 mm (6.5 in.) downstream of the leading edge of the body. At this value of x, surveys through the viscous layer in the y direction were made from z = 10.2 mm (0.40 in.) to z = 152.4 mm (6.0 in.) as detailed in Table 1.

The second measurement station was located 902 mm (35.5 in.) downstream of the leading edge. Here, surveys in the y-direction were carried out from z = 15.2 mm (0.60 in.) to z = 152.4 mm (6.0 in.) as shown in Table 2.

Two coordinate systems were employed in these experiments (fig. 7). The x-y-z Cartesian coordinates, with x in the freestream direction, y perpendicular to the flat plate, and z normal to the body surface, are defined such that x = 0 at the body leading edge, y = 0 at the plate surface, and z = 0 at the body surface. As will be explained in the next section, the local flow direction, Θ, was determined first at each value of y and z for a particular value of x by utilizing the horizontal hot-wire and the proper data acquisition program. With the value of Θ known at each y for any z station, a local s-y-n coordinate system was defined which rotated about the vertical y axis as the value of y changed (fig. 8). For each data point, the horizontal hot wire was oriented appropriately with respect to the local s-axis and the DC and RMS time-average voltages were recorded. When all of the required measurements had been completed, the probe containing the horizontal wire was removed and it was replaced with the slant-wire probe. At each y at all z stations, the slant wire was oriented either in the s-y plane previously established or at some specified angle, ψ, with respect to the s-y

plane. The DC and RMS time-average voltages were recorded as before. The choice of averaging time is discussed in Appendix A.

Throughout the tests, the hot-wire anemometer output was monitored on an oscilloscope. Close attention was paid to drift in the electronic instruments and in the temperature of the wind tunnel air (Appendix B). No measurements were made until the wind tunnel had been running for at least one hour. The hot-wire calibration and the polynomial coefficients for the linearizer were updated periodically as required.

DATA ACQUISITION AND ANALYSIS

Preliminary Considerations

The hot wire is shown schematically in figure 7 with an arbitrary orientation in both the laboratory (x,y,z) and hot-wire (s,y,n) Cartesian coordinate systems. In both coordinate systems y is measured normal to the flat plate whereas x, z, s, and n are in the plane of the plate. The hot-wire coordinates were used for data acquisition. The data results then were transformed into the laboratory coordinates for all data presentations.

The orientation of the hot wire in the wire coordinate system is specified by the two angles α and ψ. The angle α is the angle between the axis of wire rotation and a normal to the wire defined to be in the plane containing the hot wire and the axis of wire rotation. The angle ψ is the angle between the s axis and the projection of the hot wire on the s-n plane (i.e., the plane of the flat plate).

The nonlinearized voltage output of the constant-temperature anemometer is related to α, ψ, and the three instantaneous velocity components. That is,

$$E = E(U_s + u_s, U_y + u_y, u_n, \alpha, \psi)$$

In order to linearize this relationship between the voltage output and the instantaneous flow velocity, it is necessary to introduce an effective cooling velocity, U_{eff}, such that

$$E = E(U_{eff}) \tag{1}$$

where

$$U_{eff} = f(U_s + u_s, U_y + u_y, u_n, \alpha, \psi)$$

This functional relationship for U_{eff} must be determined by calibration. For the present investigation, the relationship first suggested and studied by Jorgensen (ref. 14) was used. This expression is

$$U_{eff} = \left(U_N^2 + k^2 U_T^2 + h^2 U_{BN}^2\right)^{1/2} \tag{2}$$

where U_N is the velocity component normal to the wire in the plane of the wire-support needles, U_T is the velocity component tangent to the wire, and U_{BN} is the binormal velocity component which is normal to both U_N and U_T. The coefficients k and h are determined by calibration. In terms of the angles and coordinate system of figure 7 equation (2) becomes

$$\begin{aligned} U_{eff} = \Bigg\{ & \Big\{ \Big[\left(U_s + u_s\right) \cos\psi + u_n \sin\psi \Big] \sin\alpha - \left(U_y + u_y\right) \cos\alpha \Big\}^2 \\ & + k^2 \Big\{ \Big[\left(U_s + u_s\right) \cos\psi + u_n \sin\psi \Big] \cos\alpha + \left(U_y + u_y\right) \sin\alpha \Big\}^2 \\ & + h^2 \Big\{ - \left(U_s + u_s\right) \sin\psi + u_n \cos\psi \Big\}^2 \Bigg\}^{1/2} \end{aligned} \tag{3}$$

The relation between U_{eff} and E, as expressed by equation (1), was determined by experiment for both wires used in this study. These data were then used along with the linearizer circuit of the constant-temperature anemometer to generate, for each wire, a linearized output voltage E_ℓ which is directly proportional to U_{eff}. Thus

$$E_\ell = SU_{eff} \tag{4}$$

where S is a constant of proportionality depending upon the particular hot wire. E_ℓ is decomposed into a mean or DC component, $\bar{E}_\ell$, and a fluctuating or AC component, e_ℓ, where $\bar{e}_\ell = 0$, so that equation (4) becomes

$$\bar{E}_\ell + e_\ell = SU_{eff} \tag{5}$$

In this equation, $\bar{E}_\ell$ and the root-mean-square of e_ℓ (i.e., $\sqrt{\overline{e_\ell^2}}$) are the measureable quantities which were evaluated in this investigation. Taking the mean of equation (5) gives

$$\frac{\bar{E}_\ell}{S} = \bar{U}_{eff} \tag{6}$$

Squaring equation (5) and then taking the mean and using equation (6) gives

$$\frac{\overline{e_\ell^2}}{S^2} = \overline{U_{eff}^2} - \bar{U}_{eff}^2 \tag{7}$$

Equations (3), (6), and (7) yield two equations relating $\bar{E}_\ell$ and $\overline{e_\ell^2}$ to mean values of the various velocity components and turbulence quantities for fixed values of α and ψ. This, of course, requires that U_{eff} be expanded in a truncated Taylor's series, as discussed later.

In this investigation the mean velocity components U_s and U_y and the six turbulence quantities u'_s, u'_y, u'_n, $\overline{u_s u_y}$, $\overline{u_s u_n}$, and $\overline{u_y u_n}$ were evaluated. This was accomplished using the horizontal wire ($\alpha = 0$) at the three orientations $\psi = 90^\circ$ and $\psi = \pm 45^\circ$ and using the slant wire ($\alpha = 47.3^\circ$) at the four orientations $\psi = 0$, $\psi = 180^\circ$, and $\psi = \pm 25^\circ$. The equations used to evaluate the unknowns are developed in the following section.

Development of Equations

To relate $\bar{E}_\ell$ and $\overline{e_\ell^2}$ to the eight unknowns, using equations (6) and (7), it is necessary to evaluate $\overline{U_{eff}^2}$, $\bar{U}_{eff}$, and $\bar{U}_{eff}^2$ from equation (3). The first of these simply requires squaring and averaging, yielding terms in U_s, U_y, and averages in products of the fluctuating velocity components. The latter two require that equation (3) be expanded in a truncated Taylor's series. For the hot-wire axes of figure 7, U_s is the only zeroth order velocity component while U_y, u_s, u_y, and u_n are first order terms. Therefore, for this analysis equation (3) was expanded in a series and then averaged over time to obtain $\bar{U}_{eff}$. Both $\bar{U}_{eff}$ and $\bar{U}_{eff}^2$ were truncated by neglecting third and higher order terms. After squaring and collecting terms under the square root radical, equation (3) may be rewritten in the form

$$U_{eff} = U_s\sqrt{A}\,(1+\varepsilon)^{1/2} \tag{8}$$

where ε involves first and second order terms and is given by

$$\varepsilon = 2u_s + u_s^2 + B\,(U_y^2 + 2U_y u_y + u_y^2) + Cu_n^2 + D\,(U_y + u_y + u_s U_y + u_s u_y)$$
$$+ E\,(U_y u_n + u_y u_n) + F\,(u_n + u_s u_y) \tag{9}$$

where

$$A = \cos^2\psi \sin^2\alpha + k^2\cos^2\psi\cos^2\alpha + h^2\sin^2\psi \tag{10}$$

$$B = (\cos^2\alpha + k^2\sin^2\alpha)/A \tag{11}$$

$$C = (\sin^2\psi\sin^2\alpha + k^2\sin^2\psi\cos^2\alpha + h^2\cos^2\psi)/A \tag{12}$$

$$D = 2\cos\psi\sin\alpha\cos\alpha\,(k^2-1)/A \tag{13}$$

$$E = 2\sin\psi\sin\alpha\cos\alpha\,(k^2-1)/A \tag{14}$$

$$F = 2\cos\psi\sin\psi\,(\sin^2\alpha + k^2\cos^2\alpha - 2h^2)/A \tag{15}$$

Expanding equation (8) in a Taylor's series and dropping terms of ε^3 and higher order yields

$$U_{eff} = U_s\sqrt{A}\,(1 + \tfrac{1}{2}\varepsilon - \tfrac{1}{8}\varepsilon^2), \tag{16}$$

$$\bar{U}_{eff} = U_s\sqrt{A}\,(1 + \tfrac{1}{2}\bar{\varepsilon} - \tfrac{1}{8}\overline{\varepsilon^2}), \tag{17}$$

$$\bar{U}_{eff}^2 = U_s^2 A\,(1 + \bar{\varepsilon} + \tfrac{1}{4}\bar{\varepsilon}^2 - \tfrac{1}{4}\overline{\varepsilon^2}), \tag{18}$$

and

$$\overline{U_{eff}^2} = U_s^2 A\,(1 + \bar{\varepsilon}) \tag{19}$$

Introducing equations (17-19) into equations (6) and (7) gives

$$\frac{\bar{E}_\ell}{S} = U_s\sqrt{A}\left(1 + \frac{1}{2}\,\bar{\varepsilon} - \frac{1}{8}\,\overline{\varepsilon^2}\right) \tag{20}$$

and

$$\frac{e_\ell^2}{S^2} = \frac{U_s^2 A}{4}\left(\bar{\varepsilon}^2 - \bar{\varepsilon}^2\right) \tag{21}$$

Finally, using equation (9) to evaluate $\bar{\varepsilon}$, $\bar{\varepsilon}^2$, and $\overline{\varepsilon^2}$ and dropping third and higher order terms, equations (20) and (21) become, after rearranging,

$$\frac{\bar{E}_\ell}{S} = U_s\sqrt{A}\left[1 + \left(\frac{B}{2} - \frac{D^2}{8}\right)\left(\frac{U_y^2}{U_s^2} + \frac{\overline{u_y^2}}{U_s^2}\right) + \frac{D}{2}\,\frac{U_y}{U_s}\right.$$

$$\left. + \left(\frac{C}{2} - \frac{F^2}{8}\right)\frac{\overline{u_n^2}}{U_s^2} + \left(\frac{E}{2} - \frac{DF}{4}\right)\frac{\overline{u_y u_n}}{U_s^2}\right] \tag{22}$$

and

$$\frac{\overline{e_\ell^2}}{S^2} = U_s^2 A\left[\frac{\overline{u_s^2}}{U_s^2} + \frac{D^2}{4}\,\frac{\overline{u_y^2}}{U_s^2} + \frac{F^2}{4}\,\frac{\overline{u_n^2}}{U_s^2} + D\,\frac{\overline{u_s u_y}}{U_s^2}\right.$$

$$\left. + \frac{DF}{2}\,\frac{\overline{u_y u_n}}{U_s^2} + F\,\frac{\overline{u_s u_n}}{U_s^2}\right] \tag{23}$$

Equations (22) and (23) are the general form of the hot-wire response equations used for evaluating the eight unknown velocity terms. $\bar{E}_\ell$ and $\overline{e_\ell^2}$ are the measured quantities and S is the known calibration constant discussed later. These response equations are specialized for each of the two wires at various values of ψ to evaluate the unknown velocity terms. The procedures and specific equations used to evaluate each velocity term are as follows:

(1) Evaluation of $\overline{u_s^2}$. Applying equation (23) to the horizontal ($\alpha = 0$) wire with $\psi = 90^\circ$ yields

$$\frac{(\overline{e_\ell^2})_{0,90}}{S^2} = h^2 \overline{u_s^2} \tag{24}$$

The first subscript on $\overline{e_\ell^2}$ expresses the value of α (i.e., $\alpha = 0$) and the second expresses the value of ψ (i.e., $\psi = 90^\circ$). Equation (24) has been used to evaluate $\overline{u_s^2}$.

(2) Evaluation of $\overline{u_y^2}$ and $\overline{u_s u_y}$. Applying equation (23) to the slant wire ($\alpha = 47.3^\circ$) both with $\psi = 0$ and 180° yields

$$\frac{(\overline{e_\ell^2})_{47.3,0}}{S^2} + \frac{(\overline{e_\ell^2})_{47.3,180}}{S^2} = 2(\sin^2\alpha + k^2\cos^2\alpha)\left[\overline{u_s^2} + \frac{(1-k^2)\sin^2\alpha\cos^2\alpha}{(\sin^2\alpha + k^2\cos^2\alpha)^2}\,\overline{u_y^2}\right] \tag{25}$$

and

$$\frac{(\overline{e_\ell^2})_{47.3,0}}{S^2} - \frac{(\overline{e_\ell^2})_{47.3,180}}{S^2} = 4(1-k^2)(\sin\alpha\cos\alpha)\,\overline{u_s u_y} \tag{26}$$

where $\alpha = 47.3^\circ$. Equation (25), along with $\overline{u_s^2}$ from equation (24), was used to evaluate $\overline{u_y^2}$. Equation (26) was used to evaluate $\overline{u_s u_y}$.

(3) Evaluation of U_y. Applying equation (22) to the slant wire both with $\psi = 0$ and 180° yields

$$\frac{(\bar{E}_\ell)_{47.3,180}}{S} - \frac{(\bar{E}_\ell)_{47.3,0}}{S} = 2\frac{(1-k^2)\sin\alpha\cos\alpha}{(\sin^2\alpha + k^2\cos^2\alpha)^{1/2}}\,U_y \tag{27}$$

where $\alpha = 47.3^\circ$. Equation (27) was used to evaluate U_y.

(4) Evaluation of $\overline{u_n^2}$ and $\overline{u_s u_n}$. Applying equation (23) to the horizontal wire both with $\psi = 45^\circ$ and -45° yields

$$\frac{(\overline{e_\ell^2})_{0,-45}}{S^2} + \frac{(\overline{e_\ell^2})_{0,45}}{S^2} = (k^2 + h^2)\left[\overline{u_s^2} + \left(\frac{h^2-k^2}{h^2+k^2}\right)^2 \overline{u_n^2}\right] \tag{28}$$

and

$$\frac{(\overline{e_\ell^2})_{0,-45}}{S^2} - \frac{(\overline{e_\ell^2})_{0,45}}{S^2} = 2(h^2-k^2)\overline{u_s u_n} \tag{29}$$

Equation (28) along with $\overline{u_s^2}$ from equation (24) was used to evaluate $\overline{u_n^2}$. Equation (29) was used to evaluate $\overline{u_s u_n}$.

(5) Evaluation of U_s. Applying equation (22) to the horizontal wire with $\psi = 90^\circ$ yields

$$\frac{(\bar{E}_\ell)_{0,90}}{S} = \frac{h}{U_s}\left[U_s^2 + \frac{1}{2h}(U_y^2 + \overline{u_y^2}) + \frac{k^2}{2h^2}\overline{u_n^2}\right] \tag{30}$$

Equation (30) along with $\overline{u_y^2}$, U_y, and $\overline{u_n^2}$ from equations (25), (27), and (28), respectively, was used to evaluate U_s.

(6) Evaluation of $\overline{u_y u_n}$. The cross-correlation $\overline{u_y u_n}$, which is generally small, proved to be the most difficult term to evaluate and, therefore, required special care. Applying equation (23) to the slant wire with angles ψ and $-\psi$ yields

$$\frac{(\overline{e_\ell^2})_{47.3,\psi}}{S^2} - \frac{(\overline{e^2})_{47.3,-\psi}}{S^2} = 4\cos\psi\sin\psi\left[\sin^2\alpha + k^2\cos^2\alpha - 2h^2\right]$$

$$\times\left[\overline{u_s u_n} - \frac{(1-k^2)\cos\psi\sin\alpha\cos\alpha}{(1+k^2)\cos^2\psi\sin^2\alpha + h^2\sin^2\psi}\,\overline{u_y u_n}\right] \tag{31}$$

where $\alpha = 47.3^{\circ}$ but ψ can be treated as a variable, selected for best accuracy for evaluating $\overline{u_y u_n}$. The sensitivity of the measurements to $\overline{u_y u_n}$ is a maximum when the magnitude of the coefficient of $\overline{u_y u_n}$ maximizes. Also, errors due to any inaccuracies in $\overline{u_s u_n}$ are reduced by increasing the ratio of the coefficient of $\overline{u_y u_n}$ to that of $\overline{u_s u_n}$. The variations of these coefficients with ψ are presented in figure 9 (here, h and k^2 are taken as 1 and 0.055 as discussed later). The magnitude of the coefficient of $\overline{u_y u_n}$ maximizes at about $\psi = 30^{\circ}$ (or $\psi = 150^{\circ}$) while that of $\overline{u_s u_n}$ maximizes at $\psi = 45^{\circ}$ (or $\psi = 135^{\circ}$). However, the ratio of these is a maximum at $\psi = 0$ which corresponds to the limiting case in which both coefficients approach zero. As a reasonable compromise, $\psi = 25^{\circ}$ was selected for these tests rather than $\psi = 30^{\circ}$ since the coefficient of $\overline{u_y u_n}$ is within 3% of the maximum value while the ratio of the coefficients is increased by 10%. Therefore, $\overline{u_y u_n}$ was evaluated using equation (31) with $\alpha = 47.3^{\circ}$ and $\psi = 25^{\circ}$, with $\overline{u_s u_n}$ as determined from equation (29).

Procedures and Calibrations

The orientation of the hot-wire coordinates was determined experimentally at each point in the flow field by rotating the horizontal wire ($\alpha = 0$) around its axis of rotation. A typical variation in the nonlinearized mean voltage output with angle of rotation, λ, (see fig. 7) is shown in figure 10. This bell-shaped curve is symmetrical around $\lambda = \Theta$, in which case the wire is normal to the local mean velocity vector and, thus, normal to the s axis. Also, for $\lambda = \Theta$ the mean voltage output is a maximum. This symmetry was used to evaluate Θ as follows. An estimate of Θ was first obtained from data at neighboring points in the flow field or by noting the λ for which the voltage output was apparently a maximum. Voltage outputs then were measured at 10 values of λ arranged symmetrically around this estimated Θ. Five of these values were in 1.8° increments centered around a value of λ which was 50° higher than that of the apparent maximum and five were in 1.8° increments centered around a value of λ which was 50° lower than that of the apparent maximum. Each of these sets of five data points were least-squares-fitted to a second degree polynomial. These polynomials then were used to evaluate the two λ's (near $\pm 50^{\circ}$) which yield the same voltage, the average of which gives the angle of symmetry, $\lambda = \Theta$.

The variation in the nonlinearized output voltage E with the effective velocity U_{eff}, as expressed in functional form by equation (1), was determined experimentally using a pitot-static pressure probe to evaluate U_{eff}. These tests were conducted in the freestream (i.e., $U_{eff} = V_\infty$) where the effect of turbulence is negligible. The hot wire was oriented normal to the freestream flow, the flow direction having been determined as explained above. Typical calibration results are shown in figure 11(a) for the horizontal wire. The linear relation between velocity and voltage, as given by equation (4), was obtained by fitting the nonlinear calibration data (e.g., the calibration data of fig. 11(a)) to the fourth-degree polynomial

$$U_{eff} = a_1 (E-E_o) + a_2 (E-E_o)^2 + a_3 (E-E_o)^3 + a_4 (E-E_o)^4 \tag{32}$$

where E_o is the output voltage with $U_{eff} = 0$. The coefficients a_1, a_2, a_3, and a_4 were determined by a least-squares fit to the calibration data. The operations on the right-hand side of equation (32), for given values of the coefficients and E_o, were performed by the hot-wire linearizer. This electrical analog circuitry, with an input voltage E, outputs a voltage given by

$$E_{\ell}/S = a_1 (E-E_o) + a_2 (E-E_o)^2 + a_3 (E-E_o)^3 + a_4 (E-E_o)^4$$

so that

$$E_{\ell} = SU_{eff} \tag{4}$$

The polynomial coefficents and E_o are adjustable in the circuitry in order to accommodate different calibration curves. The constant S is arbitrary and is usually selected so as to yield a convenient numerical relationship between E_{ℓ} and U_{eff}. For these tests S was selected so as to obtain 10V output at 15.24 m/s (50 ft/s). Figure 11 (b) shows the linearized form of the calibration data of figure 11 (a). Typically, the velocities are within $\pm$0.5% of the straight line approximation for the range of velocities covered herein. Calibrations like that of figure 11 were made periodically to assure that accuracy was maintained.

The binormal velocity coefficient h in equation (2) may differ from 1.0 because of wire asymmetries and the effects of the needles and needle support. Jorgensen (ref. 14) and Rodi (ref. 15) have determined that $h \cong 1.04$ for a wire similar to that of the present investigation but with the wire supported by short needles and with the needle support probe located in the stream. The needle support was outside the flow field in the present investigation and, therefore, could have no effect. Furthermore, several tests in the freestream were carried out with each wire where the flow was normal to the wire but at two angular orientations 180° apart (i.e., using opposite sides of the wire). Any differences were within data scatter. On the basis of these tests, it was concluded that the effect of wire asymmetries was negligible. The effect of the needles could not be evaluated since tests at two orientations 90° apart were impossible without constructing a new calibration facility. Because there can be no needle support effects and the wires are apparently symmetrical, the value of h must be more nearly unity than that obtained by Jorgensen and Rodi. Therefore, for these investigations it has been assumed that $h = 1.0$.

The tangential velocity coefficients k for the horizontal and slant wire were determined by testing the wires in the uniform freestream at several yaw angles λ. The magnitude of k was evaluated by least squares fitting the date to the equation

$$U_{eff}^2 = U_N^2 + k^2 U_T^2 + U_{BN}^2$$

From these tests it was determined that for the horizontal wire ($\alpha = 0$)

$$k^2 = 0.025$$

and for the slant wire ($\alpha = 47.3$)

$$k^2 = 0.055$$

Finally, it is noted that k^2 and (h-1) are at most of the same order as the first order velocity terms U_y, u_s, u_y, and u_n and, therefore, have no significant effect on the results. An inspection of equations (24 - 31) (i.e., the equations used for evaluating the unknown velocity terms) shows that they enter as coefficients of products of these first order velocities. Since terms involving triple products of these first order velocities have been dropped from the equations, it would be equally reasonable to set $k^2 = 0$ as well as $(h-1) = 0$. However, this assumption regarding k was not made in this report.

Transformation to Laboratory Coordinates

The experimental results were first determined in the hot-wire coordinates of figure 7 using the equations and procedures described in the preceding paragraphs. This Cartesian coordinate system rotates with the mean flow velocity vector and, therefore, with respect to the fixed laboratory Cartesian coordinate system as shown in figure 8. For theoretical analysis, it is usually convenient to work in the fixed laboratory coordinates. Therefore, the results expressed in the hot-wire coordinates have been transformed to the laboratory coordinates for all data presentations. This is accomplished by using the tensor transformations for Cartesian coordinate rotation.

For convenience, let the hot-wire coordinates be represented by x'_i where i = 1, 2, 3 and the laboratory coordinates be represented by x_j where j = 1, 2, 3 so that

$$x'_1 = s, \quad x'_2 = y, \quad x'_3 = n$$

and

$$x_1 = x, \quad x_2 = y, \quad x_3 = z.$$

The corresponding coordinate systems are shown in figure 12. For this particular case, rotation is about the $x_2 = x'_2 = y$ axis. The general form for the vector (first order tensor) transformation is

$$V_p = \ell_{ip} V'_i \tag{33}$$

where the indices i and p take on values 1, 2, and 3, a repeated index is held to be summed over the three values, V_i' is the i component of the vector in the hot-wire coordinates (x_i'), V_p is the i component of the vector in the laboratory coordinates (x_i), and ℓ_{ip} is the direction cosine or the cosine of the angle between x_i' and x_p. The velocity components V_i' are related to those used in the previous equations by the identities

$$V_1' \equiv U_s, \quad V_2' \equiv U_y, \quad V_3' \equiv 0 \tag{34}$$

The velocity components V_p are related to those used in the data presentations by the identities

$$V_1 \equiv U_x, \quad V_2 \equiv U_y, \quad V_3 \equiv U_z \tag{35}$$

These relationships are also indicated in figure 12.

The general form for the second order tensor transformation for the x_i' and x_j coordinates is

$$T_{pq} = \ell_{ip} \ell_{jq} T'_{ij} \tag{36}$$

where the repeated indices are again held to be summed over all three values, T_{ij}' is the ij component of the tensor in the hot-wire coordinates, and T_{pq} is the pq component of the tensor in the laboratory coordinates. The six components of each of these symmetric tensors are related to those used in the previous equations and those used in the data presentations by the identities

$$T_{ij}' \equiv \begin{bmatrix} \overline{u_s^2} & \overline{u_s u_y} & \overline{u_s u_n} \\ \overline{u_s u_y} & \overline{u_y^2} & \overline{u_y u_n} \\ \overline{u_s u_n} & \overline{u_y u_n} & \overline{u_n^2} \end{bmatrix} \tag{37}$$

and

$$T_{pq} \equiv \begin{bmatrix} \overline{u_x^2} & \overline{u_x u_y} & \overline{u_x u_z} \\ \overline{u_x u_y} & \overline{u_y^2} & \overline{u_y u_z} \\ \overline{u_x u_z} & \overline{u_y u_z} & \overline{u_z^2} \end{bmatrix} \tag{38}$$

respectively.

The velocity components in the laboratory coordinates, as given by the identities of equation (35), were evaluated using equation (33) starting with the velocity components in the hot-wire coordinates as given by the identities of equation (34). Similarly, the tensor components (i.e., the auto- and cross-correlations of the fluctuating velocities), as given by the identities of equation (38), were evaluated using equation (36) starting with the tensor components in the hot-wire coordinates as given by the identities of equation (37). The direction cosines in equations (33) and (36) vary only with the measured flow angle θ (see fig. 7).

RESULTS AND DISCUSSION

Preliminary studies regarding the quality and repeatability of the results will be discussed first. Following this, the general character of the juncture flow as deduced from contours of constant mean velocity and from vector plots in the y-z cross-section will be described. Finally, the results from the detailed measurements in the juncture will be discussed.

The main results of this experimental investigation are measured values of the mean velocity components U_x, U_y and U_z and the turbulence quantities u'_x, u'_y, u'_z, $\overline{u_x u_y}$, $\overline{u_y u_z}$, and $\overline{u_x u_z}$ at two streamwise stations in the juncture flow. These values are presented in Tables 1 and 2. Representative results have been selected for detailed graphical presentation. In addition,a collection of certain of the tabulated data, at the two streamwise stations, is presented in composite plots in order to display trends and to illustrate the relative behavior of the various quantities.

Preliminary Studies

Before systematic data-taking was begun, an evaluation of the undisturbed flow field and of the data acquisition and reduction methods was carried out by making hot-wire measurements in the turbulent boundary layer on the flat plate with the body removed. These results showed that a fully-developed two-dimensional turbulent boundary layer was well established and that the mean velocity and turbulence profiles were in good agreement with the classical data due to Klebanoff (ref. 16).

The repeatability of the data in the juncture flow was checked next and determined to be excellent . Typical results are presented in figure 13. The turbulence

measurements shown in figure 13 were made at x = 165 mm (6.5 in) and z = 30.5 mm (1.2 in.). The three data symbols represent a random selection of runs on different days and at the beginning and end of a given day. Figure 13(a), showing u'_x, is typical of the repeatability of data taken with the horizontal wire. Figure 13(b), $\overline{u_x u_y}$, shows representative repeatability of data taken with the slant wire. Figure 13(c) illustrates the repeatability of $\overline{u_y u_z}$, which is the most difficult component to measure. The method used to measure this component involved combining RMS data from both the horizontal and the slant wires. This was found to be more accurate than obtaining the component by using D.C. data from the slant wire alone, for reasons that are explained in Appendix C.

The data presented in Tables 1 and 2 and in the remaining figures are the best (i.e. most consistent) survey profiles at those several stations where more than one survey was made.

General Character of the Juncture Flow

Contours of constant mean velocity, U_x/V_∞, are shown in figure 14 at the two streamwise measurement stations. These contours show the presence of a strong counterclockwise (looking downstream) secondary flow in the juncture which is contained within a region extending about 51 mm (2.0 in.) away from the surface of the body at the upstream measurement station. At the downstream station, the secondary flow region has grown to about twice that size. The presence of the counterclockwise vortex in the juncture is more apparent in figure 14(b), where it is seen that high velocity fluid is carried down toward the plate surface at z = 25 mm (1.0 in.) while low velocity fluid is carried upward and away from the plate surface at z = 70 mm (2.7 in.). The majority of the detailed measurements described later were carried out within the region of large secondary flow activity.

The presence of the secondary flow vortex in the juncture is shown more clearly in the two vector plots in figure 15, which illustrate the velocity components in the y-z plane at the two streamwise stations. At the upstream station, x = 165 mm (6.5 in.), the vortex is stronger than that observed by Shabaka (ref. 11) at x = 156.6 mm (6.16 in.). This is to be expected, since the leading edge of the body used here was much more blunt than the one used in reference 11.

At the downstream station, figure 15(b), the vector plot suggests the presence of a second, smaller vortex having a clockwise sense and located very near the body. A similar indication is seen in the vector plots at station x = 1223 mm (48 in.) in reference 11. Comparison of the two vector plots of figure 15 indicates that the secondary flow vortex grows (diffuses) as it progresses downstream. The magnitude of the vectors shows that the vortex is also weaker at the downstream station because of the conservation of angular momentum.

The location of the effective core of the secondary flow vortex may be estimated from the vector plots of figure 15. At x = 165 mm (6.5 in.) the center is at z = 32 mm (1.25 in.) while at x = 902 mm (35.5 in.) it is located at z = 44 mm (1.75 in.). Expressed in terms of body widths, the centers are, respectively, at 0.55 and 0.78 body thicknesses away from the body surface. The weaker vortex studied in reference 11 was located closer to the body (0.36 body widths) at x = 156.6 mm (6.16 in.) and was only 0.46 body widths away from the body at x = 1223 mm (48 in.). As other investigators (refs. 10 and 11) have observed, the secondary flow vortex moves slightly away from the body surface as it proceeds downstream.

Considering the vertical (y) location of the vortex center, the approximate values from figure 15 are 8.9 mm (0.35 in.) at the upstream station and 17.8 mm (0.70 in.) at the downstream station. The ratios of these y values to the local thickness of the essentially two-dimensional boundary layer are 0.33 and 0.54 at the two measurement stations. In contrast, corresponding ratios estimated from reference 11 are 0.58 and 0.48 at comparable streamwise stations. Thus, in terms of local undisturbed boundary layer thickness, the stronger vortex in the juncture is located much nearer the surface of the flat plate near the body leading edge than is the weaker vortex (ref. 11). Also, the normalized height to the vortex center apparently increases with distance downstream for the stronger vortex but decreases for the weaker one.

The fact that the strong secondary flow is confined to a narrow region near the body surface is indicated in the vector plots of figure 15 and confirmed by the profiles in figure 16. In the latter figure, one mean flow and two turbulence profiles are presented at z = 152 mm (6.0 in.) and compared with the classical two-dimensional boundary layer measurements of Klebanoff (ref. 16). The measured mean streamwise velocity profile, figure 16 (a), agrees very well with the two-dimensional reference profile except in the region near the plate surface where the measured profile is slightly

less full. The difference is attributed to the slight effect of the body on the boundary layer flow and to the lower Reynolds number for the present experiments. Similar disagreements are seen in the normal stress profiles of figure 16 (b) and in the shear stress profiles of figure 16 (c). The disagreement in the outer third of the profile in figure 16 (b) is because the turbulent intensity in the free stream for these experiments (0.5%) was greater than that for the reference work. Figure 16 indicates that the flow in the viscous layer on the flat plate at z = 152 mm (6.0 in.) can be said to be effectively two-dimensional.

The skewing of the two-dimensional boundary layer on the flat plate, which was noted in the introduction, is illustrated in figure 17. This figure shows the variation of the local mean flow direction, θ, with distance above the flat plate as a function of x and z. The skewing is much more pronounced at the upstream station, as expected. At the upstream station, the mean flow is directed toward the body (θ negative) at the outer edge of the viscous region and away from the body (θ positive) closer to the plate surface. At the downstream station, the skewing of the mean flow is confined to about the lower half of the viscous region. It is this angle θ, the angle between the s and x axes as determined from measurements with the horizontal wire, that specifies the s-n plane for the slant wire measurements.

Mean Velocities and Turbulence Stresses

Selected graphs of the mean velocity components U_x, U_y and U_z and the six turbulence stresses are shown in figure 18 as a function of distance above the plate at the upstream measuring station. Comparable results at the downstream measuring station are given in figure 19. As has been discussed, the results at the largest value of z at both stations correspond to those for an effectively two-dimensional boundary layer. Thus, the curves for the largest z may be used as bases of comparison when studying the behavior of the flow in the juncture in figures 18 and 19. Also, in examining figures 18 and 19, it should be kept in mind that, from the vector plots (fig. 15), the effective core of the secondary flow is located at approximately z = 32 mm (1.25 in.) at the upstream measuring station and z = 44 mm (1.75 in.) at the downstream measuring station.

The profiles of the x-component of mean velocity, figures 18 (a) and 19 (a), bear out the overall behavior of the juncture flow which was deduced from the contours of constant mean velocity in figure 14 and the vector plots of figure 15. Near the body (small values of z), the mean velocity profiles are fuller than those for the undisturbed two-dimensional boundary layer, indicating that high momentum fluid is being transported towards the plate surface by the action of the secondary flow. At an intermediate distance from the body surface, and particularly near the effective core of the secondary flow, the profiles are distorted. Further outboard, the profiles have a smaller velocity magnitude for the same height above the plate than do the comparable undisturbed boundary layer profiles. This is due to the fact that low momentum fluid is being transported upward and away from the plate surface by the action of the secondary flow.

A comparison of the profiles of the y-component of mean velocity, U_y, is shown in figures 18 (b) and 19 (b).* These profiles again demonstrate the counterclockwise vortical motion of the secondary flow. Inboard of the effective vortex center, there is an appreciable downwash in the viscous layer at the upstream measuring station. Outboard of the vortex center the upwash is greater at the downstream measuring station. The maximum pitch angle of the velocity vector in the juncture flow is about three degrees.

Profiles of the z-component of mean velocity, U_z, are shown in figure 18 (c) and 19 (c). These profiles indicate the skewing of the boundary layer as previously noted in the discussion of the yaw angle profiles (fig. 17). The information in figures 18 (c) and 19 (c) is similar to that in figure 17 and again illustrates the presence of the secondary flow vortex. The large velocity gradients in the U_x and U_z profiles at the upstream measuring station near the surface of the body indicate a considerable increase in flat-plate shear stress over that for a conventional two-dimensional boundary layer.

The profiles describing the distribution of the turbulence stresses in the juncture, which are found in the remaining plots in figures 18 and 19, point out the important result that the secondary flow in the juncture has large effects on the turbulence as well as on the mean flow. That is, the secondary flow in the juncture re-distributes the turbulence as well as changing the mean flow direction.

---

*Profiles of the y-component of mean velocity, U_y, presented in an interim Status Report show too great an upwash and are unreliable for reasons explained in Appendix D.

The turbulent normal stress u'_x, figures 18 (d) and 19 (d), is reduced near the body and increased outboard of the effective core of the secondary flow when compared with the undisturbed two-dimensional boundary-layer values. At both measuring stations, all the curves coalesce into a single curve near the flat plate, indicating that there is an equilibrium in the wall layer. Near the effective core of the secondary flow the normal stress increases considerably at the upstream station but does not have such an abrupt behavior at the downstream station. This is perhaps because the secondary flow has diffused with distance downstream.

The distribution of the turbulent normal stress, u'_y, figures 18 (e) and 19 (e), has the same qualitative behavior as that described earlier for the normal stress u'_x. Because the u'_y data had to be obtained using the slant wire, and the sensor portion could not be positioned very near the plate surface, the coalescing of the curves near $y = 0$ noted with regard to u'_x is not present in the u'_y plots. Between the body and the vortex center, the values of u'_y are lower than those for a two-dimensional boundary layer, while outboard of the center they are considerably higher, particularly at the upstream station.

The distribution of the turbulent normal stress u'_z, figures 18 (f) and 19 (f), shows a trend similar to that for u'_y in the sense that the values are lower than those for a two-dimensional boundary layer inboard of the vortex core and higher in the outboard regions.

Profiles of turbulent shear stress $\overline{u_x u_y}$ are shown in figures 18 (g) and 19 (g), and indicate a transport of turbulent shear stress by the secondary flow. The turbulent shear stress near the surface of the body (i.e. inboard of the vortex center) is very small at the upstream station, while at the downstream station it becomes negative at the outer edge of the viscous region. Near the vortex center, the distributions become highly distorted.

The turbulent shear stress $\overline{u_x u_z}$, figures 18 (h) and 19 (h), is significant in this juncture flow. At the downstream station the large values observed at $z = 15$ mm (0.6 in.) are due to the boundary layer on the vertical body.

As has been mentioned, there is scatter in the data for the shear stress $\overline{u_y u_z}$ (figs. 18 (i) and 19 (i)). Nevertheless, this shear stress is not zero, as it would be for a two-dimensional boundary layer, and inspection of these figures reveals significant values of $\overline{u_y u_z}$, with those profiles near and outboard of the vortex center being highly distorted.

A summary of the behavior of the secondary flow in the juncture, both as regards mean flow and turbulence, is presented in figures 20 and 21. It is instructive to follow the trends in the various quantities and their relative behaviors by studying these figures. In so doing, keep in mind that the profiles at z = 152 mm (6.0 in.) represent the behavior of a two-dimensional turbulent boundary layer with no secondary flow. It is also useful to recall that at the upstream station (fig. 20) the effective core of the secondary flow is at approximately z = 32 mm (1.25 in.) and at the downstream station (fig. 21) it is located at z = 44 mm (1.75 in.). Inspection of the curves in figures 20 and 21 shows that the trends in the results are smooth and consistent. The turbulent stresses are seen to vary quite substantially in both the y and z directions as a result of the presence of the secondary flow system. There is considerable evidence of similarity between the turbulent shear stresses and the mean-flow strain rates. This is important in eddy viscosity modeling of shear stresses, and should be investigated further. Also, there is some evidence of similarity between the variations in the turbulent stress components.

CONCLUDING REMARKS

The hot-wire measurements carried out in the juncture formed by a flat plate and a body of constant thickness having a 1.5:1 elliptical leading edge have led to results from which the following conclusions may be drawn.

1. The experimental results for the mean flow and turbulence components show clear and consistent trends.
2. The secondary flow in the juncture transports mean momentum toward the flat plate near the body surface and away from the flat plate further outboard from the body. This results in the mean velocity profiles being changed considerably from those for a two-dimensional boundary layer.
3. The secondary flow in the juncture also transports turbulence and has a large effect on the distribution of the turbulence stresses.
4. In the juncture flow, there is considerable evidence of similarity between the turbulent shear stresses and the mean-flow strain rates. Also, there is some evidence of similarity between the variations in the turbulent stress components. These points should be investigated further.

5. The strength of the secondary flow vortex in the juncture increases as the leading edge of a body of constant thickness is made more blunt. This stronger vortex has an effective core which is located closer to the surface of the body than is the weaker vortex caused by a leading edge of smaller fineness ratio.
6. The secondary flow vortex in the juncture diffuses as downstream distance from the body leading edge increases.

APPENDIX A

TIME AVERAGING

In the experiments reported here, the data reduction method used to find the mean velocity components and turbulence stresses was based upon analog (voltage) measurements. The method utilizes the time-averaged mean (D.C.) voltage and/or RMS voltage at each point in the flow. This time averaging was accomplished by transferring the linearized voltage output of the hot-wire anemometer and the voltage signal from the true RMS meter to an integrating digital voltmeter. The maximum integrating time of the HP-2401C digital voltmeter is one second. Longer averaging times were obtained by making repeated calls to the voltmeter from the computer and then arithmetically averaging the several integrated voltages. The time interval between calls was about 16 milliseconds.

The question arises as to the proper total time or number of data points for averaging. It was found that the scatter in some calculated velocity and stress components was sensitive to the averaging time, so this matter was investigated.

The uncertainty in the measured value of the turbulent shear stress $\overline{u_y u_n}$ (the shear stress in the hot-wire coordinate system) for different averaging times is shown in figure 22.

The calculation of $\overline{u_y u_n}$ involves taking the difference of two time-averaged RMS voltages. Also present in the equations is a previously determined value of $\overline{u_s u_n}$. This quantity was specified at a representative value and held constant for these calculations.

Over one thousand data samples (successive RMS voltage readings) were taken at an averaging time of one second each at $\psi = 0^{o}$ and at a representative value of y. The standard deviation of these voltage samples was calculated and introduced into the data reduction scheme as variations in the voltages around typical reference values. These typical reference voltages were obtained from a survey at the particular x and z using moderate averaging times, and were used to compute reference values of $\overline{u_y u_n}$. The result is shown in figure 22 as a plus/minus scatter in $\overline{u_y u_n}$ from the reference values. Averaging times of greater than one second (i.e. greater than the integrating time of the HP-2401C voltmeter) were obtained by arithmetically averaging the one-second

data samples in groups. As is apparent from figure 22, the scatter in the calculated shear stress is greatly reduced if long averaging times are used (i.e. a large number of data points are averaged) during the voltage measurements. The data reduction process then becomes a compromise between desired accuracy and the time required to take the data.

The relationship between scatter and averaging time was checked for the other mean flow and stress components in a similar way. On the basis of the findings it was decided that an averaging time of 30 seconds (the average of 30 readings each integrated over 1 second) would be used for all voltages used in the determination of U_y, u'_y, $\overline{u_s u_y}$, and $\overline{u_y u_n}$. It was concluded that a one second averaging time would be adequate for readings taken to determine U_s, U_n, u'_s, u'_n, and $\overline{u_s u_n}$ since the scatter in these results was relatively insensitive to the averaging time. After allowing for tunnel warm-up, a typical hot-wire survey took 30-90 minutes depending upon the averaging time and the number of y ordinates (16 or 24) at which measurements were taken.

APPENDIX B

EFFECT OF FLOW TEMPERATURE VARIATIONS ON HOT-WIRE ANEMOMETER MEASUREMENTS

Consider the hot-wire response equation

$$\frac{E^2}{T_w - T_f} = A + B\sqrt{U_{eff}} \tag{B-1}$$

where U_{eff} is the effective cooling velocity, E is the nonlinear output voltage and A and B are calibration coefficients. T_w and T_f are the wire temperature and flow temperature, respectively. For a given flow velocity, the right side of equation (B-1) remains constant. This implies that E is directly proportional to $(T_w - T_f)$. The same argument holds for E_o, the nonlinear output voltage at zero velocity.

For a given overheat ratio, (T_w/T_f), the anemometer circuitry maintains the sensor temperature at a constant level. However, the temperature of the air flow in a wind tunnel can increase over a period of time before relative stabilization occurs (fig. 23). This temperature rise would be sensed as an apparent drop in the flow velocity.

Various methods can be used for compensating the output voltage for this temperature variation effect. Some of these methods are:

(1) Measurements can be made after the flow temperature has reached a constant value.

(2) The overheat ratio can be adjusted, within limits, so as to maintain a constant value of $(T_w - T_f)$.

(3) An accurate record of the flow temperature can be kept and used to correct the data later.

Generally, these procedures are either cumbersome or excessively time-consuming. Two other methods of correction for temperature variation effects were considered in the course of this work and are described below. The second method was the one used to correct the data presented herein.

The first method considered was a "Two-Point" correction procedure. The calibration curve of the wire (for details, see Procedures and Calibrations) yields the

value of E corresponding to $U_{eff}=V_\infty$ as well as the value of E_o. These two voltages E_o and E, which correspond to $U_{eff}=0$ and $U_{eff}=V_\infty$, respectively, are used to set the span of the linearized output. At the calibration temperature, the linear output curve (fig. 24) passes through the origin. Decreases in the voltages E_o and E, as the flow temperature increases, result in a downward shift in the output curve and a change in the slope (fig. 24). If E_o can be measured frequently enough so as to offset the input voltage to the linearizer as an update correction, then the linearized output curve will continue to pass through the origin. Hence, the slope of an updated calibration curve can be obtained by measuring the linearized output voltage $(E_\ell)_{new}$ in the usual way at the edge of the boundary layer where $U_{eff}=V_\infty$. Finally, this new slope can be used to scale up (or scale down) all of the measured voltages to their corresponding values at the calibration temperature. Thus,

$$(E_\ell)_{corrected} = (E_\ell)_{measured} \times \frac{(slope)_{calibration\ temp.}}{(slope)_{new}} \qquad (B\text{-}2)$$

The problem with this "Two-Point" correction method of adjusting E_o and the slope of the linear output curve is that it requires many measurements of E_o. This means that the wind tunnel must be stopped frequently in order to provide a zero-velocity environment for the wire.

For this reason, a "One-Point" temperature correction method was employed here. In this approach, the input voltage to the linearizer is offset by E_o only at the beginning of a series of measurements, which typically take several hours to complete. At the end of each boundary-layer survey, a new slope of the linearized output curve is determined by assuming that the curve still passes through the origin and then measuring the value of E at the boundary-layer edge when $U_{eff}=V_\infty$ (fig. 24). This new slope then is used to scale all of the voltages measured during that particular survey by using equation (B-2). Of course, the new slope is approximate because the actual curve may no longer pass through the origin.

This method of using the approximate slope introduces small errors in measuring effective velocities when these effective velocities are well below the freestream value. Calculations based on a typical calibration curve show that a change of 3^oC

(5.4°F) in flow temperature introduces a maximum error of less than 1% in the measurement of effective velocity over the operating range of 7 m/s (23 ft /sec.) to 17 m/s (56 ft/sec.).

In order to reduce this error still further, the wind tunnel was run for one hour before the initial value of E_o was measured. This bypassed the period of time during which the flow temperature increased most rapidly (fig. 23). Also, if the measurements were to take more than four or five hours, the flow temperature was monitored and the wind tunnel was stopped and E_o updated after every 1.0°C (1.8°F) temperature rise. Using the "One-Point" correction method in this way introduced a maximum error of less than 0.5% in the effective velocities that were measured in these experiments.

APPENDIX C

MEASUREMENT OF $\overline{u_y u_n}$

The turbulent shearing stress $\overline{u_y u_n}$, which is generally small, proved to be the most difficult stress component to measure, and finding a satisfactory method required special study.

After examination of the basic wire-response equations, the most straightforward way to evaluate $\overline{u_y u_n}$ is by taking the difference of two mean voltages, $\bar{E}_\ell$. These two mean voltages are measured with the slant wire oriented at a nominal $\alpha = \pm 45^\circ$ in the measurement or s-y plane, i.e., at $\psi = 0^\circ$ and $\psi = 180^\circ$. With these choices of angles, ψ, the response equations simplify so that the two mean voltage equations contain only $\overline{u_y u_n}$ as unknowns and the solution is accomplished.

When the values of $\overline{u_y u_n}$ were calculated at $z = 152$ mm (6.0 in.) using the difference of two mean voltages, $\bar{E}_\ell$, it was found that the result was an order of magnitude larger than expected. It was determined that the problem lay in the variation of the free stream velocity, V_∞ . Recall that the readings with the slant wire were made sequentially rather than simultaneously, since the probe had only a single sensor. Even though V_∞ was held constant to within $\pm$ 0.5%, this small difference introduced a difference in the two values of mean voltage, $\bar{E}_\ell$, which was sufficient to mask the small difference in $\bar{E}_\ell$ which was attributable to $\overline{u_y u_n}$. Averaging the readings of $\bar{E}_\ell$ over a very long time, in an attempt to suppress the V_∞ variation, did not improve the quality of the results.

In order to examine the possiblity of obtaining $\overline{u_y u_n}$ from other measurements than the difference of two mean voltages, the wire-response equations were derived in full for arbitrary values of α and ψ . From this it was observed that $\overline{u_y u_n}$ also could be determined, using the slant wire, as the difference of two time-averaged RMS voltages, hence eliminating the DC voltage drift due to the small variations in V_∞ . However, in order to find $\overline{u_y u_n}$ from measured RMS voltages, the necessary two equations also contain the quantity $\overline{u_s u_n}$, which is determined from horizontal wire data and hence is subject to experimental error. Accordingly, values of ψ were selected at which the coefficients of the unknown $\overline{u_y y_n}$ were large while the coefficients of $\overline{u_s u_n}$ were small. The choice of the appropriate values of ψ is discussed in the main text of this report under Development of the Equations, part 6.

APPENDIX D

MEASUREMENT PROBLEMS IN EVALUATING U_y

The determination of the vertical component of mean velocity, U_y, involves a measurement of the time-averaged DC voltage $\bar{E}_\ell$ with the slant wire at two orientations ($\psi = 0^\circ, 180^\circ$) in the s-y measurement plane.

The data for this experiment were collected by first making all of the measurements in the s-y plane at the upstream station, using first the horizontal wire and then the slant wire. A complete set of measurements then was made at the downstream station. Finally, the instrumented slide was moved back to the upstream measurement station in order to complete the measurements there and also to make some final repeatability checks. Over the outer half of the boundary layer, the new values of U_y showed poor repeatability when compared with the values determined earlier at the upstream station, with the new measurements indicating a larger upwash corresponding to a pitch angle increment of about 1.5°.

At first, it was thought that the wind tunnel flow had changed or that some hardware had shifted during the course of the experiments, and considerable effort was expended in checking the hot-wire probe, cleaning the screens in the wind tunnel, verifying model alignment, and so on. When these efforts produced no change in U_y, the slant wire probe again was scrutinized in detail. After many trials, the cause of the problem was discovered. Referring to figure 5, the two needles supporting the slant wire pass through two holes in the surface plug, and the needles move in and out of these holes as the measurement height, y, is changed. The holes in the surface plug were purposely made small (about twice the diameter of the needles) so as to minimize inflow-outflow interference when the wire was close to the flat plate. This clearance was carefully checked after the probe was fabricated.

The surface plug in the original design was made in one piece. It was press-fit into the probe holder and held by three set screws. During the detailed re-examination of the probe, it was found that the surface plug had rotated slightly at some time during the experiment, presumably at about the beginning of the downstream measurements. As a result, one needle was touching the surface plug. Thus, as the needles were moved in and out of the holes during a survey, one needle bent slightly since it was not perfectly aligned with the vertical direction of motion. As a result, the slant wire

experienced a slight change in tension. None of this was visible to the eye, even with an optical comparator, but change in axial force on the wire was detected as a change of about 0.01 ohms in the cold resistance. This small change in wire resistance varied as the needles were extended into the flow, and this resistance change was sufficient to cause the observed change in U_y.

The probe was fitted with a new surface plug which was split (fig. 5) and the hole clearance was increased slightly. No differential resistance changes were observed after this modification, and the new values of U_y determined with the modified probe repeated those measured much earlier at the upstream station.

This needle interference did not have an observable effect on the turbulence stresses measured with the slant wire. However, it was decided to repeat all slant wire measurements at both measuring stations using the new surface plug. These are the data presented in this report.

During the close examination of the slant-wire probe while investigating the needle interference problem, it was also discovered that the axis of rotation of the probe was not exactly parallel to the y axis, the divergence angle being approximately 0.25°. Thus, as the slant wire was rotated in the s-y plane from $\psi = 0^{\circ}$ to $\psi = 180^{\circ}$ the angle that the slant wire made with the horizontal was not constant, as had been assumed earlier, but rather was increased by about 0.5° at one orientation and decreased by 0.5° at the other. This correction has been incorporated into the data reduction program used in calculating the results presented in this report.

REFERENCES

1. Gessner, F. B., "The Origin of Secondary Flow in Turbulent Flow Along a Corner", J. Fluid Mechanics, Vol. 58, Part 1, 1973.

2. Bragg, G. M., "The Turbulent Boundary Layer in a Corner", J. Fluid Mechanics, Vol. 36, Part 3, pp. 485-503, November, 1974.

3. Johnston, J. P., "Internal Flows", Topics in Applied Physics, Vol. 12, Turbulence (P. Bradshaw, Editor), 2nd Edition, Springer-Verlag, New York, 1978.

4. Baker, A. J., Manhardt P. D., and Orzechowski, J.A., "Numerical Prediction of Turbulent Three-Dimensional Juncture Region Flow Using the Parabolic Navier Stokes Equation", NASA CR-159024, March, 1979.

5. Gessner, F. B., Po, J. K., and Emery, A. F., "Measurements of Developing Turbulent Flow in a Square Duct", Turbulent Shear Flows I (F. Durst, et al, Editors), Springer-Verlag, New York, 1979.

6. Treaster, A. L., Jacobs, P. P., and Gurney, G. B., "Correcting for the Sidewall Boundary Layer in Subsonic Two-Dimensional Airfoil/Hydrofoil Testing". Applied Research Laboratory, Penn State University, Tech Memo 81-176, August, 1981 (AD-A104562).

7. Hawthorne, W. R., "The Secondary Flow About Struts and Airfoils", Jour. Aero. Sc., Vol. 21, No. 9, pp. 588-608, September, 1954.

8. Kuchemann, D., "Some Remarks on the Interference Between A Swept Wing and a Fuselage", AGARD Conference Proceedings No. 71, Aerodynamic Interference, September,1970.

9. Barber, T. J., "An Investigation of Strut-Wall Intersection Losses", AIAA Journal of Aircraft, Vol. 15, No. 10, pp. 676-681, October, 1978.

10. Oguz, E. A., "An Experimental Investigation of the Turbulent Flow in the Junction of a Flat Plate and a Body of Constant Thickness", Ph.D. Thesis, Georgia Inst. of Technology, 1981.

11. Shabaka, I. M. M. A., "Turbulent Flow in an Idealized Wing-Body Junction", Ph.D. Thesis, Imperial College, London, April, 1979.

12. Shabaka, I. M. M. A., and Bradshaw, P., "Turbulent Flow in an Idealized Wing-Body Junction", AIAA Journal, Vol. 19, No. 12, February, 1981.

13. Hubbartt, J., McMahon, H., and Oguz, E., "Exploratory Tests of Flow in Wing-Root Junctions", Georgia Institute of Technology, School of Aerospace Engineering, Final Report, Contract No. P.O. CK27034P, Lockheed-Georgia Company, Marietta, Georgia, March, 1976.

14. Jorgensen, F. E., "Directional Sensitivity of Wire and Fiber-Film Probes", DISA Information Bulletin No. 11, 1971, pp. 31-37.

15. Rodi, W., "A New Method of Analyzing Hot-Wire Signals in a Highly Turbulent Flow, and its Evaluation in a Round Jet", DISA Information Bulletin No. 17, 1975, pp. 9-18.

16. Klebanoff, P. S., "Characteristics of Turbulence in a Boundary Layer with Zero Pressure Gradient", NACA TN 317E (1954).

Table 1
Mean velocities and turbulence stresses in the juncture (x = 165 mm.).

z (mm)	y (mm)	y (in.)	$\frac{U_x}{V_\infty}$	$\frac{U_y}{V_\infty}$	$\frac{U_z}{V_\infty}$	$\frac{u'_x}{V_\infty}$	$\frac{u'_y}{V_\infty}$	$\frac{u'_z}{V_\infty}$	$-\frac{\overline{u_x u_y}}{V_\infty^2}\times10^4$	$-\frac{\overline{u_x u_z}}{V_\infty^2}\times10^4$	$-\frac{\overline{u_y u_z}}{V_\infty^2}\times10^4$
152.4	.5	.02	.47	-	-.002	.087	-	.042	-	.3	-
	.8	.03	.53	-	-.002	.083	-	.044	-	.9	-
	1.0	.04	.57	-	-.001	.077	-	.044	-	1.0	-
	1.3	.05	.58	-	0.000	.075	-	.046	-	-1.0	-
	1.5	.06	.60	-	-.001	.075	-	.040	-	-.9	-
	1.8	.07	.62	-	.001	.074	-	.040	-	-.1	-
	2.0	.08	.62	-	.003	.073	-	.039	-	-.5	-
	2.3	.09	.65	.005	.001	.069	.049	.044	14.2	-.6	-1.7
	2.5	.10	.66	.007	0.000	.071	.042	.035	13.9	-.0	-1.4
	3.8	.15	.70	.003	.002	.066	.046	.035	12.8	.2	.3
	5.1	.20	.73	.002	.003	.061	.049	.042	12.0	.8	1.5
	6.4	.25	.77	.001	.003	.061	.044	.037	11.1	-.1	-1.1
	7.6	.30	.80	.005	.001	.059	.043	.036	10.5	1.0	.6
	8.9	.35	.81	.002	.001	.057	.041	.035	10.0	.2	1.1
	10.2	.40	.84	.004	0.000	.054	.045	.039	9.4	.9	.4
	11.4	.45	.85	.001	-.001	.051	.045	.036	8.8	.9	3.2
	12.7	.50	.88	.005	0.000	.052	.039	.032	7.9	.3	1.0
	15.2	.60	.90	.002	-.003	.047	.039	.032	6.6	.1	.4
	17.8	.70	.93	.003	-.003	.042	.037	.030	4.8	.0	.2
	20.3	.80	.95	.001	0.000	.037	.036	.028	3.7	-.0	.7
	22.9	.90	.97	0.000	0.000	.031	.032	.023	2.1	.5	1.0
	25.4	1.00	.98	0.000	-.002	.022	.030	.021	.0	.3	-.3
	27.9	1.10	1.00	.002	.002	.015	.025	.016	-.1	.1	-.8
	31.8	1.25	1.00	-	0.000	.008	-	.012	-	.3	-

Table 1. Continued.

z (mm)	y (mm)	y (in.)	$\frac{U_x}{V_\infty}$	$\frac{U_y}{V_\infty}$	$\frac{U_z}{V_\infty}$	$\frac{u'_x}{V_\infty}$	$\frac{u'_y}{V_\infty}$	$\frac{u'_z}{V_\infty}$	$-\frac{\overline{u_x u_y}}{V_\infty^2}\times 10^4$	$-\frac{\overline{u_x u_z}}{V_\infty^2}\times 10^4$	$-\frac{\overline{u_y u_z}}{V_\infty^2}\times 10^4$
76.2	.5	.02	.48	-	.004	.087	-	.043	-	-.7	-
	.8	.03	.53	-	.006	.082	-	.039	-	-1.3	-
	1.0	.04	.56	-	.005	.080	-	.042	-	-1.2	-
	1.3	.05	.58	-	.007	.075	-	.043	-	-1.2	-
	1.5	.06	.60	-	.005	.074	-	.043	-	-.8	-
	1.8	.07	.62	-	.006	.072	-	.044	-	-.3	-
	2.0	.08	.64	-	.006	.071	-	.044	-	-.4	-
	2.3	.09	.64	.004	.008	.074	.038	.036	13.2	-.1	3.4
	2.5	.10	.65	.004	.007	.070	.046	.040	13.4	.6	3.9
	3.8	.15	.71	.003	.010	.066	.044	.043	11.9	.1	2.3
	5.1	.20	.74	.004	.010	.063	.047	.039	9.2	.6	1.2
	6.4	.25	.77	.006	.008	.060	.043	.036	9.1	1.5	66.2
	7.6	.30	.80	.005	.008	.059	.048	.036	11.3	2.8	1.8
	8.9	.35	.82	.004	.007	.056	.044	.038	9.5	1.7	3.4
	10.2	.40	.84	.007	.003	.055	.044	.038	8.9	1.6	1.8
	11.4	.45	.85	.006	0.000	.054	.045	.040	9.1	1.7	3.1
	12.7	.50	.88	.006	.002	.054	.040	.037	8.2	1.9	4.1
	15.2	.60	.90	.005	0.000	.050	.041	.036	7.1	.7	3.7
	17.8	.70	.93	.005	-.003	.045	.038	.035	5.4	1.1	3.6
	20.3	.80	.96	.007	-.002	.040	.036	.029	3.4	-.4	.7
	22.9	.90	.98	.005	-.003	.034	.031	.024	2.8	.1	2.2
	25.4	1.00	1.00	.007	-.007	.027	.028	.023	.4	.3	2.3
	27.9	1.10	1.01	.005	-.005	.005	.032	.025	-.4	.3	1.9
	31.8	1.25	1.01	-	-.005	.016	-	.020	-	.0	-

Table 1. - Continued.

z (mm)	y (mm)	y (in.)	$\frac{U_x}{V_\infty}$	$\frac{U_y}{V_\infty}$	$\frac{U_z}{V_\infty}$	$\frac{u'_x}{V_\infty}$	$\frac{u'_y}{V_\infty}$	$\frac{u'_z}{V_\infty}$	$-\frac{\overline{u_x u_y}}{V_\infty^2}\times10^4$	$-\frac{\overline{u_x u_z}}{V_\infty^2}\times10^4$	$-\frac{\overline{u_y u_z}}{V_\infty^2}\times10^4$
50.8	.5	.02	.46	-	.024	.086	-	.049	-	-5.8	-
	.8	.03	.52	-	.029	.084	-	.047	-	-6.8	-
	1.0	.04	.55	-	.028	.081	-	.045	-	-5.6	-
	1.3	.05	.58	-	.029	.078	-	.047	-	-4.4	-
	1.5	.06	.60	-	.027	.078	-	.046	-	-3.3	-
	1.8	.07	.61	-	.029	.079	-	.043	-	-5.6	-
	2.0	.08	.63	-	.035	.074	-	.051	-	-3.8	-
	2.3	.09	.63	.001	.031	.075	.048	.046	14.1	-3.4	4.1
	2.5	.10	.65	.001	.029	.076	.045	.043	14.2	-4.0	3.6
	3.8	.15	.69	-.001	.028	.071	.047	.043	12.6	-2.0	2.3
	5.1	.20	.73	0.000	.025	.068	.049	.044	11.7	-.1	-3.5
	6.4	.25	.75	0.000	.020	.065	.049	.044	11.3	2.2	-.9
	7.6	.30	.78	0.000	.016	.063	.050	.046	11.2	3.3	-.5
	8.9	.35	.80	.003	.011	.063	.049	.045	10.5	4.0	-2.7
	10.2	.40	.82	.002	.004	.062	.054	.047	10.8	3.3	-.4
	11.4	.45	.84	.002	-.003	.062	.051	.045	10.7	2.4	-1.5
	12.7	.50	.85	.003	-.007	.060	.053	.045	10.2	2.2	-1.5
	15.2	.60	.89	.001	-.014	.059	.045	.037	8.1	1.4	-.1
	17.8	.70	.92	-.002	-.011	.052	.047	.035	6.4	1.2	.5
	20.3	.80	.95	-.006	-.018	.047	.042	.032	4.3	.4	1.9
	22.9	.90	.97	-.007	-.019	.039	.041	.030	2.5	.3	.9
	25.4	1.00	.99	-.010	-.019	.032	.036	.021	.3	.6	2.8
	27.9	1.10	1.01	-.013	-.019	.021	.034	.017	-1.1	.0	.6
	31.8	1.25	1.02	-	-.018	.010	-	.016	-	.1	-

Table 1. - Continued.

z (mm)	y (mm)	y (in.)	$\frac{U_x}{V_\infty}$	$\frac{U_y}{V_\infty}$	$\frac{U_z}{V_\infty}$	$\frac{u'_x}{V_\infty}$	$\frac{u'_y}{V_\infty}$	$\frac{u'_z}{V_\infty}$	$-\frac{\overline{u_x u_y}}{V_\infty^2}\times10^4$	$-\frac{\overline{u_x u_z}}{V_\infty^2}\times10^4$	$-\frac{\overline{u_y u_z}}{V_\infty^2}\times10^4$
45.7	.5	.02	.48	-	.034	.090	-	.045	-	-5.0	-
	.8	.03	.54	-	.038	.085	-	.048	-	-4.8	-
	1.0	.04	.57	-	.040	.082	-	.050	-	-4.3	-
	1.3	.05	.59	-	.043	.082	-	.048	-	-3.4	-
	1.5	.06	.61	-	.045	.081	-	.046	-	-2.7	-
	1.8	.07	.62	-	.044	.081	-	.043	-	-2.9	-
	2.0	.08	.64	-	.045	.079	-	.046	-	-3.2	-
	2.3	.09	.65	.003	.044	.078	.048	.048	15.7	-1.9	.5
	2.5	.10	.66	.005	.046	.078	.049	.046	16.0	-2.7	-3.6
	3.8	.15	.70	.007	.043	.076	.046	.040	15.3	.1	-3.9
	5.1	.20	.73	.008	.036	.070	.053	.050	15.0	2.7	-7.8
	6.4	.25	.76	.012	.029	.069	.056	.046	14.9	4.5	-4.3
	7.6	.30	.79	.014	.021	.067	.058	.048	15.0	5.4	-4.7
	8.9	.35	.79	.013	.011	.065	.061	.049	15.0	4.2	-4.2
	10.2	.40	.81	.013	-.003	.067	.061	.049	15.5	4.5	-7.5
	11.4	.45	.83	.011	-.010	.067	.060	.044	15.2	3.3	-6.5
	12.7	.50	.85	.008	-.018	.065	.062	.045	14.8	2.7	-1.4
	15.2	.60	.88	.003	-.023	.058	.060	.045	11.4	1.3	1.9
	17.8	.70	.92	-.001	-.024	.053	.054	.040	7.0	1.0	.4
	20.3	.80	.95	-.005	-.023	.046	.046	.034	4.5	-.1	.4
	22.9	.90	.97	-.008	-.022	.039	.041	.031	2.1	.6	.8
	25.4	1.00	1.00	-.012	-.021	.033	.034	.021	.3	.0	1.2
	27.9	1.10	1.01	-.014	-.021	.028	.033	.023	-1.4	.4	3.1
	31.8	1.25	1.02	-	-.018	.011	-	.019	-	-.3	-

Table 1. - Continued.

z (mm)	y (mm)	y (in.)	$\frac{U_x}{V_\infty}$	$\frac{U_y}{V_\infty}$	$\frac{U_z}{V_\infty}$	$\frac{u'_x}{V_\infty}$	$\frac{u'_y}{V_\infty}$	$\frac{u'_z}{V_\infty}$	$-\frac{\overline{u_x u_y}}{V_\infty^2}\times 10^4$	$-\frac{\overline{u_x u_z}}{V_\infty^2}\times 10^4$	$-\frac{\overline{u_y u_z}}{V_\infty^2}\times 10^4$
40.6	.5	.02	.47	-	.047	.088	-	.051	-	-5.1	-
	.8	.03	.52	-	.053	.084	-	.059	-	-6.2	-
	1.0	.04	.56	-	.058	.084	-	.054	-	-5.9	-
	1.3	.05	.58	-	.061	.083	-	.058	-	-7.8	-
	1.5	.06	.61	-	.067	.084	-	.053	-	-5.8	-
	1.8	.07	.62	-	.068	.082	-	.053	-	-6.8	-
	2.0	.08	.64	-	.068	.080	-	.060	-	-6.0	-
	2.3	.09	.65	.016	.068	.078	.061	.059	13.4	-5.6	8.9
	2.5	.10	.67	.018	.065	.081	.053	.056	12.6	-5.1	4.9
	3.8	.15	.70	.023	.062	.074	.054	.054	9.8	-4.3	-1.0
	5.1	.20	.73	.027	.055	.068	.060	.053	8.8	-1.0	-1.3
	6.4	.25	.74	.029	.040	.067	.061	.051	9.7	.2	-5.5
	7.6	.30	.76	.029	.024	.065	.066	.050	10.8	2.6	-6.1
	8.9	.35	.77	.026	.005	.060	.066	.045	13.0	1.4	-9.8
	10.2	.40	.78	.019	-.008	.071	.065	.046	15.0	1.1	-5.9
	11.4	.45	.80	.019	-.020	.073	.065	.045	16.5	1.2	-5.9
	12.7	.50	.81	.011	-.024	.076	.058	.037	16.5	1.4	-2.2
	15.2	.60	.87	.006	-.030	.071	.055	.035	13.7	.6	-.2
	17.8	.70	.91	-.003	-.029	.060	.051	.035	9.2	.1	2.2
	20.3	.80	.94	-.009	-.030	.049	.047	.032	5.3	.7	4.4
	22.9	.90	.97	-.013	-.032	.040	.041	.025	1.9	.2	2.8
	25.4	1.00	.99	-.016	-.028	.030	.039	.019	.2	-.0	1.2
	27.9	1.10	1.00	-.016	-.026	.019	.033	.018	-1.3	-.1	2.2
	31.8	1.25	1.02	-	-.016	.009	-	.014	-	.2	-

Table 1. - Continued.

z (mm)	y (mm)	y (in.)	$\frac{U_x}{V_\infty}$	$\frac{U_y}{V_\infty}$	$\frac{U_z}{V_\infty}$	$\frac{u'_x}{V_\infty}$	$\frac{u'_y}{V_\infty}$	$\frac{u'_z}{V_\infty}$	$-\frac{\overline{u_x u_y}}{V_\infty^2} \times 10^4$	$-\frac{\overline{u_x u_z}}{V_\infty^2} \times 10^4$	$-\frac{\overline{u_y u_z}}{V_\infty^2} \times 10^4$
35.6	.5	.02	.53	-	.060	.092	-	.058	-	-17.1	-
	.8	.03	.58	-	.060	.090	-	.056	-	-17.6	-
	1.0	.04	.63	-	.072	.091	-	.057	-	-19.9	-
	1.3	.05	.64	-	.076	.089	-	.060	-	-20.0	-
	1.5	.06	.67	-	.079	.090	-	.053	-	-20.2	-
	1.8	.07	.69	-	.079	.087	-	.054	-	-18.8	-
	2.0	.08	.71	-	.080	.086	-	.057	-	-21.5	-
	2.3	.09	.72	.012	.079	.084	.039	.055	9.5	-19.3	3.5
	2.5	.10	.74	.013	.080	.081	.039	.055	8.1	-18.3	3.3
	3.8	.15	.77	.013	.075	.070	.050	.057	3.1	-12.9	-5.2
	5.1	.20	.77	.014	.060	.063	.062	.054	.1	-7.6	-5.1
	6.4	.25	.78	.014	.039	.060	.070	.054	-.0	-3.1	-3.6
	7.6	.30	.78	.013	.023	.060	.074	.055	2.1	.1	-4.9
	8.9	.35	.78	.009	.003	.064	.073	.053	5.3	1.3	-2.8
	10.2	.40	.79	.008	-.014	.069	.070	.048	9.3	.5	-1.9
	11.4	.45	.82	.001	-.023	.073	.066	.045	12.3	1.5	2.8
	12.7	.50	.84	.003	-.029	.074	.064	.042	14.0	-.4	.5
	15.2	.60	.87	-.006	-.033	.069	.061	.044	13.3	-.4	5.3
	17.8	.70	.91	-.011	-.035	.058	.056	.040	8.5	-.3	5.8
	20.3	.80	.95	-.017	-.033	.049	.046	.033	4.1	-.9	3.5
	22.9	.90	.98	-.020	-.032	.037	.043	.026	1.4	-.5	3.1
	25.4	1.00	1.00	-.021	-.030	.028	.038	.026	-.6	-.9	1.8
	27.9	1.10	1.01	-.021	-.029	.018	.033	.020	-1.7	-.9	.2
	31.8	1.25	1.02	-	-.020	.009	-	.014	-	.1	-

Table 1. - Continued.

z (mm)	y (mm)	y (in.)	$\frac{U_x}{V_\infty}$	$\frac{U_y}{V_\infty}$	$\frac{U_z}{V_\infty}$	$\frac{u'_x}{V_\infty}$	$\frac{u'_y}{V_\infty}$	$\frac{u'_z}{V_\infty}$	$-\frac{\overline{u_x u_y}}{V_\infty^2}\times 10^4$	$-\frac{\overline{u_x u_z}}{V_\infty^2}\times 10^4$	$-\frac{\overline{u_y u_z}}{V_\infty^2}\times 10^4$
33.0	.5	.02	.52	-	.071	.094	-	.055	-	-19.1	-
	.8	.03	.58	-	.080	.095	-	.057	-	-22.2	-
	1.0	.04	.62	-	.084	.091	-	.060	-	-22.7	-
	1.3	.05	.65	-	.085	.089	-	.061	-	-21.9	-
	1.5	.06	.66	-	.085	.089	-	.053	-	-22.2	-
	1.8	.07	.68	-	.084	.088	-	.055	-	-22.7	-
	2.0	.08	.71	-	.088	.080	-	.054	-	-22.1	-
	2.3	.09	.71	.013	.085	.085	.033	.054	7.7	-21.1	-6.4
	2.5	.10	.74	.012	.085	.082	.037	.055	7.1	-20.1	-8.6
	3.8	.15	.77	.011	.078	.073	.027	.050	1.4	-14.4	-8.2
	5.1	.20	.79	.010	.063	.064	.054	.053	-1.2	-7.6	-4.1
	6.4	.25	.78	.010	.042	.061	.067	.057	-.1	-3.4	-1.4
	7.6	.30	.78	.006	.020	.061	.072	.055	2.6	.1	-.7
	8.9	.35	.79	.004	-.003	.066	.069	.053	5.9	2.9	4.0
	10.2	.40	.80	.005	-.014	.069	.069	.050	9.2	1.1	1.9
	11.4	.45	.82	.003	-.023	.071	.067	.047	12.6	1.4	7.2
	12.7	.50	.82	0.000	-.029	.075	.057	.043	13.7	1.0	7.7
	15.2	.60	.88	.002	-.034	.072	.049	.038	13.4	-1.0	11.0
	17.8	.70	.92	-.004	-.035	.062	.040	.035	9.1	-1.0	6.7
	20.3	.80	.95	-.004	-.033	.048	.039	.033	4.8	-1.5	4.6
	22.9	.90	.97	-.008	-.032	.038	.033	.029	2.1	-.8	3.1
	25.4	1.00	1.00	-.007	-.030	.029	.028	.027	.2	-.2	2.1
	27.9	1.10	1.01	-.007	-.028	.019	.024	.021	-.6	.1	1.7
	31.8	1.25	1.02	-	-.020	.008	-	.010	-	.3	-

Table 1. - Continued.

z (mm)	y (mm)	y (in.)	$\frac{U_x}{V_\infty}$	$\frac{U_y}{V_\infty}$	$\frac{U_z}{V_\infty}$	$\frac{u'_x}{V_\infty}$	$\frac{u'_y}{V_\infty}$	$\frac{u'_z}{V_\infty}$	$-\frac{\overline{u_x u_y}}{V_\infty^2} \times 10^4$	$-\frac{\overline{u_x u_z}}{V_\infty^2} \times 10^4$	$-\frac{\overline{u_y u_z}}{V_\infty^2} \times 10^4$
38.5	.5	.02	.57	-	.094	.094	-	.050	-	-15.8	-
	.8	.03	.64	-	.103	.091	-	.046	-	-14.3	-
	1.0	.04	.68	-	.109	.087	-	.049	-	-14.0	-
	1.3	.05	.71	-	.106	.086	-	.043	-	-12.6	-
	1.5	.06	.74	-	.108	.081	-	.046	-	-14.0	-
	1.8	.07	.77	-	.110	.077	-	.047	-	-11.9	-
	2.0	.08	.77	-	.109	.073	-	.045	-	-10.6	-
	2.3	.09	.77	.009	.107	.071	.026	.046	6.4	-12.0	-9.1
	2.5	.10	.80	.007	.107	.067	.035	.044	4.7	-9.8	-5.8
	3.0	.15	.81	.001	.086	.059	.052	.045	.4	-7.5	-7.1
	5.1	.20	.82	-.005	.064	.058	.059	.048	.2	-5.0	-6.1
	6.4	.25	.80	-.006	.042	.062	.063	.047	1.9	-4.4	-8.0
	7.6	.30	.80	-.007	.021	.063	.068	.052	4.7	-2.8	-6.5
	8.9	.35	.80	-.008	-.007	.067	.068	.050	7.7	-2.2	-5.6
	10.2	.40	.82	-.008	-.026	.071	.063	.049	10.8	-.7	.4
	11.4	.45	.82	-.007	-.033	.073	.061	.050	12.5	-2.3	-.5
	12.7	.50	.84	-.006	-.041	.074	.056	.046	13.3	-2.8	1.0
	15.2	.60	.89	-.006	-.042	.070	.044	.040	12.3	-2.5	3.1
	17.8	.70	.94	-.007	-.039	.059	.036	.036	7.6	-1.4	4.1
	20.3	.80	.97	-.004	-.037	.047	.035	.028	4.0	-1.0	.2
	22.9	.90	.99	-.004	-.038	.033	.034	.026	2.0	-.9	1.0
	25.4	1.00	1.01	-.004	-.035	.022	.032	.021	.2	-.4	2.1
	27.9	1.10	1.02	-.004	-.032	.015	.025	.014	-.7	-.1	-.2
	31.8	1.25	1.02	-	-.018	.008	-	.014	-	-.2	-

Table 1. - Continued.

z (mm)	y (mm)	y (in.)	$\frac{U_x}{V_\infty}$	$\frac{U_y}{V_\infty}$	$\frac{U_z}{V_\infty}$	$\frac{u'_x}{V_\infty}$	$\frac{u'_y}{V_\infty}$	$\frac{u'_z}{V_\infty}$	$-\frac{\overline{u_x u_y}}{V_\infty^2} \times 10^4$	$-\frac{\overline{u_x u_z}}{V_\infty^2} \times 10^4$	$-\frac{\overline{u_y u_z}}{V_\infty^2} \times 10^4$
27.9	.5	.02	.59	-	.089	.094	-	.047	-	-12.7	-
	.8	.03	.66	-	.099	.089	-	.049	-	-12.4	-
	1.0	.04	.71	-	.103	.085	-	.048	-	-9.0	-
	1.3	.05	.73	-	.108	.081	-	.044	-	-9.3	-
	1.5	.06	.76	-	.105	.081	-	.034	-	-10.2	-
	1.8	.07	.77	-	.103	.073	-	.047	-	-7.4	-
	2.0	.08	.79	-	.102	.069	-	.048	-	-7.3	-
	2.3	.09	.80	-.010	.100	.065	.031	.041	3.3	-6.7	-4.3
	2.5	.10	.81	-.016	.099	.064	.031	.041	2.6	-9.4	-7.7
	3.8	.15	.84	-.024	.081	.055	.049	.042	-1.1	-5.5	-8.8
	5.1	.20	.83	-.029	.052	.055	.059	.048	-.7	-4.0	-7.5
	6.4	.25	.83	-.032	.036	.058	.061	.051	.9	-3.6	-5.3
	7.6	.30	.82	-.036	.013	.062	.064	.051	4.1	-3.2	-4.5
	8.9	.35	.83	-.038	-.007	.067	.059	.050	6.2	-2.6	-2.8
	10.2	.40	.85	-.039	-.028	.069	.058	.049	8.3	-2.3	-.5
	11.4	.45	.85	-.039	-.033	.070	.054	.047	10.8	-2.2	3.6
	12.7	.50	.86	-.037	-.039	.072	.045	.043	10.7	-4.5	.2
	15.2	.60	.89	-.034	-.042	.063	.045	.043	9.2	-2.9	5.2
	17.8	.70	.94	-.031	-.039	.053	.040	.035	5.8	-1.4	3.2
	20.3	.80	.98	-.030	-.038	.042	.037	.031	2.6	-1.7	1.1
	22.9	.90	.99	-.030	-.035	.030	.038	.030	.3	-1.8	1.2
	25.4	1.00	1.00	-.030	-.033	.020	.034	.021	-1.8	.3	2.4
	27.9	1.10	1.02	-.029	-.028	.013	.028	.019	-1.6	-.4	-.5
	31.8	1.25	1.02	-	-.020	.007	-	.018	-	-.1	-

Table 1. - Continued.

z (mm)	y (mm)	y (in.)	$\frac{U_x}{V_\infty}$	$\frac{U_y}{V_\infty}$	$\frac{U_z}{V_\infty}$	$\frac{u'_x}{V_\infty}$	$\frac{u'_y}{V_\infty}$	$\frac{u'_z}{V_\infty}$	$-\frac{\overline{u_x u_y}}{V_\infty^2}\times 10^4$	$-\frac{\overline{u_x u_z}}{V_\infty^2}\times 10^4$	$-\frac{\overline{u_y u_z}}{V_\infty^2}\times 10^4$
25.4	.5	.02	.61	-	.082	.095	-	.045	-	-13.9	-
	.8	.03	.67	-	.086	.089	-	.046	-	-9.0	-
	1.0	.04	.71	-	.090	.087	-	.039	-	-8.2	-
	1.3	.05	.75	-	.087	.083	-	.045	-	-8.9	-
	1.5	.06	.77	-	.088	.078	-	.042	-	-7.1	-
	1.8	.07	.80	-	.088	.073	-	.044	-	-5.2	-
	2.0	.08	.81	-	.087	.068	-	.039	-	-6.3	-
	2.3	.09	.82	-.016	.084	.062	.032	.044	1.9	-5.0	-3.2
	2.5	.10	.83	-.021	.080	.059	.038	.044	.9	-5.4	-3.6
	3.0	.15	.85	-.027	.065	.052	.048	.040	-1.0	-4.5	-6.4
	5.1	.20	.85	-.037	.046	.053	.055	.042	-.9	-3.8	-5.5
	6.4	.25	.85	-.042	.028	.056	.056	.046	.4	-3.5	-6.2
	7.6	.30	.85	-.043	.007	.061	.054	.045	2.2	-3.4	-5.4
	8.9	.35	.86	-.045	-.005	.065	.052	.047	3.9	-3.9	-4.4
	10.2	.40	.86	-.047	-.021	.067	.048	.046	5.0	-3.4	-.7
	11.4	.45	.87	-.048	-.030	.066	.047	.045	6.4	-3.5	1.2
	12.7	.50	.89	-.043	-.037	.067	.039	.044	6.4	-5.2	-1.0
	15.2	.60	.92	-.041	-.042	.058	.041	.039	5.5	-4.0	.9
	17.8	.70	.95	-.041	-.035	.048	.039	.033	3.4	-2.3	2.0
	20.3	.80	.99	-.036	-.036	.038	.036	.030	1.3	-1.4	4.3
	22.9	.90	1.00	-.034	-.037	.027	.036	.026	-.5	-1.5	1.5
	25.4	1.00	1.01	-.032	-.032	.019	.030	.020	-1.7	-.1	1.4
	27.9	1.10	1.02	-.032	-.027	.010	.029	.016	-2.2	-.4	.2
	31.8	1.25	1.02	-	-.018	.006	-	.014	-	-.0	-

Table 1. - Continued.

z (mm)	y (mm)	y (in.)	$\frac{U_x}{V_\infty}$	$\frac{U_y}{V_\infty}$	$\frac{U_z}{V_\infty}$	$\frac{u'_x}{V_\infty}$	$\frac{u'_y}{V_\infty}$	$\frac{u'_z}{V_\infty}$	$-\frac{\overline{u_x u_y}}{V_\infty^2}\times 10^4$	$-\frac{\overline{u_x u_z}}{V_\infty^2}\times 10^4$	$-\frac{\overline{u_y u_z}}{V_\infty^2}\times 10^4$
22.9	.5	.02	.63	-	.075	.089	-	.038	-	-8.6	-
	.8	.03	.78	-	.079	.091	-	.045	-	-9.5	-
	1.0	.04	.73	-	.079	.087	-	.048	-	-8.8	-
	1.3	.05	.78	-	.076	.083	-	.044	-	-9.8	-
	1.5	.06	.79	-	.076	.078	-	.042	-	-8.3	-
	1.8	.07	.81	-	.076	.072	-	.042	-	-6.5	-
	2.0	.08	.82	-	.071	.069	-	.041	-	-6.4	-
	2.3	.09	.84	-.017	.070	.064	.028	.037	2.5	-6.2	-5.2
	2.5	.10	.85	-.022	.070	.060	.032	.039	1.3	-4.9	-3.3
	3.8	.15	.86	-.033	.050	.049	.059	.040	-5.8	-3.3	-7.7
	5.1	.20	.87	-.042	.035	.050	.052	.039	-.3	-3.3	.4
	6.4	.25	.87	-.047	.018	.053	.052	.039	1.3	-3.8	-5.6
	7.6	.30	.86	-.046	.005	.056	.051	.042	2.1	-3.8	-4.2
	8.9	.35	.88	-.049	-.006	.060	.045	.040	3.2	-3.1	-1.3
	10.2	.40	.89	-.049	-.019	.060	.044	.045	4.2	-3.9	-2.2
	11.4	.45	.90	-.047	-.028	.059	.042	.043	4.4	-4.2	-2.8
	12.7	.50	.91	-.047	-.032	.058	.036	.038	4.8	-2.9	1.9
	15.2	.60	.94	-.045	-.034	.053	.030	.036	3.5	-3.6	.8
	17.8	.70	.97	-.043	-.037	.042	.037	.035	1.6	-2.5	.5
	20.3	.80	.99	-.043	-.035	.034	.034	.025	.8	-1.3	.2
	22.9	.90	1.00	-.039	-.030	.025	.032	.018	-1.3	-.1	1.1
	25.4	1.00	1.01	-.037	-.032	.014	.031	.019	-1.7	-.1	.9
	27.9	1.10	1.01	-.036	-.028	.010	.027	.016	-2.0	.1	1.0
	31.8	1.25	1.02	-	-.023	.005	-	.012	-	-.0	-

Table 1. Continued.

z (mm)	y (mm)	y (in.)	$\frac{U_x}{V_\infty}$	$\frac{U_y}{V_\infty}$	$\frac{U_z}{V_\infty}$	$\frac{u'_x}{V_\infty}$	$\frac{u'_y}{V_\infty}$	$\frac{u'_z}{V_\infty}$	$-\frac{\overline{u_x u_y}}{V_\infty^2}\times 10^4$	$-\frac{\overline{u_x u_z}}{V_\infty^2}\times 10^4$	$-\frac{\overline{u_y u_z}}{V_\infty^2}\times 10^4$
20.3	.5	.02	.63	-	.063	.098	-	.042	-	-9.0	-
	.8	.03	.71	-	.068	.096	-	.044	-	-10.4	-
	1.0	.04	.76	-	.072	.093	-	.040	-	-10.8	-
	1.3	.05	.80	-	.070	.087	-	.038	-	-9.8	-
	1.5	.06	.82	-	.066	.080	-	.039	-	-8.3	-
	1.8	.07	.83	-	.065	.073	-	.043	-	-7.9	-
	2.0	.08	.85	-	.065	.067	-	.041	-	-5.9	-
	2.3	.09	.86	-.012	.061	.063	.021	.042	1.2	-4.9	-1.1
	2.5	.10	.86	-.014	.058	.060	.023	.039	.2	-4.7	-1.2
	3.8	.15	.88	-.024	.038	.049	.041	.036	-1.3	-3.7	-3.8
	5.1	.20	.88	-.027	.022	.048	.045	.036	-.5	-3.1	-2.3
	6.4	.25	.89	-.036	.008	.049	.048	.036	.3	-2.4	-.8
	7.6	.30	.90	-.038	.002	.051	.046	.039	1.1	-3.1	-1.2
	8.9	.35	.91	-.042	-.011	.053	.043	.039	1.9	-4.0	-2.2
	10.2	.40	.92	-.039	-.021	.052	.045	.042	2.1	-3.0	.1
	11.4	.45	.93	-.040	-.029	.053	.039	.038	2.5	-3.0	-.1
	12.7	.50	.94	-.040	-.028	.052	.036	.037	2.4	-2.9	2.1
	15.2	.60	.97	-.039	-.034	.047	.035	.035	2.0	-2.5	1.8
	17.8	.70	.98	-.036	-.034	.039	.035	.029	1.0	-1.6	2.8
	20.3	.80	1.00	-.038	-.035	.031	.034	.025	-.4	-.8	3.4
	22.9	.90	1.01	-.033	-.032	.021	.031	.019	-1.1	-.2	2.6
	25.4	1.00	1.02	-.029	-.027	.012	.030	.016	-1.8	-.0	1.5
	27.9	1.10	1.02	-.028	-.027	.009	.027	.014	-2.2	.2	1.3
	31.8	1.25	1.03	-	-.025	.006	-	.012	-	-.2	-

Table 1. - Continued.

z (mm)	y (mm)	y (in.)	$\frac{U_x}{V_\infty}$	$\frac{U_y}{V_\infty}$	$\frac{U_z}{V_\infty}$	$\frac{u'_x}{V_\infty}$	$\frac{u'_y}{V_\infty}$	$\frac{u'_z}{V_\infty}$	$-\frac{\overline{u_x u_y}}{V_\infty^2}\times 10^4$	$-\frac{\overline{u_x u_z}}{V_\infty^2}\times 10^4$	$-\frac{\overline{u_y u_z}}{V_\infty^2}\times 10^4$
15.2	.5	.02	.64	-	.047	.100	-	.038	-	-8.6	-
	.8	.03	.75	-	.054	.100	-	.027	-	-10.3	-
	1.0	.04	.79	-	.054	.091	-	.037	-	-9.4	-
	1.3	.05	.84	-	.051	.084	-	.030	-	-8.4	-
	1.5	.06	.85	-	.050	.073	-	.033	-	-8.4	-
	1.8	.07	.86	-	.048	.065	-	.040	-	-5.9	-
	2.0	.08	.87	-	.046	.059	-	.037	-	-5.1	-
	2.3	.09	.88	-.016	.040	.054	.020	.035	-.1	-3.6	-.3
	2.5	.10	.88	-.018	.038	.050	.027	.036	-.3	-3.5	-.4
	3.8	.15	.90	-.025	.017	.044	.039	.032	-.6	-2.5	.3
	5.1	.20	.91	-.033	.005	.043	.041	.030	-.1	-2.3	.7
	6.4	.25	.91	-.033	.006	.044	.040	.031	.8	-2.3	.6
	7.6	.30	.92	-.036	-.013	.044	.041	.033	1.3	-1.8	1.3
	8.9	.35	.93	-.037	-.021	.044	.040	.034	1.5	-2.5	.6
	10.2	.40	.94	-.037	-.026	.044	.037	.032	1.8	-1.8	2.0
	11.4	.45	.96	-.040	-.028	.042	.038	.032	1.5	-2.0	1.5
	12.7	.50	.96	-.042	-.030	.042	.035	.031	1.5	-2.2	1.7
	15.2	.60	.97	-.041	-.029	.037	.033	.030	.7	-1.4	1.9
	17.8	.70	1.00	-.039	-.028	.032	.031	.020	-.2	-1.8	2.1
	20.3	.80	1.01	-.039	-.026	.024	.027	.015	-.9	.8	3.6
	22.9	.90	1.02	-.036	-.027	.015	.030	.017	-1.8	-.1	1.1
	25.4	1.00	1.02	-.034	-.027	.010	.027	.017	-1.9	-.1	.5
	27.9	1.10	1.02	-.033	-.025	.007	.025	.013	-2.0	-.2	.1
	31.8	1.25	1.03	-	-.025	.005	-	.013	-	-.1	-

Table 1. - Concluded.

z (mm)	y (mm)	y (in.)	$\frac{U_x}{V_\infty}$	$\frac{U_y}{V_\infty}$	$\frac{U_z}{V_\infty}$	$\frac{u'_x}{V_\infty}$	$\frac{u'_y}{V_\infty}$	$\frac{u'_z}{V_\infty}$	$-\frac{\overline{u_x u_y}}{V_\infty^2}\times 10^4$	$-\frac{\overline{u_x u_z}}{V_\infty^2}\times 10^4$	$-\frac{\overline{u_y u_z}}{V_\infty^2}\times 10^4$
10.2	.5	.02	.70	-	.023	.097	-	.024	-	-2.7	-
	.8	.03	.79	-	.028	.090	-	.025	-	-1.2	-
	1.0	.04	.84	-	.025	.075	-	.026	-	1.4	-
	1.3	.05	.87	-	.018	.067	-	.027	-	-.2	-
	1.5	.06	.88	-	.015	.060	-	.022	-	.5	-
	1.8	.07	.89	-	.009	.052	-	.030	-	1.9	-
	2.0	.08	.89	-	.012	.049	-	.032	-	1.4	-
	2.3	.09	.89	-.018	.005	.049	.020	.022	.3	1.5	2.7
	2.5	.10	.90	-.021	.002	.047	.033	.026	.7	.7	1.4
	3.0	.15	.91	-.034	-.008	.044	.037	.027	1.4	.9	3.5
	5.1	.20	.92	-.037	-.018	.043	.035	.030	1.7	.4	3.5
	6.4	.25	.94	-.043	-.023	.042	.034	.030	1.7	-.1	3.5
	7.6	.30	.95	-.040	-.025	.039	.035	.031	1.7	-1.4	1.8
	8.9	.35	.96	-.040	-.028	.037	.034	.033	1.5	-1.4	2.5
	10.2	.40	.97	-.042	-.030	.037	.032	.027	1.4	-1.4	2.1
	11.4	.45	.98	-.041	-.031	.036	.029	.026	1.2	-1.2	2.7
	12.7	.50	.99	-.036	-.031	.034	.030	.027	1.1	-1.3	1.3
	15.2	.60	1.00	-.036	-.033	.029	.028	.023	.6	-1.3	1.0
	17.8	.70	1.01	-.037	-.028	.021	.027	.023	-.1	-.3	1.5
	20.3	.80	1.02	-.031	-.030	.016	.024	.016	-.5	-.4	.6
	22.9	.90	1.02	-.029	-.030	.011	.021	.016	-.8	-.3	.4
	25.4	1.00	1.02	-.025	-.030	.009	.020	.013	-.9	-.0	.4
	27.9	1.10	1.02	-.025	-.028	.008	.018	.013	-.9	.0	.3
	31.8	1.25	1.02	-	-.030	.007	-	.014	-	.1	-

Table 2
Mean velocities and turbulence stresses in the juncture (x = 902 mm).

z (mm)	y (mm)	y (in.)	$\frac{U_x}{V_\infty}$	$\frac{U_y}{V_\infty}$	$\frac{U_z}{V_\infty}$	$\frac{u'_x}{V_\infty}$	$\frac{u'_y}{V_\infty}$	$\frac{u'_z}{V_\infty}$	$-\frac{\overline{u_x u_y}}{V_\infty^2}\times 10^4$	$-\frac{\overline{u_x u_z}}{V_\infty^2}\times 10^4$	$-\frac{\overline{u_y u_z}}{V_\infty^2}\times 10^4$
152.4	.5	.02	.46	-	-.006	.087	-	.041	-	1.1	-
	.8	.03	.51	-	-.005	.082	-	.041	-	.6	-
	1.0	.04	.53	-	-.004	.078	-	.043	-	-.2	-
	1.3	.05	.55	-	-.005	.074	-	.046	-	1.4	-
	1.5	.06	.57	-	-.004	.073	-	.046	-	-.0	-
	1.8	.07	.58	-	-.003	.072	-	.046	-	.7	-
	2.0	.08	.60	-	-.002	.072	-	.042	-	.4	-
	2.3	.09	.60	.006	-.002	.071	.051	.043	13.9	1.3	3.2
	2.5	.10	.60	.007	-.004	.070	.052	.044	13.2	.1	-.4
	3.8	.15	.64	.006	-.003	.068	.054	.046	13.7	-.4	4.5
	5.1	.20	.68	.004	-.002	.068	.053	.040	12.9	-.0	3.6
	6.4	.25	.71	.004	-.004	.067	.050	.042	12.5	.6	5.9
	7.6	.30	.74	.001	-.004	.065	.052	.043	12.3	-.3	4.2
	8.9	.35	.76	.004	-.003	.064	.050	.043	11.6	.2	4.4
	10.2	.40	.78	.004	0.000	.065	.043	.041	10.6	-1.1	3.0
	11.4	.45	.79	.003	.001	.063	.045	.041	10.3	-.8	5.7
	12.7	.50	.81	.002	0.000	.061	.046	.044	10.4	-.9	4.2
	15.2	.60	.84	.001	.001	.057	.044	.041	8.3	.0	6.9
	17.8	.70	.87	.004	.002	.053	.044	.040	7.3	-.6	4.0
	20.3	.80	.90	.004	.003	.050	.039	.035	5.8	-.4	3.5
	22.9	.90	.92	.004	.002	.044	.042	.036	4.8	.1	5.1
	25.4	1.00	.95	.001	-.002	.040	.039	.033	3.3	.0	3.0
	27.9	1.10	.96	.003	0.000	.035	.036	.032	1.9	-.4	1.3
	33.0	1.30	1.00	-	-.003	.023	-	.022	-	.0	-

Table 2. - Continued.

z (mm)	y (mm)	y (in.)	$\frac{U_x}{V_\infty}$	$\frac{U_y}{V_\infty}$	$\frac{U_z}{V_\infty}$	$\frac{u'_x}{V_\infty}$	$\frac{u'_y}{V_\infty}$	$\frac{u'_z}{V_\infty}$	$-\frac{\overline{u_x u_y}}{V_\infty^2}\times 10^4$	$-\frac{\overline{u_x u_z}}{V_\infty^2}\times 10^4$	$-\frac{\overline{u_y u_z}}{V_\infty^2}\times 10^4$
114.3	.5	.02	.44	-	-.004	.084	-	.041	-	.7	-
	.8	.03	.49	-	-.005	.078	-	.045	-	-.1	-
	1.0	.04	.51	-	-.004	.076	-	.042	-	-.1	-
	1.3	.05	.53	-	-.004	.073	-	.045	-	-.6	-
	1.5	.06	.55	-	-.004	.070	-	.040	-	.3	-
	1.8	.07	.55	-	-.003	.070	-	.044	-	-.3	-
	2.0	.08	.57	-	-.002	.068	-	.045	-	.4	-
	2.3	.09	.57	.009	-.003	.069	.054	.044	13.1	.8	3.4
	2.5	.10	.59	.006	-.003	.070	.052	.045	12.4	.1	.8
	3.8	.15	.64	.006	-.002	.068	.053	.041	13.1	1.1	4.5
	5.1	.20	.66	.008	-.002	.066	.053	.041	12.5	-.4	3.1
	6.4	.25	.68	.005	0.000	.065	.053	.043	12.7	.1	2.0
	7.6	.30	.70	.007	-.001	.066	.050	.043	12.4	-.6	2.9
	8.9	.35	.73	.008	0.000	.062	.053	.046	11.5	1.2	5.1
	10.2	.40	.75	.006	.001	.064	.046	.042	11.3	-.8	5.0
	11.4	.45	.77	.011	.001	.062	.047	.044	10.5	.7	6.3
	12.7	.50	.79	.006	0.000	.061	.047	.043	10.7	.1	6.1
	15.2	.60	.82	.011	0.000	.060	.043	.041	8.9	.2	6.5
	17.8	.70	.85	.008	-.001	.055	.046	.042	8.2	.8	4.4
	20.3	.80	.88	.011	-.003	.053	.041	.043	6.5	.8	4.4
	22.9	.90	.91	.011	.002	.048	.041	.040	5.7	1.3	7.0
	25.4	1.00	.93	.009	-.002	.046	.038	.034	4.0	.3	2.9
	27.9	1.10	.95	.010	0.000	.042	.033	.030	3.2	.2	2.8
	33.0	1.30	.99	-	-.002	.031	-	.025	-	1.1	-

Table 2. - Continued.

z (mm)	y (mm)	y (in.)	$\frac{U_x}{V_\infty}$	$\frac{U_y}{V_\infty}$	$\frac{U_z}{V_\infty}$	$\frac{u'_x}{V_\infty}$	$\frac{u'_y}{V_\infty}$	$\frac{u'_z}{V_\infty}$	$-\frac{\overline{u_x u_y}}{V_\infty^2}\times 10^4$	$-\frac{\overline{u_x u_z}}{V_\infty^2}\times 10^4$	$-\frac{\overline{u_y u_z}}{V_\infty^2}\times 10^4$
88.9	.5	.02	.44	-	-.002	.085	-	.036	-	-.6	-
	.8	.03	.47	-	-.002	.079	-	.040	-	-.4	-
	1.0	.04	.51	-	-.002	.076	-	.039	-	.7	-
	1.3	.05	.52	-	-.002	.072	-	.044	-	1.4	-
	1.5	.06	.54	-	-.002	.071	-	.042	-	-.3	-
	1.8	.07	.55	-	-.001	.069	-	.048	-	2.2	-
	2.0	.08	.57	-	-.002	.070	-	.044	-	1.2	-
	2.3	.09	.56	.005	0.000	.071	.047	.041	12.2	.1	2.0
	2.5	.10	.58	.006	0.000	.069	.052	.047	12.3	1.2	-.3
	3.8	.15	.62	.005	.002	.066	.053	.043	12.4	1.7	4.6
	5.1	.20	.65	.003	.005	.067	.050	.039	12.3	2.6	6.4
	6.4	.25	.67	.004	.004	.066	.050	.042	12.1	2.8	5.5
	7.6	.30	.69	.004	.004	.065	.049	.045	11.2	2.7	4.5
	8.9	.35	.71	.004	.002	.064	.051	.045	11.2	2.8	4.5
	10.2	.40	.73	.004	0.000	.065	.047	.043	11.1	2.5	6.5
	11.4	.45	.75	.005	-.003	.063	.049	.045	10.9	4.2	9.3
	12.7	.50	.76	.003	-.004	.064	.047	.048	10.8	4.0	6.2
	15.2	.60	.80	.004	-.003	.062	.046	.045	10.1	4.1	10.7
	17.8	.70	.83	.004	0.000	.063	.039	.042	9.8	4.2	7.9
	20.3	.80	.86	.003	-.003	.059	.043	.047	8.1	4.6	8.2
	22.9	.90	.88	.004	-.005	.059	.034	.042	6.8	4.0	5.9
	25.4	1.00	.90	.006	-.002	.054	.039	.042	6.4	3.3	8.0
	27.9	1.10	.93	.006	0.000	.050	.035	.039	4.9	3.0	5.3
	33.0	1.30	.98	-	-.005	.042	-	.027	-	1.5	-

Table 2. - Continued.

z (mm)	y (mm)	y (in.)	$\frac{U_x}{V_\infty}$	$\frac{U_y}{V_\infty}$	$\frac{U_z}{V_\infty}$	$\frac{u'_x}{V_\infty}$	$\frac{u'_y}{V_\infty}$	$\frac{u'_z}{V_\infty}$	$-\frac{\overline{u_x u_y}}{V_\infty^2} \times 10^4$	$-\frac{\overline{u_x u_z}}{V_\infty^2} \times 10^4$	$-\frac{\overline{u_y u_z}}{V_\infty^2} \times 10^4$
76.2	.5	.02	.38	-	.003	.078	-	.036	-	-.7	-
	.8	.03	.44	-	.004	.075	-	.036	-	.5	-
	1.0	.04	.46	-	.003	.073	-	.032	-	.7	-
	1.3	.05	.47	-	.005	.069	-	.039	-	1.9	-
	1.5	.06	.49	-	.007	.067	-	.039	-	.8	-
	1.8	.07	.50	-	.005	.066	-	.040	-	1.8	-
	2.0	.08	.51	-	.006	.066	-	.039	-	.3	-
	2.3	.09	.52	.006	.006	.064	.053	.039	10.7	1.4	-2.5
	2.5	.10	.52	.009	.005	.065	.052	.040	11.3	2.1	1.4
	3.8	.15	.55	.007	.008	.063	.055	.040	11.3	1.6	1.3
	5.1	.20	.59	.011	.008	.060	.060	.043	12.1	2.1	3.1
	6.4	.25	.61	.012	.006	.062	.055	.040	11.3	1.2	-1.6
	7.6	.30	.64	.016	.007	.062	.054	.038	11.5	.9	-.6
	8.9	.35	.65	.015	.006	.061	.055	.043	11.4	2.7	2.6
	10.2	.40	.67	.016	.004	.062	.055	.044	11.9	1.4	-.3
	11.4	.45	.69	.017	.004	.062	.054	.043	11.9	2.8	3.2
	12.7	.50	.70	.017	0.000	.064	.053	.039	11.8	2.7	1.3
	15.2	.60	.75	.016	-.003	.067	.049	.041	12.3	3.8	3.8
	17.8	.70	.77	.014	-.003	.066	.050	.042	12.2	4.1	5.6
	20.3	.80	.80	.014	-.001	.067	.048	.042	12.1	4.2	5.2
	22.9	.90	.83	.012	-.004	.065	.045	.040	10.8	3.3	6.4
	25.4	1.00	.86	.012	-.003	.064	.042	.041	10.8	4.6	9.4
	27.9	1.10	.89	.010	-.003	.061	.039	.040	8.8	2.5	5.8
	33.0	1.30	.94	-	-.003	.050	-	.036	-	2.3	-

Table 2. - Continued.

z (mm)	y (mm)	y (in.)	$\frac{U_x}{V_\infty}$	$\frac{U_y}{V_\infty}$	$\frac{U_z}{V_\infty}$	$\frac{u'_x}{V_\infty}$	$\frac{u'_y}{V_\infty}$	$\frac{u'_z}{V_\infty}$	$-\frac{\overline{u_x u_y}}{V_\infty^2}\times 10^4$	$-\frac{\overline{u_x u_z}}{V_\infty^2}\times 10^4$	$-\frac{\overline{u_y u_z}}{V_\infty^2}\times 10^4$
71.1	.5	.02	.40	-	.010	.079	-	.037	-	-6.7	-
	.8	.03	.45	-	.012	.072	-	.045	-	-6.8	-
	1.0	.04	.48	-	.013	.071	-	.042	-	-4.9	-
	1.3	.05	.49	-	.015	.069	-	.041	-	-4.9	-
	1.5	.06	.51	-	.014	.064	-	.045	-	-4.4	-
	1.8	.07	.51	-	.015	.066	-	.047	-	-5.6	-
	2.0	.08	.52	-	.015	.065	-	.043	-	-4.6	-
	2.3	.09	.54	.013	.016	.066	.044	.042	10.6	-6.4	-2.6
	2.5	.10	.55	.012	.015	.064	.047	.046	10.7	-6.6	-3.3
	3.8	.15	.58	.014	.010	.063	.048	.042	10.6	-7.4	-5.1
	5.1	.20	.62	.016	.018	.060	.052	.044	10.9	-6.1	-6.7
	6.4	.25	.65	.018	.018	.060	.051	.046	10.4	-6.5	-4.6
	7.6	.30	.66	.022	.014	.061	.049	.043	9.7	-5.6	-3.6
	8.9	.35	.69	.025	.012	.062	.048	.042	10.0	-6.7	-4.5
	10.2	.40	.69	.023	.004	.060	.052	.040	9.9	-4.5	-3.2
	11.4	.45	.72	.025	.006	.060	.050	.042	10.6	-3.1	-1.8
	12.7	.50	.73	.026	.003	.059	.053	.043	10.4	-2.2	-.4
	15.2	.60	.74	.023	-.003	.060	.056	.042	11.6	-.8	1.4
	17.8	.70	.78	.020	-.008	.061	.055	.046	11.7	.3	1.5
	20.3	.80	.80	.022	-.003	.062	.054	.045	11.8	1.4	2.1
	22.9	.90	.84	.018	-.004	.065	.048	.043	11.6	2.7	7.3
	25.4	1.00	.86	.016	-.005	.063	.049	.044	11.1	2.1	7.6
	27.9	1.10	.89	.014	-.006	.059	.050	.041	10.3	1.9	3.9
	33.0	1.30	.95	-	-.003	.052	-	.037	-	2.0	-

Table 2. - Continued.

z (mm)	y (mm)	y (in.)	$\frac{U_x}{V_\infty}$	$\frac{U_y}{V_\infty}$	$\frac{U_z}{V_\infty}$	$\frac{u'_x}{V_\infty}$	$\frac{u'_y}{V_\infty}$	$\frac{u'_z}{V_\infty}$	$-\frac{\overline{u_x u_y}}{V_\infty^2} \times 10^4$	$-\frac{\overline{u_x u_z}}{V_\infty^2} \times 10^4$	$-\frac{\overline{u_y u_z}}{V_\infty^2} \times 10^4$
66.0	.5	.02	.44	-	.019	.083	-	.037	-	-8.3	-
	.8	.03	.49	-	.022	.079	-	.042	-	-7.9	-
	1.0	.04	.52	-	.024	.076	-	.041	-	-7.2	-
	1.3	.05	.54	-	.024	.072	-	.044	-	-7.9	-
	1.5	.06	.54	-	.024	.070	-	.046	-	-7.7	-
	1.8	.07	.56	-	.026	.069	-	.044	-	-8.3	-
	2.0	.08	.58	-	.027	.067	-	.045	-	-8.6	-
	2.3	.09	.57	.015	.028	.068	.041	.045	11.0	-9.3	-.4
	2.5	.10	.59	.009	.029	.068	.039	.043	10.7	-9.6	-1.0
	3.0	.15	.63	.015	.032	.066	.043	.041	10.0	-9.6	1.4
	5.1	.20	.67	.017	.034	.064	.044	.044	9.5	-11.2	-1.5
	6.4	.25	.68	.021	.032	.064	.044	.043	9.2	-10.0	-3.4
	7.6	.30	.71	.026	.030	.061	.048	.045	7.8	-10.2	1.1
	8.9	.35	.73	.026	.025	.062	.044	.044	7.5	-10.0	.8
	10.2	.40	.74	.029	.019	.062	.043	.042	7.1	-9.4	-4.6
	11.4	.45	.75	.028	.016	.060	.047	.044	6.9	-8.9	-1.9
	12.7	.50	.75	.026	.013	.059	.045	.041	7.5	-7.4	1.4
	15.2	.60	.78	.023	.004	.055	.053	.047	8.0	-4.8	-1.8
	17.8	.70	.80	.024	-.004	.057	.051	.044	9.1	-3.5	-.4
	20.3	.80	.83	.021	-.004	.057	.053	.048	10.5	-1.1	2.5
	22.9	.90	.84	.020	0.000	.060	.049	.044	10.6	-.1	4.1
	25.4	1.00	.86	.018	-.002	.060	.049	.043	10.5	.6	4.8
	27.9	1.10	.89	.014	-.002	.057	.051	.044	10.1	.7	6.0
	33.0	1.30	.94	-	-.002	.053	-	.037	-	.6	-

Table 2. - Continued.

z (mm)	y (mm)	y (in.)	$\frac{U_x}{V_\infty}$	$\frac{U_y}{V_\infty}$	$\frac{U_z}{V_\infty}$	$\frac{u'_x}{V_\infty}$	$\frac{u'_y}{V_\infty}$	$\frac{u'_z}{V_\infty}$	$-\frac{\overline{u_x u_y}}{V_\infty^2}\times 10^4$	$-\frac{\overline{u_x u_z}}{V_\infty^2}\times 10^4$	$-\frac{\overline{u_y u_z}}{V_\infty^2}\times 10^4$
61.0	.5	.02	.48	-	.023	.087	-	.039	-	-10.1	-
	.8	.03	.53	-	.025	.081	-	.043	-	-7.7	-
	1.0	.04	.56	-	.027	.076	-	.045	-	-6.9	-
	1.3	.05	.58	-	.028	.074	-	.047	-	-7.4	-
	1.5	.06	.59	-	.030	.072	-	.045	-	-8.9	-
	1.8	.07	.62	-	.032	.071	-	.046	-	-9.6	-
	2.0	.08	.61	-	.030	.069	-	.047	-	-6.5	-
	2.3	.09	.62	.011	.030	.070	.046	.044	11.0	-7.2	4.9
	2.5	.10	.63	.014	.033	.068	.049	.048	11.3	-8.2	2.4
	3.8	.15	.69	.014	.037	.067	.047	.041	9.8	-8.4	3.9
	5.1	.20	.70	.015	.037	.063	.053	.045	9.0	-9.0	3.7
	6.4	.25	.74	.017	.036	.063	.047	.035	7.5	-8.1	3.4
	7.6	.30	.77	.019	.034	.060	.052	.039	6.3	-9.3	3.7
	8.9	.35	.78	.021	.030	.058	.052	.042	5.9	-9.4	2.5
	10.2	.40	.80	.022	.025	.057	.049	.038	5.3	-10.0	2.1
	11.4	.45	.79	.023	.010	.056	.050	.042	4.4	-9.5	.5
	12.7	.50	.80	.024	.015	.055	.048	.041	4.5	-7.7	2.1
	15.2	.60	.81	.024	.004	.054	.049	.041	5.2	-6.1	1.1
	17.8	.70	.83	.023	0.000	.053	.051	.044	6.0	-4.7	2.4
	20.3	.80	.84	.020	-.003	.053	.052	.043	8.4	-3.0	1.7
	22.9	.90	.86	.021	-.003	.056	.051	.041	9.4	-1.8	3.7
	25.4	1.00	.88	.016	-.002	.056	.052	.044	9.7	-.8	4.1
	27.9	1.10	.90	.012	-.003	.055	.051	.044	9.2	-.3	4.2
	33.0	1.30	.96	-	0.000	.051	-	.037	-	.0	-

Table 2. - Continued.

z (mm.)	y (mm)	y (in.)	$\frac{U_x}{V_\infty}$	$\frac{U_y}{V_\infty}$	$\frac{U_z}{V_\infty}$	$\frac{u'_x}{V_\infty}$	$\frac{u'_y}{V_\infty}$	$\frac{u'_z}{V_\infty}$	$-\frac{\overline{u_x u_y}}{V_\infty^2}\times 10^4$	$-\frac{\overline{u_x u_z}}{V_\infty^2}\times 10^4$	$-\frac{\overline{u_y u_z}}{V_\infty^2}\times 10^4$
55.9	.5	.02	.51	-	.026	.086	-	.048	-	-10.0	-
	.8	.03	.55	-	.029	.082	-	.048	-	-7.2	-
	1.0	.04	.59	-	.033	.079	-	.045	-	-5.8	-
	1.3	.05	.61	-	.033	.076	-	.044	-	-6.5	-
	1.5	.06	.62	-	.035	.072	-	.050	-	-4.9	-
	1.8	.07	.64	-	.035	.073	-	.047	-	-5.9	-
	2.0	.08	.67	-	.036	.072	-	.046	-	-6.1	-
	2.3	.09	.68	.011	.036	.071	.044	.044	12.1	-5.0	5.9
	2.5	.10	.68	.008	.038	.070	.045	.042	11.7	-4.4	6.1
	3.8	.15	.72	.011	.041	.066	.045	.039	10.3	-6.8	6.0
	5.1	.20	.76	.012	.044	.061	.051	.042	8.5	-5.8	3.5
	6.4	.25	.79	.014	.043	.058	.058	.035	7.2	-5.7	5.3
	7.6	.30	.81	.012	.038	.054	.049	.040	4.9	-7.3	4.5
	8.9	.35	.82	.010	.033	.050	.052	.042	3.9	-6.8	1.5
	10.2	.40	.85	.014	.027	.052	.048	.038	3.3	-7.5	1.5
	11.4	.45	.84	.017	.023	.051	.046	.036	2.1	-7.3	.7
	12.7	.50	.85	.017	.010	.049	.048	.037	2.7	-7.3	-.8
	15.2	.60	.84	.016	.007	.049	.048	.039	2.9	-6.8	1.9
	17.8	.70	.85	.016	.003	.048	.049	.040	4.3	-5.0	3.8
	20.3	.80	.87	.014	-.002	.050	.049	.041	5.9	-4.1	5.3
	22.9	.90	.88	.009	-.002	.053	.046	.039	7.7	-3.0	3.5
	25.4	1.00	.89	.014	-.002	.052	.049	.039	7.8	-1.8	6.3
	27.9	1.10	.91	.009	-.003	.053	.048	.040	7.9	-1.4	6.2
	33.0	1.30	.97	-	-.003	.048	-	.036	-	-1.5	-

Table 2. - Continued.

z (mm)	y (mm)	y (in.)	$\frac{U_x}{V_\infty}$	$\frac{U_y}{V_\infty}$	$\frac{U_z}{V_\infty}$	$\frac{u'_x}{V_\infty}$	$\frac{u'_y}{V_\infty}$	$\frac{u'_z}{V_\infty}$	$-\frac{\overline{u_x u_y}}{V_\infty^2} \times 10^4$	$-\frac{\overline{u_x u_z}}{V_\infty^2} \times 10^4$	$-\frac{\overline{u_y u_z}}{V_\infty^2} \times 10^4$
50.8	.5	.02	.54	-	.030	.089	-	.046	-	-6.8	-
	.8	.03	.50	-	.032	.083	-	.046	-	-5.9	-
	1.0	.04	.62	-	.039	.078	-	.052	-	-5.6	-
	1.3	.05	.64	-	.039	.077	-	.047	-	-5.2	-
	1.5	.06	.66	-	.039	.075	-	.048	-	-3.6	-
	1.8	.07	.67	-	.041	.073	-	.049	-	-3.7	-
	2.0	.08	.69	-	.043	.071	-	.047	-	-4.3	-
	2.3	.09	.69	.008	.045	.070	.046	.048	13.1	-4.4	3.5
	2.5	.10	.70	.010	.045	.068	.048	.049	12.8	-4.0	3.7
	3.8	.15	.75	.007	.050	.066	.044	.041	10.8	-4.6	4.9
	5.1	.20	.79	.007	.050	.059	.048	.041	8.6	-4.3	3.2
	6.4	.25	.81	.008	.047	.053	.048	.041	6.5	-4.1	3.6
	7.6	.30	.84	.007	.047	.050	.045	.038	4.3	-4.7	1.6
	8.9	.35	.86	.002	.041	.048	.043	.036	2.9	-4.5	1.8
	10.2	.40	.87	.005	.038	.046	.044	.036	1.9	-5.5	1.5
	11.4	.45	.88	.000	.028	.043	.046	.040	1.0	-6.2	-.9
	12.7	.50	.88	.000	.018	.044	.045	.039	.6	-5.8	.2
	15.2	.60	.88	.003	.011	.044	.046	.039	1.4	-4.9	.8
	17.8	.70	.89	.005	.005	.044	.048	.041	2.8	-5.8	1.5
	20.3	.80	.88	.008	.002	.047	.046	.039	4.6	-3.9	3.4
	22.9	.90	.89	.005	-.003	.048	.047	.039	5.5	-3.5	3.6
	25.4	1.00	.90	.005	-.005	.049	.048	.039	6.6	-2.3	4.8
	27.9	1.10	.93	.003	-.003	.049	.048	.040	6.3	-3.8	2.6
	33.0	1.30	.96	-	-.003	.045	-	.034	-	-.8	-

Table 2. - Continued.

z (mm)	y (mm)	y (in.)	$\frac{U_x}{V_\infty}$	$\frac{U_y}{V_\infty}$	$\frac{U_z}{V_\infty}$	$\frac{u'_x}{V_\infty}$	$\frac{u'_y}{V_\infty}$	$\frac{u'_z}{V_\infty}$	$-\frac{\overline{u_x u_y}}{V_\infty^2} \times 10^4$	$-\frac{\overline{u_x u_z}}{V_\infty^2} \times 10^4$	$-\frac{\overline{u_y u_z}}{V_\infty^2} \times 10^4$
45.7	.5	.02	.54	-	.026	.092	-	.045	-	-7.7	-
	.8	.03	.60	-	.030	.086	-	.046	-	-5.5	-
	1.0	.04	.62	-	.031	.080	-	.050	-	-3.8	-
	1.3	.05	.65	-	.034	.078	-	.048	-	-3.7	-
	1.5	.06	.66	-	.036	.076	-	.047	-	-2.0	-
	1.8	.07	.68	-	.036	.074	-	.051	-	-3.2	-
	2.0	.08	.70	-	.038	.072	-	.050	-	-2.9	-
	2.3	.09	.70	.009	.037	.071	.046	.049	13.7	-2.1	3.2
	2.5	.10	.72	.010	.040	.071	.045	.045	13.5	-3.3	4.9
	3.8	.15	.77	.006	.044	.065	.046	.045	11.5	-2.8	4.2
	5.1	.20	.81	.003	.044	.059	.045	.040	9.2	-2.8	2.4
	6.4	.25	.84	.005	.041	.054	.044	.040	6.7	-2.9	2.3
	7.6	.30	.87	.003	.041	.049	.042	.034	4.4	-2.9	2.7
	8.9	.35	.88	.003	.032	.045	.041	.038	2.8	-3.3	2.4
	10.2	.40	.91	.003	.029	.042	.043	.037	1.2	-3.9	.6
	11.4	.45	.90	.003	.027	.042	.043	.035	.3	-4.5	2.1
	12.7	.50	.91	.005	.027	.042	.041	.036	.2	-4.0	-.2
	15.2	.60	.92	.005	.014	.041	.044	.038	.3	-4.5	1.2
	17.8	.70	.91	.002	.002	.042	.046	.040	1.0	-5.1	.9
	20.3	.80	.91	.002	-.005	.042	.048	.042	3.1	-4.0	2.6
	22.9	.90	.92	.003	-.008	.044	.047	.037	4.4	-3.2	3.8
	25.4	1.00	.93	.001	-.008	.045	.047	.036	4.9	-2.2	4.8
	27.9	1.10	.94	.003	-.007	.045	.045	.036	4.8	-3.0	3.6
	33.0	1.30	.98	-	-.002	.042	-	.038	-	-1.2	-

Table 2. - Continued.

z (mm)	y (mm)	y (in.)	$\frac{U_x}{V_\infty}$	$\frac{U_y}{V_\infty}$	$\frac{U_z}{V_\infty}$	$\frac{u'_x}{V_\infty}$	$\frac{u'_y}{V_\infty}$	$\frac{u'_z}{V_\infty}$	$-\frac{\overline{u_x u_y}}{V_\infty^2}\times 10^4$	$-\frac{\overline{u_x u_z}}{V_\infty^2}\times 10^4$	$-\frac{\overline{u_y u_z}}{V_\infty^2}\times 10^4$
40.6	.5	.02	.55	-	.021	.093	-	.046	-	-6.2	-
	.8	.03	.60	-	.025	.085	-	.052	-	-4.1	-
	1.0	.04	.64	-	.026	.081	-	.053	-	-2.9	-
	1.3	.05	.65	-	.027	.078	-	.053	-	-1.8	-
	1.5	.06	.68	-	.028	.076	-	.048	-	-1.9	-
	1.8	.07	.69	-	.030	.075	-	.049	-	-2.6	-
	2.0	.08	.70	-	.029	.073	-	.051	-	-1.5	-
	2.3	.09	.72	.004	.030	.075	.038	.044	14.1	-1.6	5.1
	2.5	.10	.74	.005	.034	.073	.042	.047	13.7	-1.7	4.6
	3.8	.15	.77	.001	.036	.068	.041	.041	11.6	-1.9	5.4
	5.1	.20	.83	.001	.039	.062	.041	.041	9.4	-2.7	1.2
	6.4	.25	.87	-.003	.038	.054	.043	.042	7.0	-1.5	3.8
	7.6	.30	.89	-.002	.036	.049	.040	.037	4.9	-2.2	1.3
	8.9	.35	.91	-.003	.033	.045	.038	.036	2.3	-2.5	2.0
	10.2	.40	.93	-.004	.029	.040	.041	.036	.9	-3.2	.4
	11.4	.45	.93	-.004	.026	.038	.041	.036	.2	-4.5	-.8
	12.7	.50	.93	-.003	.021	.039	.041	.035	-.1	-3.7	1.0
	15.2	.60	.94	-.004	.013	.039	.040	.034	.4	-4.1	.6
	17.8	.70	.94	-.003	.005	.041	.041	.034	1.3	-3.8	3.6
	20.3	.80	.94	-.000	0.000	.042	.042	.033	2.0	-4.0	1.0
	22.9	.90	.95	-.005	-.002	.040	.044	.036	2.8	-3.4	3.6
	25.4	1.00	.96	-.007	-.005	.042	.043	.033	3.2	-2.9	3.0
	27.9	1.10	.97	-.003	-.005	.040	.043	.032	3.2	-2.0	3.5
	33.0	1.30	.99	-	-.002	.033	-	.028	-	-1.3	-

Table 2. - Continued.

z (mm.)	y (mm)	y (in.)	$\frac{U_x}{V_\infty}$	$\frac{U_y}{V_\infty}$	$\frac{U_z}{V_\infty}$	$\frac{u'_x}{V_\infty}$	$\frac{u'_y}{V_\infty}$	$\frac{u'_z}{V_\infty}$	$-\frac{\overline{u_x u_y}}{V_\infty^2} \times 10^4$	$-\frac{\overline{u_x u_z}}{V_\infty^2} \times 10^4$	$-\frac{\overline{u_y u_z}}{V_\infty^2} \times 10^4$
35.6	.5	.02	.56	-	.018	.092	-	.050	-	-3.2	-
	.8	.03	.60	-	.018	.087	-	.048	-	-2.3	-
	1.0	.04	.63	-	.020	.083	-	.049	-	-2.6	-
	1.3	.05	.66	-	.022	.078	-	.051	-	-1.2	-
	1.5	.06	.68	-	.025	.077	-	.051	-	-.7	-
	1.8	.07	.69	-	.025	.076	-	.053	-	-1.0	-
	2.0	.08	.71	-	.027	.075	-	.050	-	-.8	-
	2.3	.09	.72	.008	.029	.074	.044	.049	14.9	-1.4	3.2
	2.5	.10	.73	.003	.028	.073	.044	.048	14.5	-.5	4.2
	3.8	.15	.78	.002	.033	.069	.042	.043	12.7	-.7	5.5
	5.1	.20	.84	-.003	.035	.063	.043	.043	10.2	-.9	6.3
	6.4	.25	.87	-.001	.038	.057	.040	.039	8.8	-1.8	1.4
	7.6	.30	.90	-.002	.028	.051	.037	.038	5.5	-.6	4.0
	8.9	.35	.92	-.004	.026	.044	.037	.037	3.3	-1.2	3.5
	10.2	.40	.93	-.003	.023	.039	.038	.036	1.6	-2.5	1.3
	11.4	.45	.95	-.004	.020	.037	.037	.034	.6	-3.0	-.6
	12.7	.50	.95	-.005	.020	.035	.038	.032	.0	-3.5	-.0
	15.2	.60	.96	-.005	.012	.035	.038	.032	.1	-3.4	.8
	17.8	.70	.95	-.006	.008	.036	.039	.032	.7	-3.4	.8
	20.3	.80	.97	-.006	.005	.036	.040	.033	1.3	-3.4	1.3
	22.9	.90	.97	-.007	.002	.036	.039	.032	1.7	-2.7	1.3
	25.4	1.00	.98	-.008	.002	.036	.039	.029	1.7	-2.1	2.9
	27.9	1.10	.99	-.004	0.000	.033	.039	.030	1.5	-2.1	1.7
	33.0	1.30	1.00	-	.002	.025	-	.023	-	-1.1	-

Table 2. - Continued.

z (mm)	y (mm)	y (in.)	$\frac{U_x}{V_\infty}$	$\frac{U_y}{V_\infty}$	$\frac{U_z}{V_\infty}$	$\frac{u'_x}{V_\infty}$	$\frac{u'_y}{V_\infty}$	$\frac{u'_z}{V_\infty}$	$-\frac{\overline{u_x u_y}}{V_\infty^2}\times 10^4$	$-\frac{\overline{u_x u_z}}{V_\infty^2}\times 10^4$	$-\frac{\overline{u_y u_z}}{V_\infty^2}\times 10^4$
30.5	.5	.02	.56	-	.014	.094	-	.046	-	-3.6	-
	.8	.03	.61	-	.015	.087	-	.050	-	-.7	-
	1.0	.04	.63	-	.015	.082	-	.050	-	-.1	-
	1.3	.05	.66	-	.018	.079	-	.052	-	-.9	-
	1.5	.06	.67	-	.020	.078	-	.049	-	-.2	-
	1.8	.07	.69	-	.020	.078	-	.049	-	-.1	-
	2.0	.08	.70	-	.022	.075	-	.054	-	-1.4	-
	2.3	.09	.72	.005	.023	.075	.045	.049	15.2	-.2	4.6
	2.5	.10	.73	.005	.024	.073	.047	.050	14.7	.6	7.0
	3.8	.15	.79	.001	.028	.070	.045	.045	13.3	.0	7.4
	5.1	.20	.83	-.002	.028	.066	.041	.044	11.1	-.9	3.4
	6.4	.25	.86	-.003	.026	.058	.044	.044	9.0	-.7	3.9
	7.6	.30	.90	-.003	.024	.054	.034	.039	6.2	-1.4	1.9
	8.9	.35	.92	-.007	.021	.046	.035	.036	3.7	-.9	3.0
	10.2	.40	.95	-.006	.020	.040	.037	.033	2.4	-1.3	1.7
	11.4	.45	.95	-.007	.017	.036	.034	.030	.9	-1.8	1.8
	12.7	.50	.97	-.011	.015	.033	.035	.030	.2	-1.7	2.1
	15.2	.60	.97	-.010	.012	.031	.036	.029	-.2	-2.4	1.5
	17.8	.70	.97	-.010	.008	.031	.037	.029	.3	-2.4	1.5
	20.3	.80	.98	-.009	.007	.031	.036	.029	.4	-2.1	1.6
	22.9	.90	.99	-.010	.005	.030	.035	.026	.5	-1.7	2.0
	25.4	1.00	.99	-.008	.005	.029	.034	.024	.4	-1.9	1.2
	27.9	1.10	1.00	-.007	.005	.026	.034	.024	.2	-1.4	1.9
	33.0	1.30	1.01	-	.005	.018	-	.021	-	-.4	-

Table 2. - Continued.

z (mm.)	y (mm)	y (in.)	$\frac{U_x}{V_\infty}$	$\frac{U_y}{V_\infty}$	$\frac{U_z}{V_\infty}$	$\frac{u'_x}{V_\infty}$	$\frac{u'_y}{V_\infty}$	$\frac{u'_z}{V_\infty}$	$-\frac{\overline{u_x u_y}}{V_\infty^2}\times 10^4$	$-\frac{\overline{u_x u_z}}{V_\infty^2}\times 10^4$	$-\frac{\overline{u_y u_z}}{V_\infty^2}\times 10^4$
25.4	.5	.02	.55	-	.010	.092	-	.053	-	-3.1	-
	.8	.03	.60	-	.012	.087	-	.049	-	-2.1	-
	1.0	.04	.62	-	.012	.081	-	.055	-	-.5	-
	1.3	.05	.65	-	.014	.080	-	.049	-	.3	-
	1.5	.06	.67	-	.015	.076	-	.053	-	1.1	-
	1.8	.07	.68	-	.015	.076	-	.053	-	.4	-
	2.0	.08	.70	-	.017	.075	-	.050	-	.2	-
	2.3	.09	.71	.006	.015	.074	.049	.053	16.0	.6	5.3
	2.5	.10	.72	.006	.019	.072	.050	.054	15.6	1.5	8.3
	3.8	.15	.78	.002	.020	.071	.043	.044	13.7	.9	8.0
	5.1	.20	.82	0.000	.020	.066	.044	.046	11.9	.4	6.4
	6.4	.25	.86	.002	.020	.062	.040	.042	9.7	-.0	5.9
	7.6	.30	.90	-.004	.017	.056	.033	.039	7.1	1.0	7.0
	8.9	.35	.92	-.001	.014	.049	.030	.036	4.7	-.2	2.7
	10.2	.40	.95	-.005	.015	.041	.032	.033	2.7	-.5	4.2
	11.4	.45	.96	-.005	.012	.034	.034	.034	1.4	-1.9	.6
	12.7	.50	.97	-.007	.010	.031	.032	.030	.2	-1.3	1.6
	15.2	.60	1.00	-.007	.010	.027	.033	.030	-.3	-1.1	1.7
	17.8	.70	1.01	-.008	.007	.025	.033	.028	-.2	-1.2	1.5
	20.3	.80	1.00	-.007	.007	.025	.031	.024	-.2	-.9	2.2
	22.9	.90	1.01	-.007	.009	.021	.033	.023	-.4	-.8	1.8
	25.4	1.00	1.02	-.005	.009	.019	.030	.022	-.1	-.4	3.6
	27.9	1.10	1.02	-.007	.009	.017	.028	.021	-.6	-.6	.8
	33.0	1.30	1.02	-	.009	.013	-	.018	-	-.0	-

Table 2. - Concluded.

z (mm)	y (mm)	y (in.)	$\frac{U_x}{V_\infty}$	$\frac{U_y}{V_\infty}$	$\frac{U_z}{V_\infty}$	$\frac{u'_x}{V_\infty}$	$\frac{u'_y}{V_\infty}$	$\frac{u'_z}{V_\infty}$	$-\frac{\overline{u_x u_y}}{V_\infty^2} \times 10^4$	$-\frac{\overline{u_x u_z}}{V_\infty^2} \times 10^4$	$-\frac{\overline{u_y u_z}}{V_\infty^2} \times 10^4$
15.2	.5	.02	.52	-	.003	.089	-	.049	-	-2.3	-
	.8	.03	.57	-	.002	.084	-	.050	-	-.3	-
	1.0	.04	.60	-	.003	.080	-	.049	-	1.1	-
	1.3	.05	.62	-	.001	.077	-	.053	-	1.6	-
	1.5	.06	.63	-	-.002	.076	-	.049	-	2.1	-
	1.8	.07	.65	-	-.005	.075	-	.050	-	2.3	-
	2.0	.08	.67	-	-.008	.074	-	.050	-	2.4	-
	2.3	.09	.67	.005	-.007	.073	.053	.049	17.0	2.3	5.6
	2.5	.10	.69	.004	-.010	.074	.051	.046	16.7	2.1	6.0
	3.0	.15	.74	.002	-.013	.070	.052	.046	15.5	3.1	4.7
	5.1	.20	.79	.001	-.021	.066	.050	.043	13.6	4.1	6.9
	6.4	.25	.82	-.003	-.023	.061	.047	.042	10.7	3.6	5.4
	7.6	.30	.85	-.001	-.021	.056	.043	.038	8.1	4.5	7.2
	8.9	.35	.89	-.006	-.019	.052	.038	.035	4.0	5.0	7.7
	10.2	.40	.90	-.007	-.016	.048	.036	.036	2.7	5.7	6.8
	11.4	.45	.91	-.007	-.013	.047	.033	.035	.9	5.6	6.9
	12.7	.50	.91	-.010	-.013	.048	.028	.034	.1	6.7	8.0
	15.2	.60	.92	-.008	-.008	.050	.027	.035	-.5	7.2	6.9
	17.8	.70	.92	-.007	-.005	.051	.022	.033	-.4	7.6	7.4
	20.3	.80	.93	-.006	-.003	.050	.024	.033	-.5	7.2	7.1
	22.9	.90	.93	-.007	-.003	.048	.026	.033	-.4	6.8	5.9
	25.4	1.00	.93	-.004	-.003	.048	.024	.034	-.7	6.9	6.1
	27.9	1.10	.94	-.004	-.005	.047	.023	.033	-1.0	6.5	5.3
	33.0	1.30	.94	-	-.003	.045	-	.032	-	6.3	-

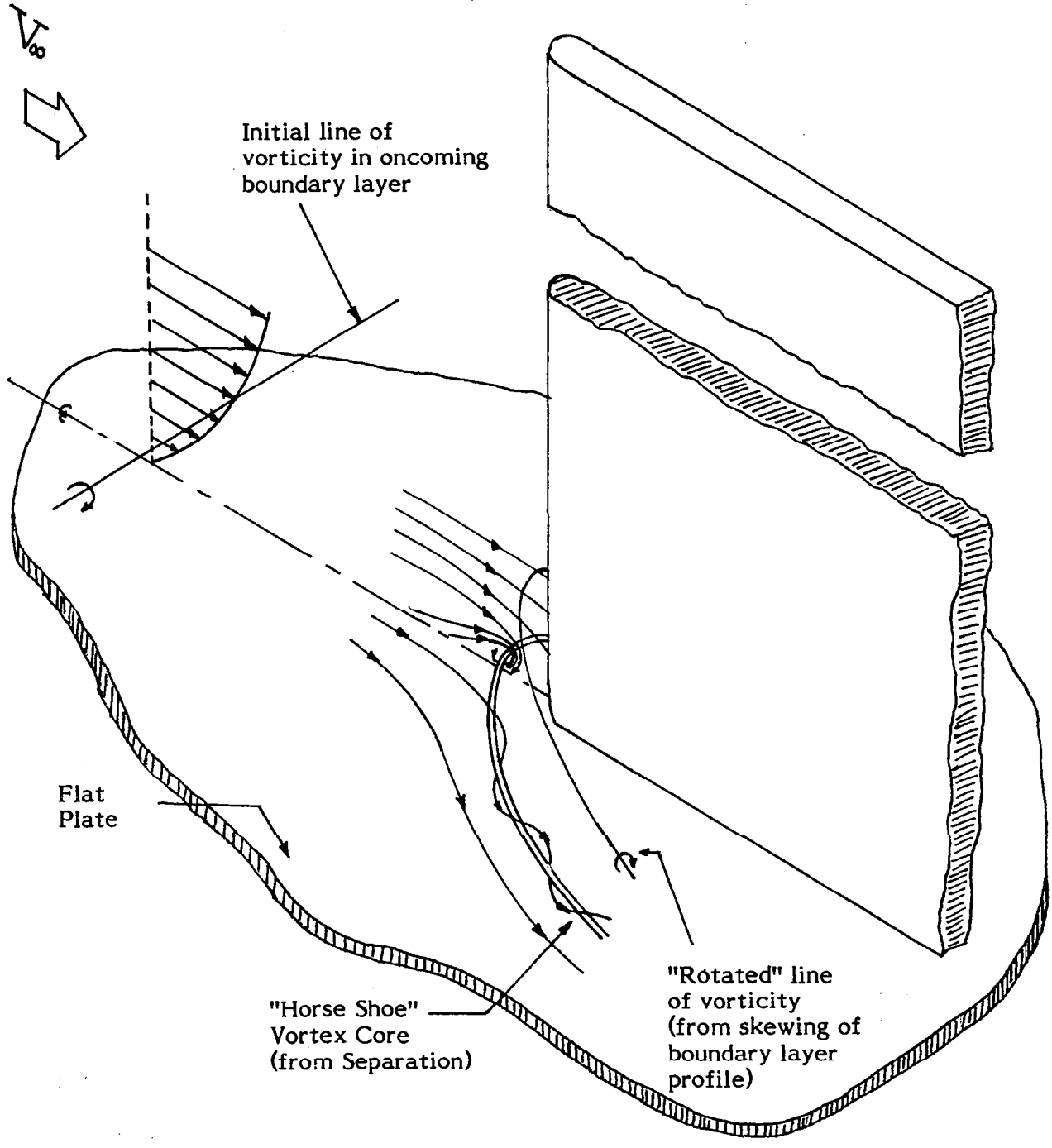

Figure 1. - Schematic of the flow in a juncture .

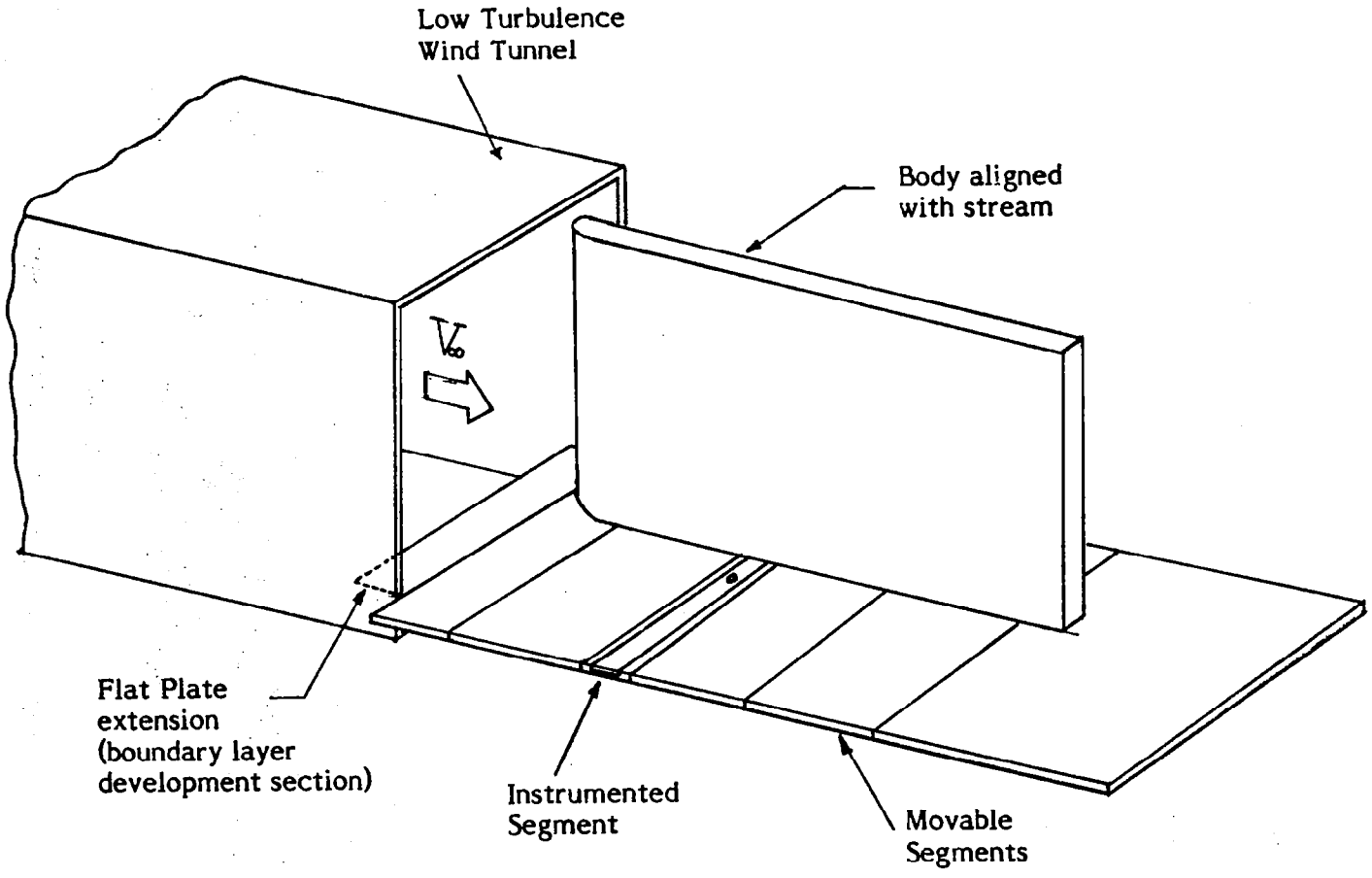

Figure 2. - Flat Plate and body at the exit of the wind tunnel.

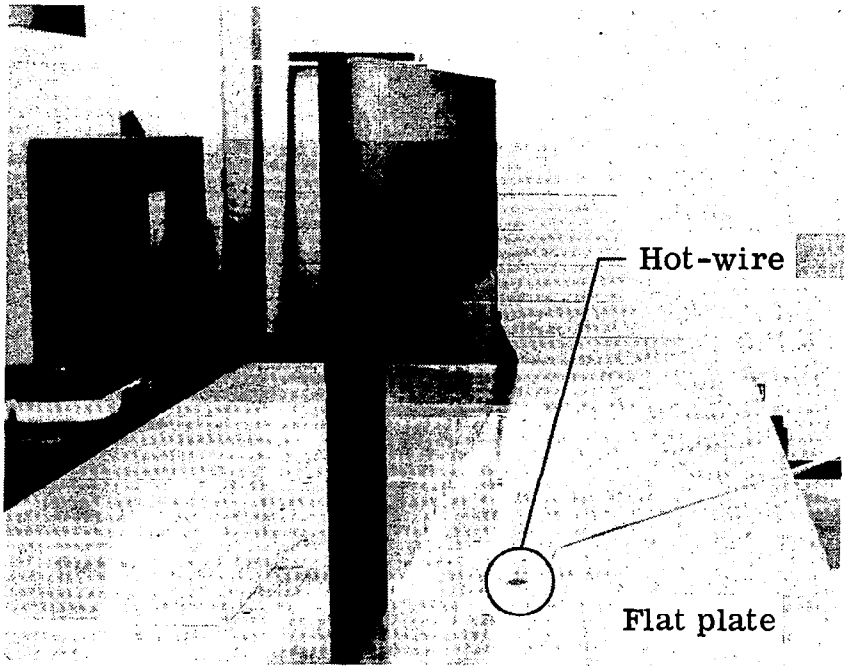

(a) View looking downstream

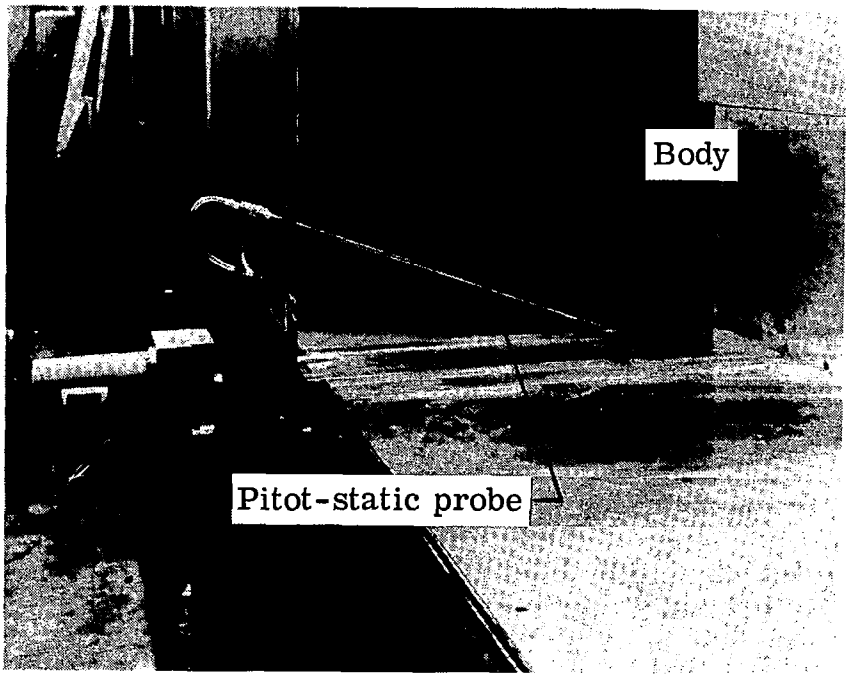

(b) View looking upstream

Figure 3.- Experimental set-up.

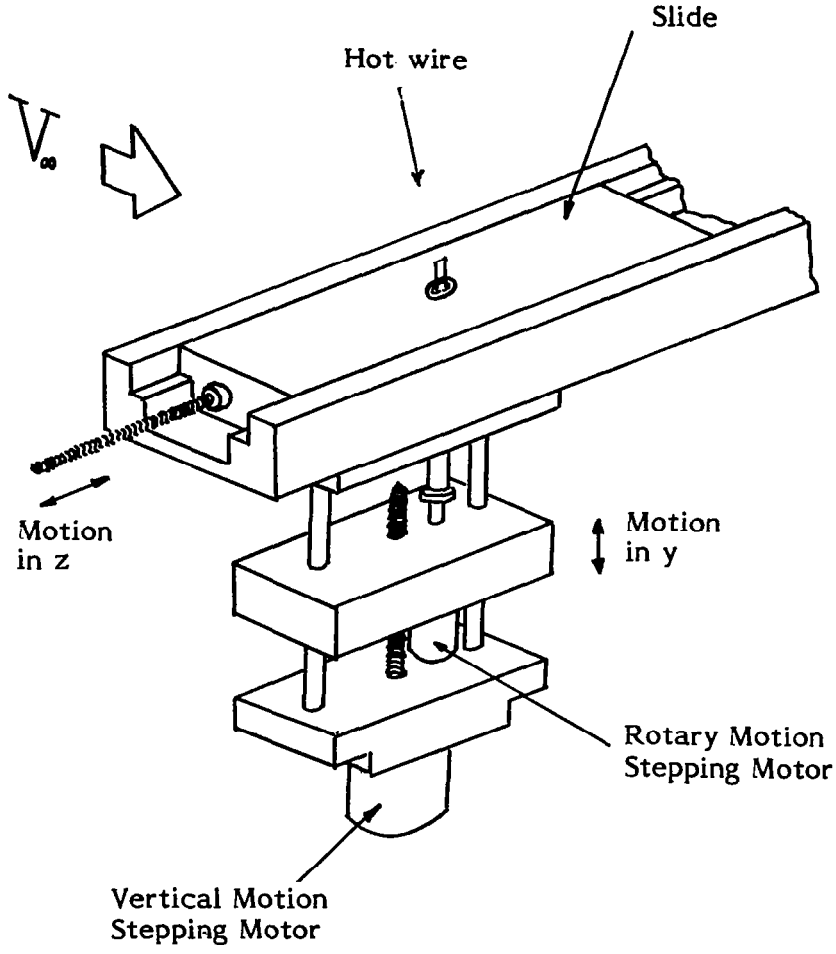

Figure 4. - Details of instrumented segment.

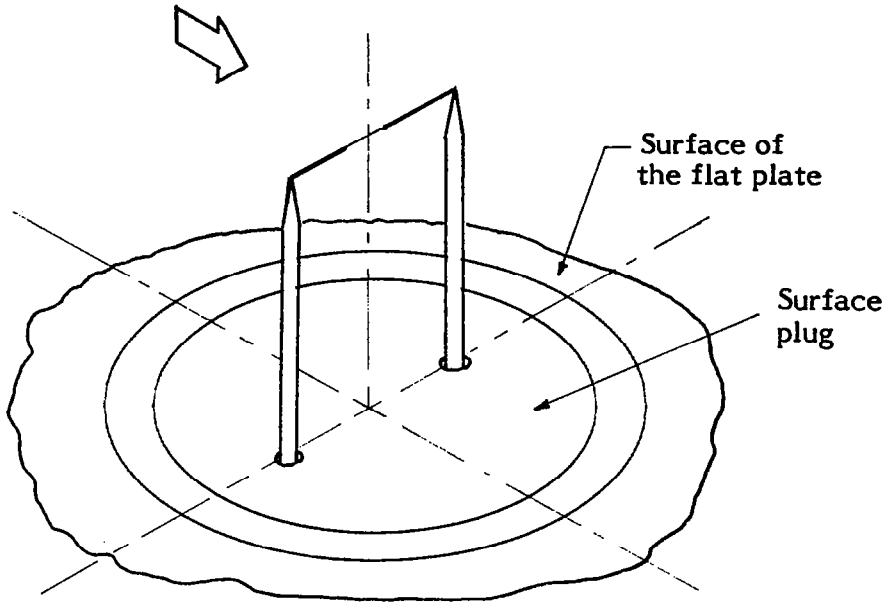

(a) Horizontal wire.

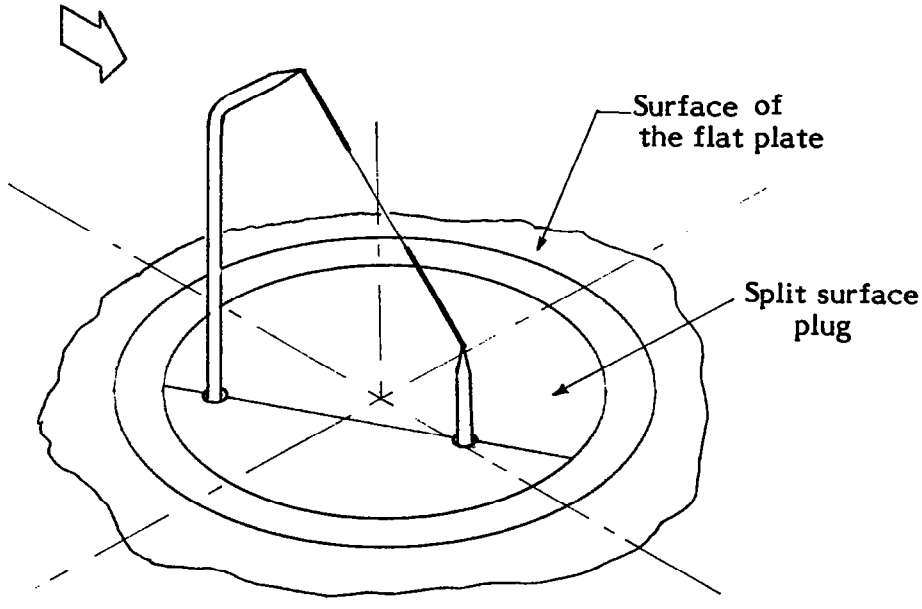

(b) Slant wire.

Figure 5. Details of hot wires.

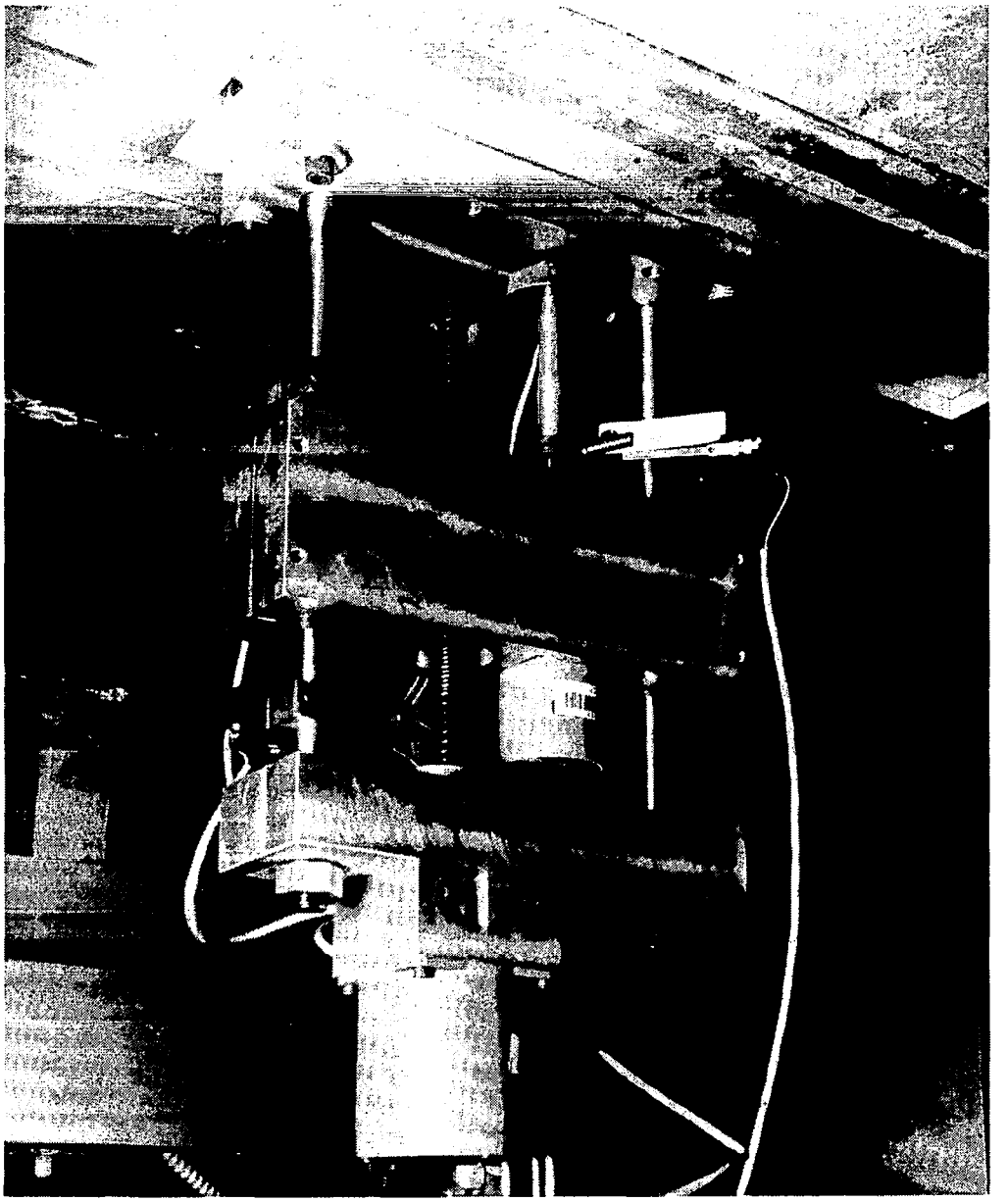

Figure 6.- Probe actuator.

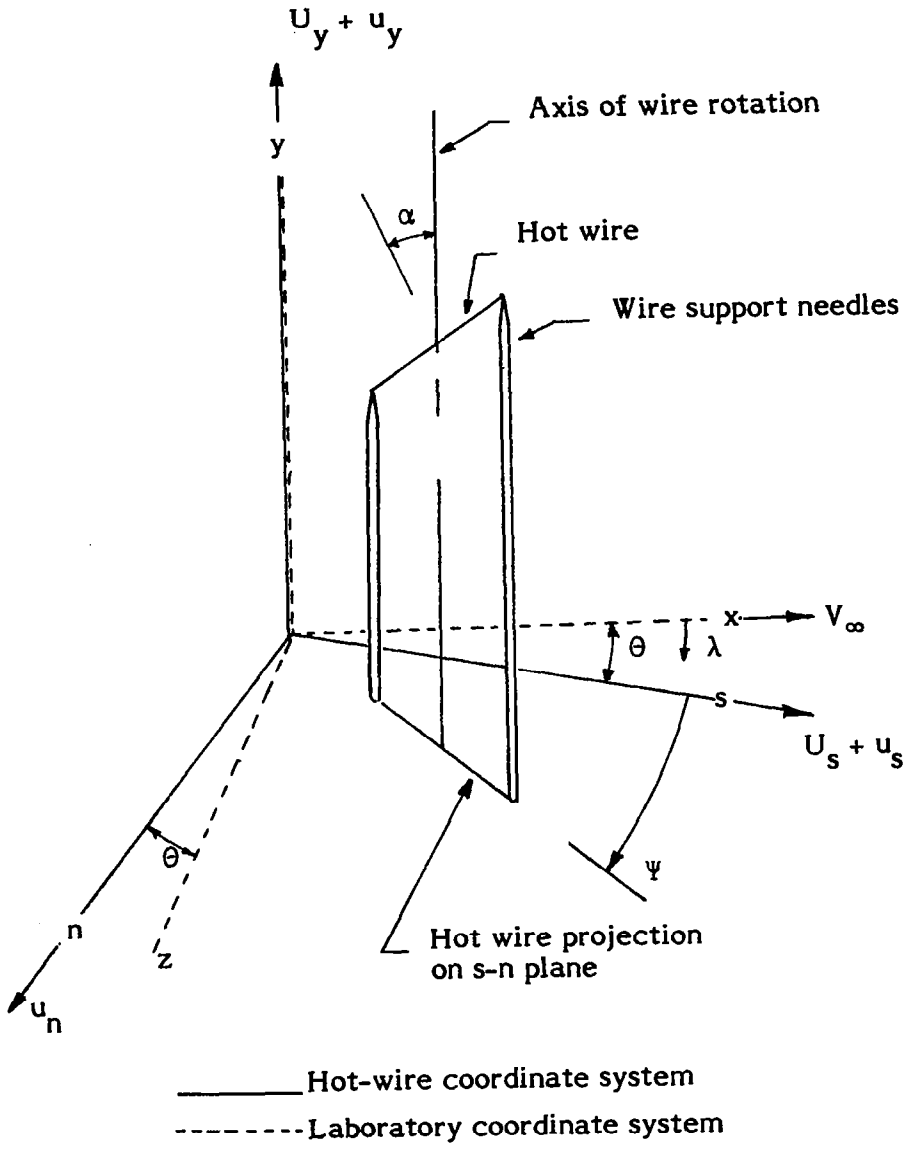

Figure 7. - Schematic of hot wire in the Cartesian coordinate system.

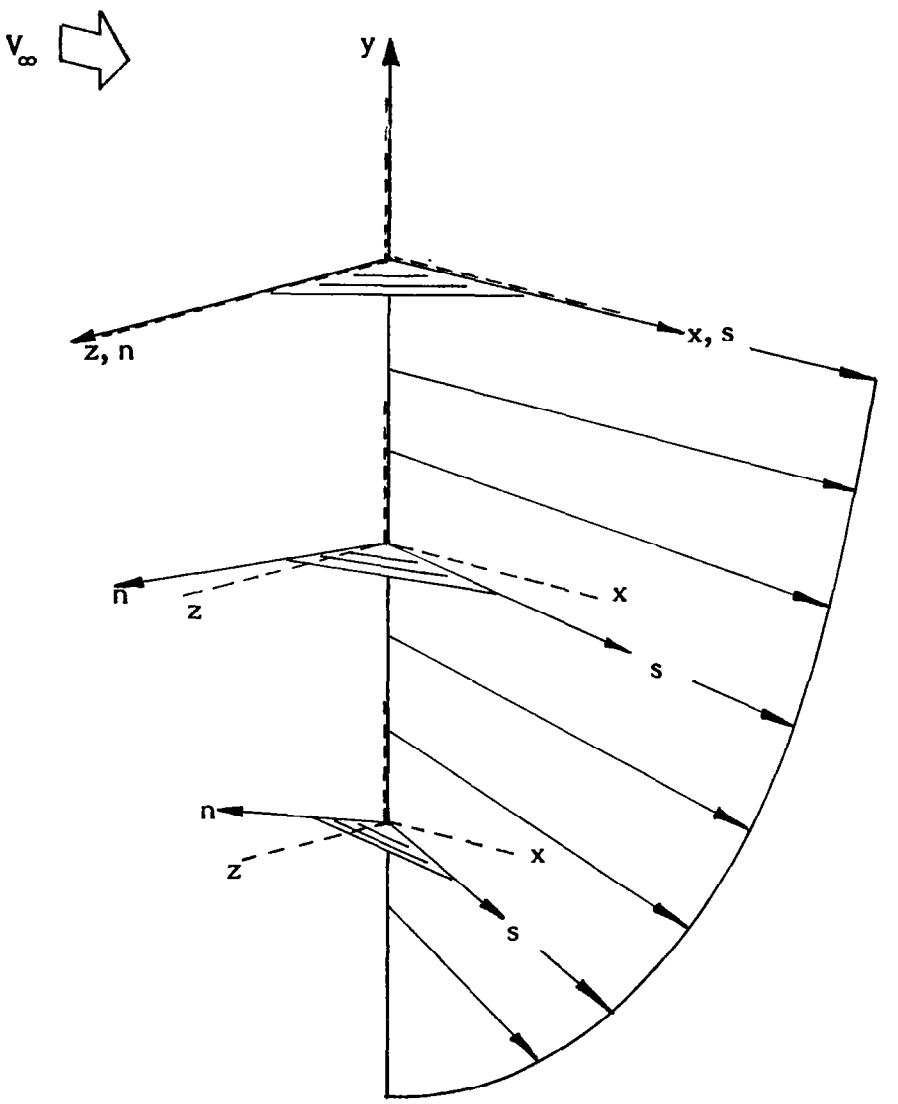

Hot-wire coordinates

Laboratory coordinates

Figure 8. - Coordinate Axes.

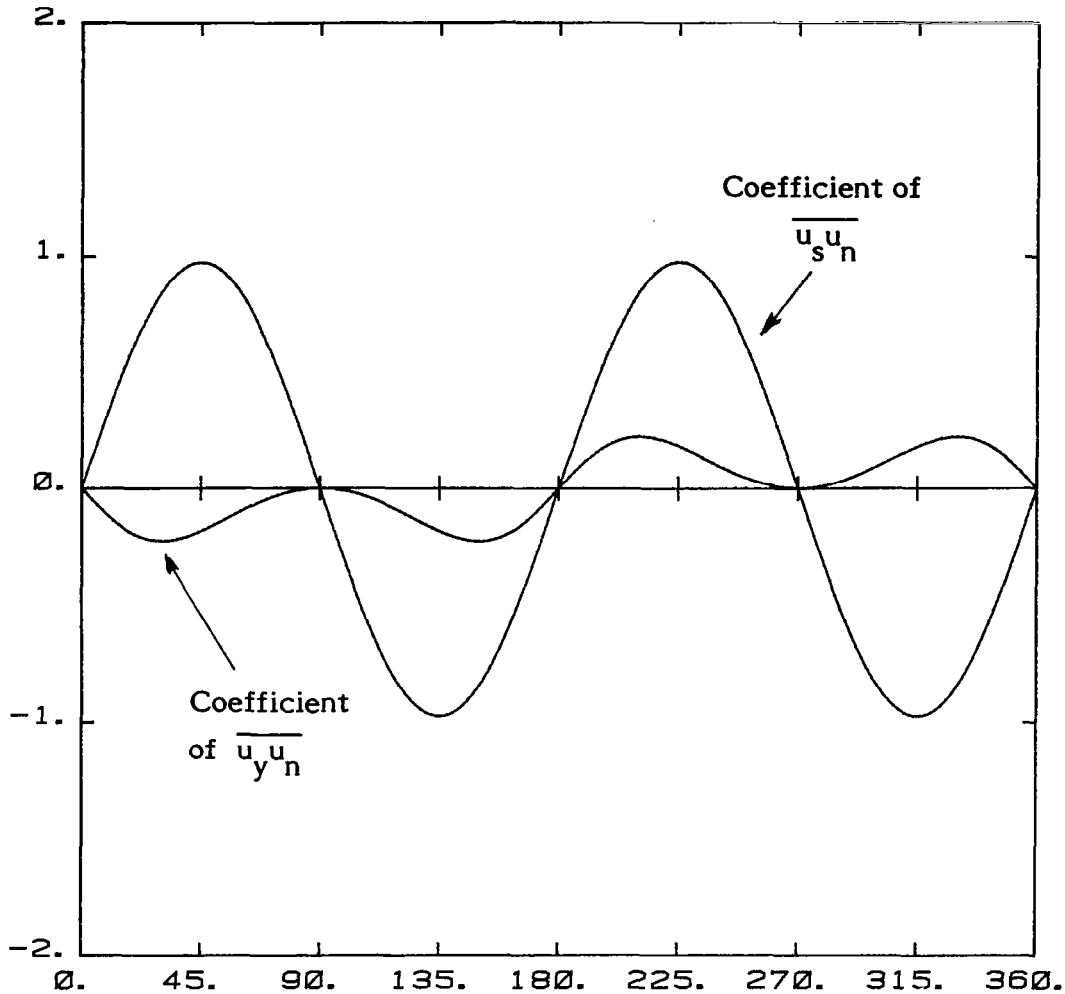

Figure 9. - Variation of coefficients of $\overline{u_y u_n}$ and $\overline{u_s u_n}$ with yaw angle ψ .

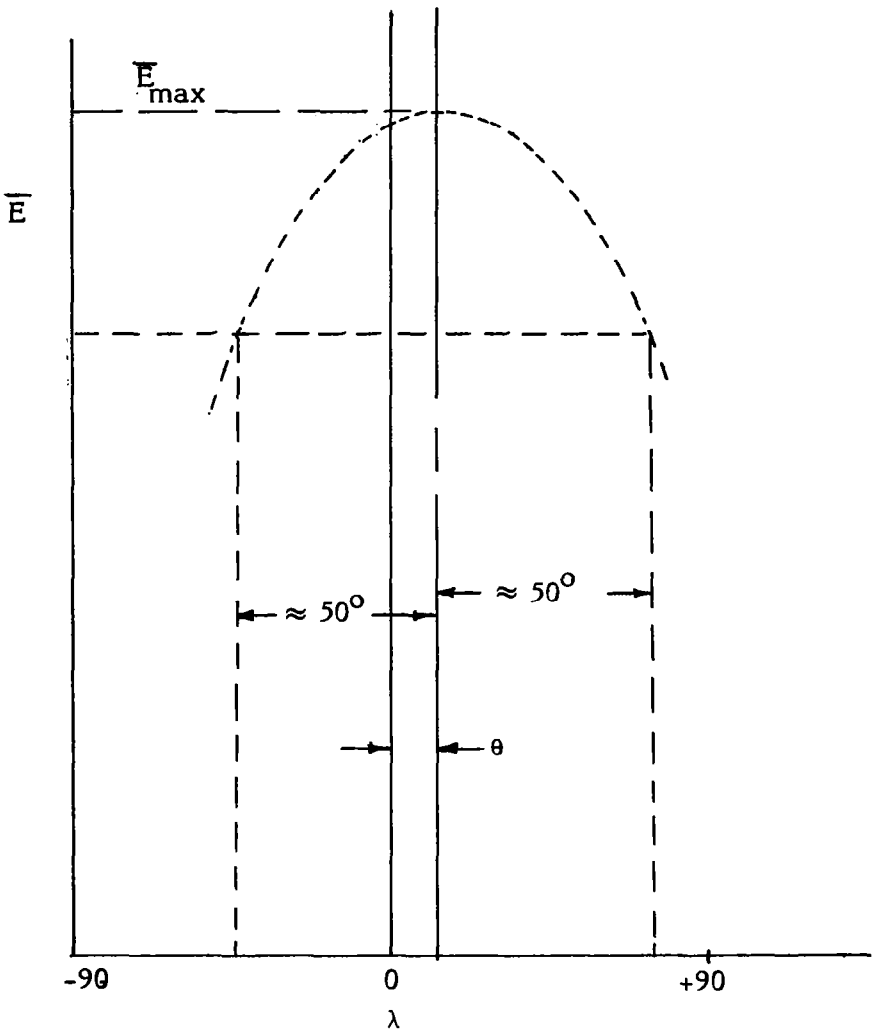

Figure 10. - Typical variation in mean voltage output with angle of rotation. Horizontal wire ($\alpha = 0$).

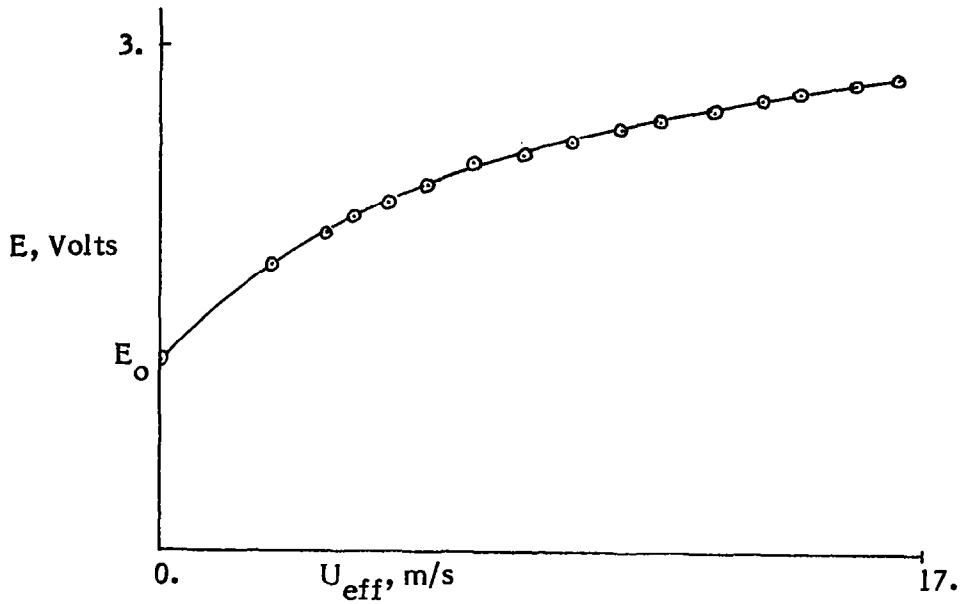

(a) Nonlinear results.

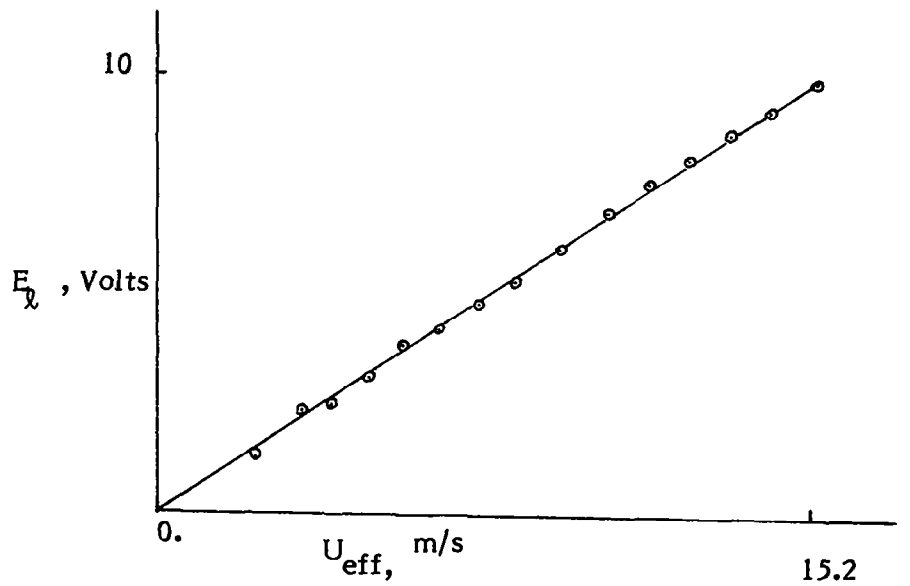

(b) Linearized results.

Figure 11. - Typical hot-wire calibration results. Straight wire ($\alpha = 0$).

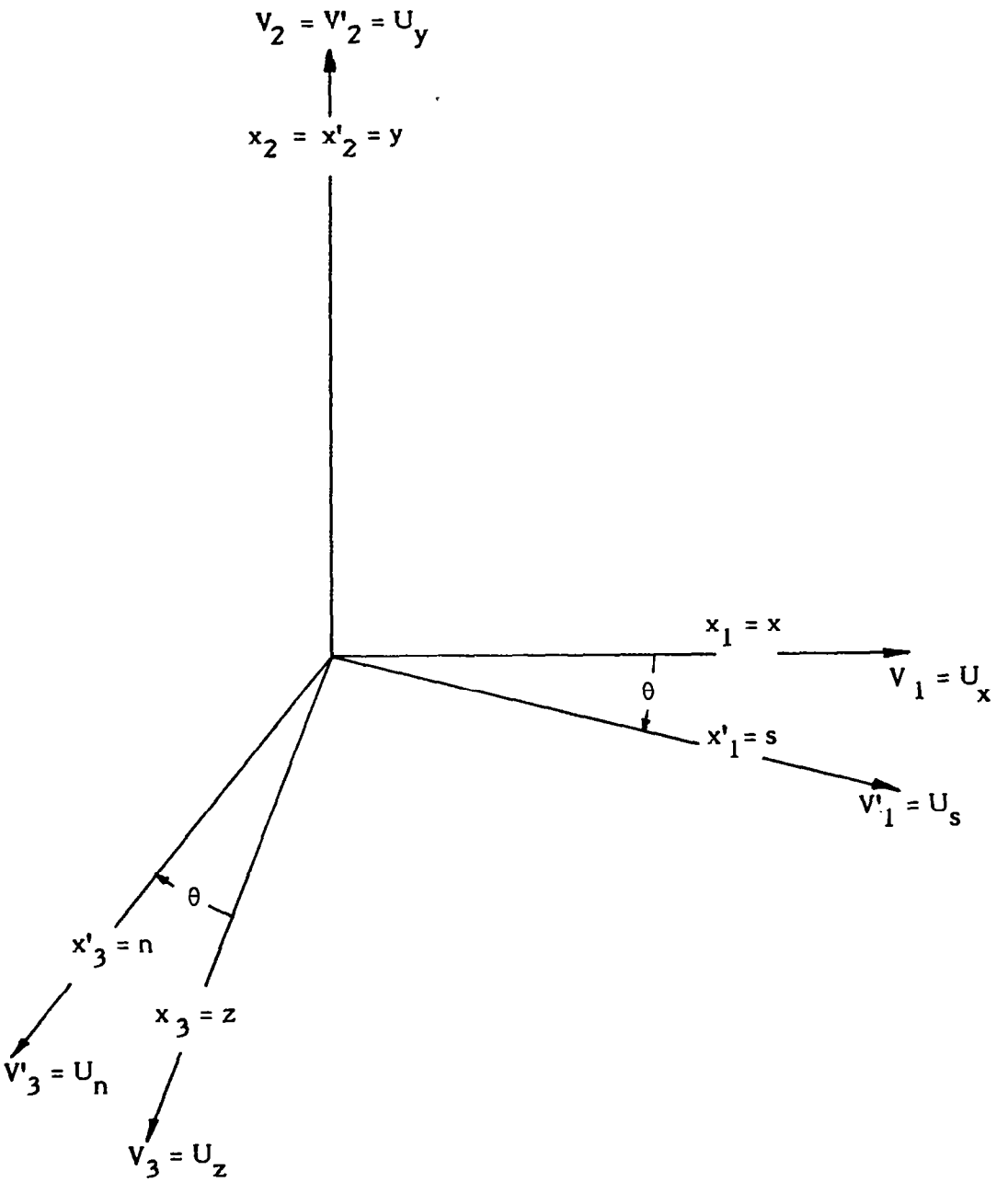

Figure 12. - The two Cartesian co-ordinate systems.

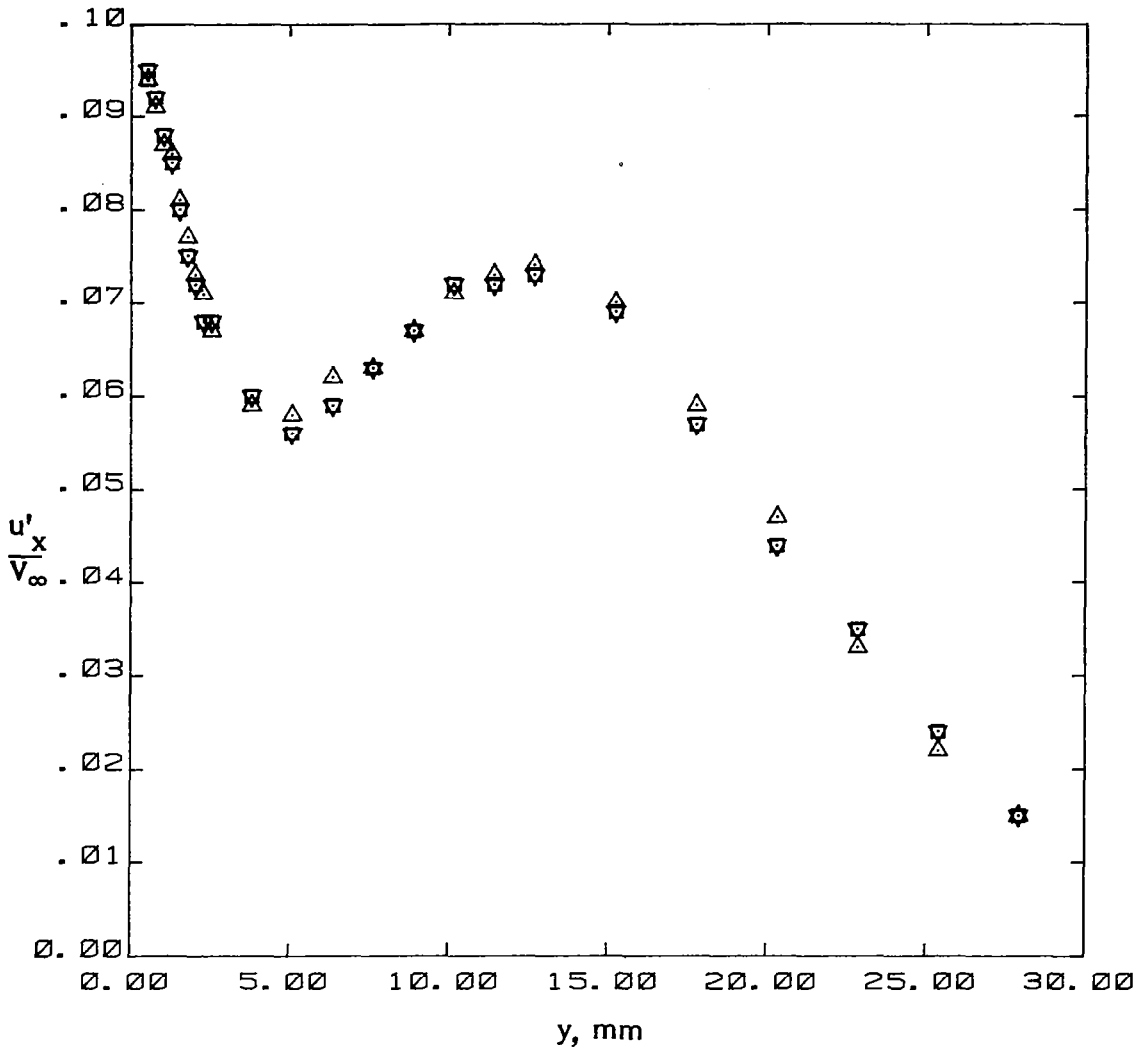

(a) Turbulent normal stress u'_x.

Figure 13. - Repeatability of results in the juncture flow.

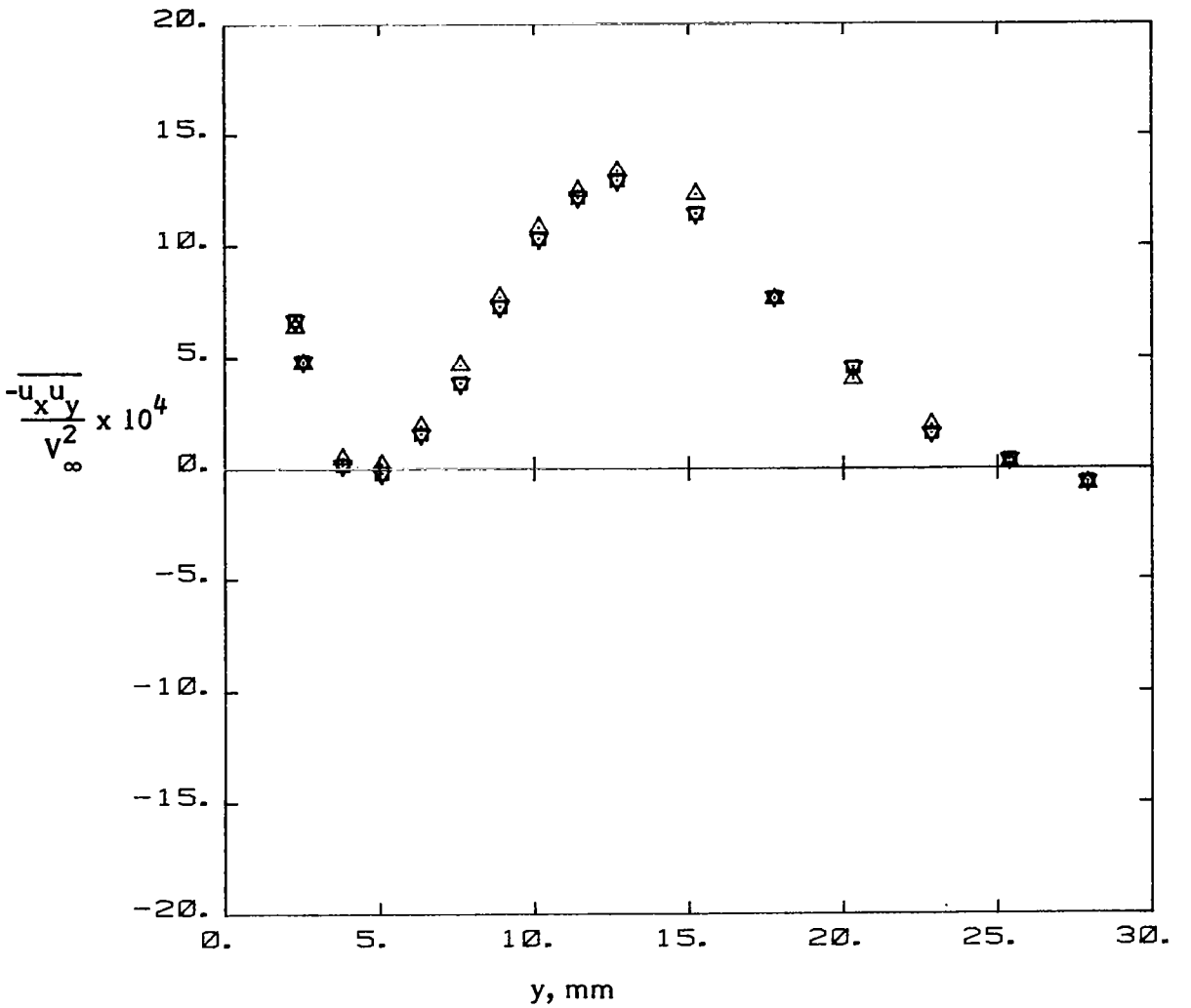

(b) Turbulent shear stress $\overline{u_x u_y}$.

Figure 13. - Continued.

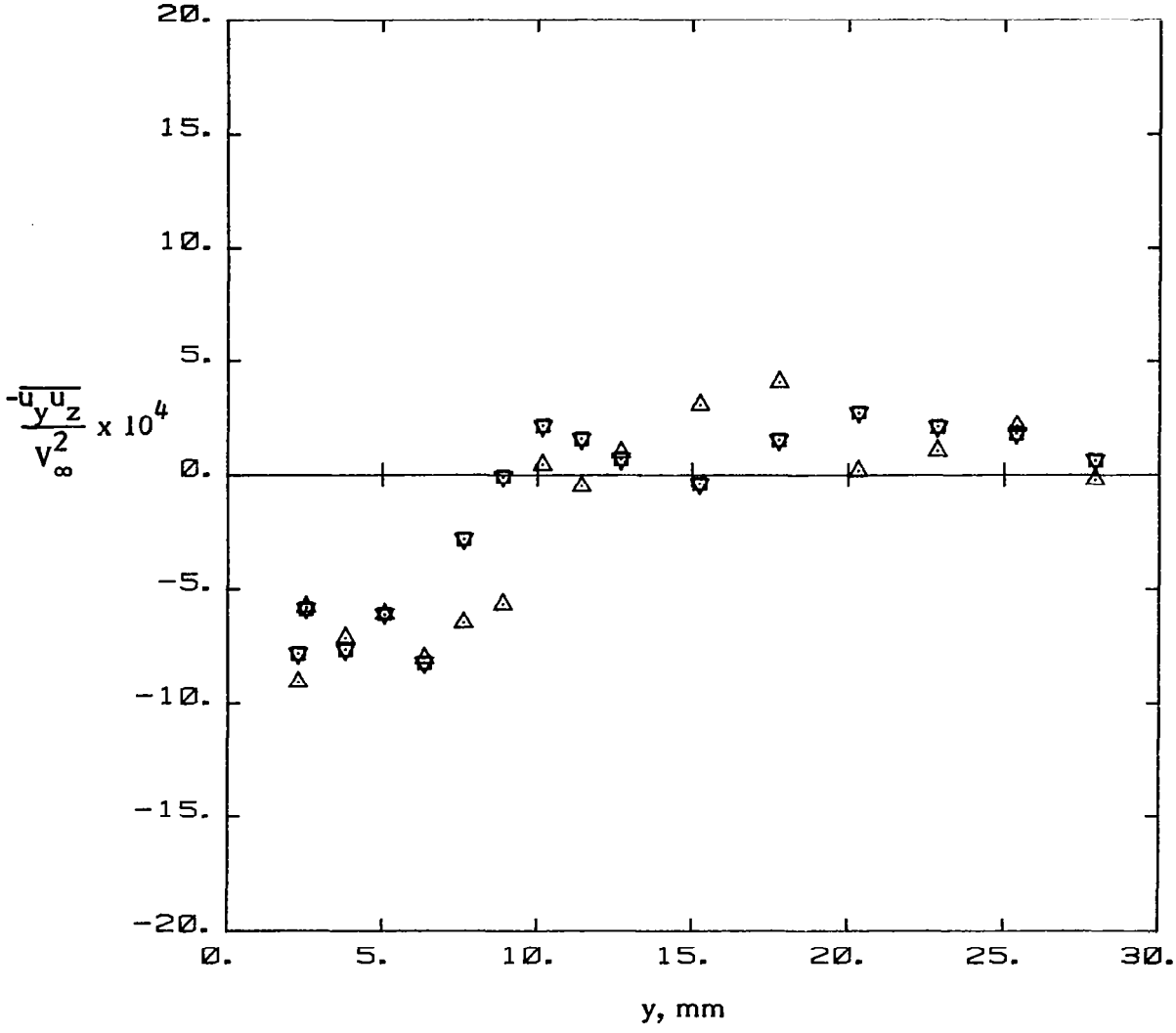

(c) Turbulent shear stress $\overline{u_y u_z}$.

Figure 13. - Concluded.

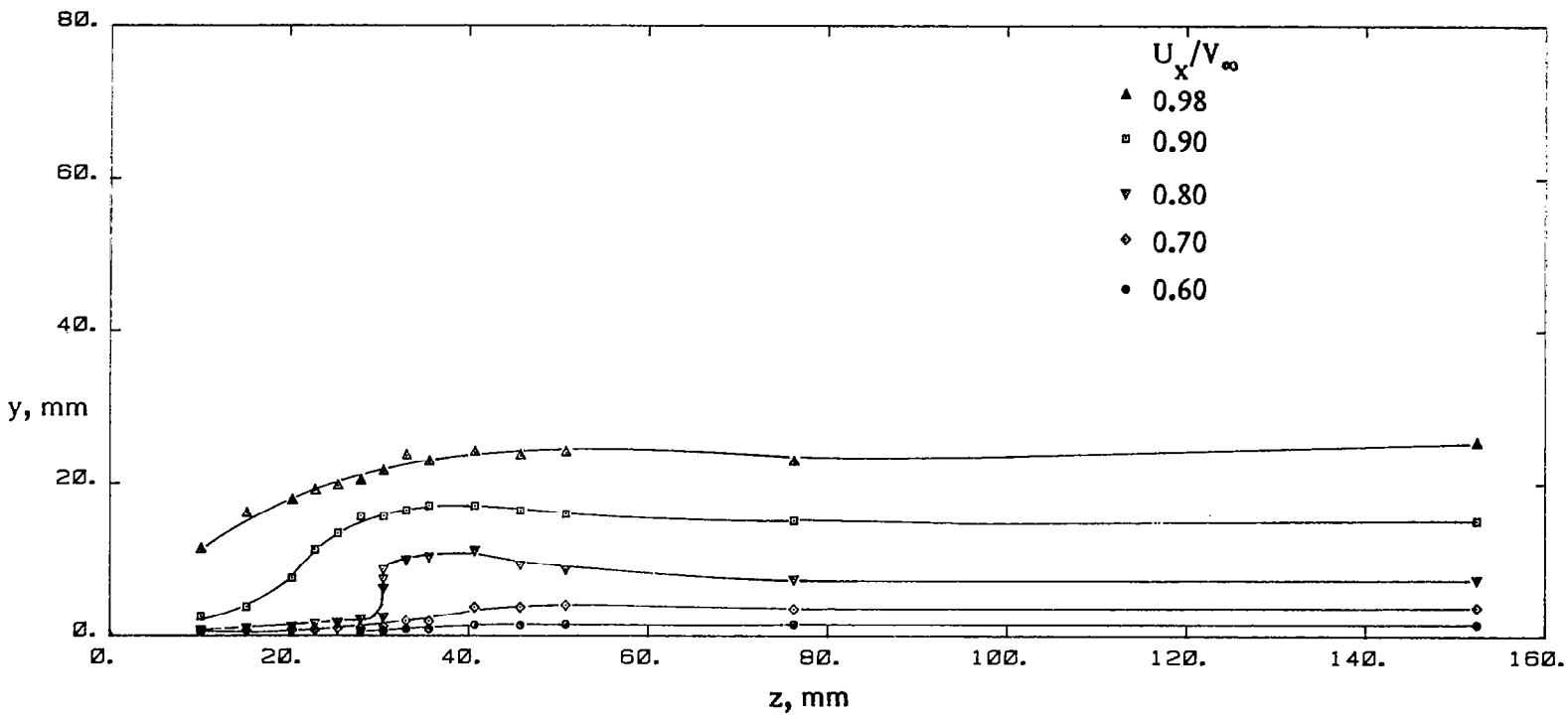

(a) x = 165 mm.

Figure 14. - Contour plot of mean velocity U_x.

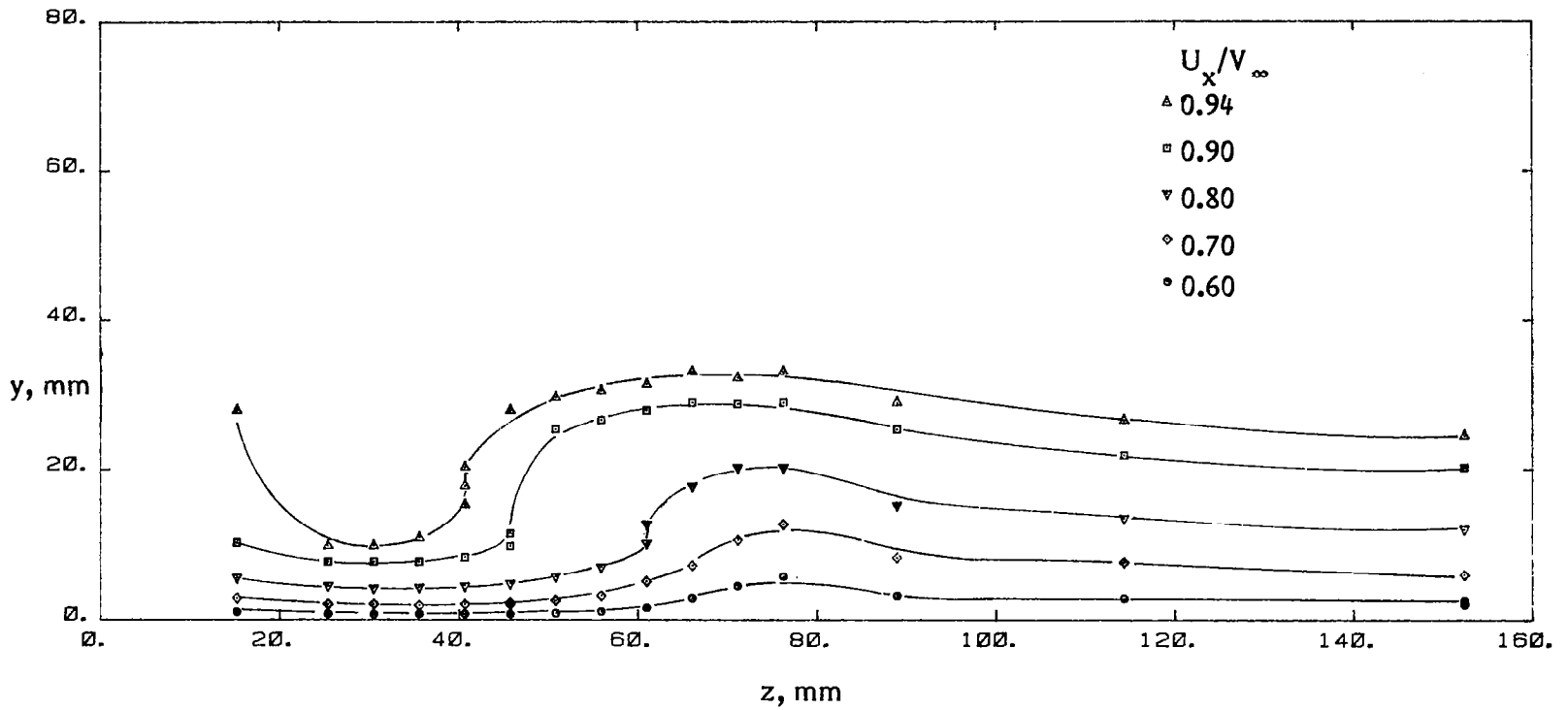

(b) x = 902 mm.

Figure 14. - Concluded .

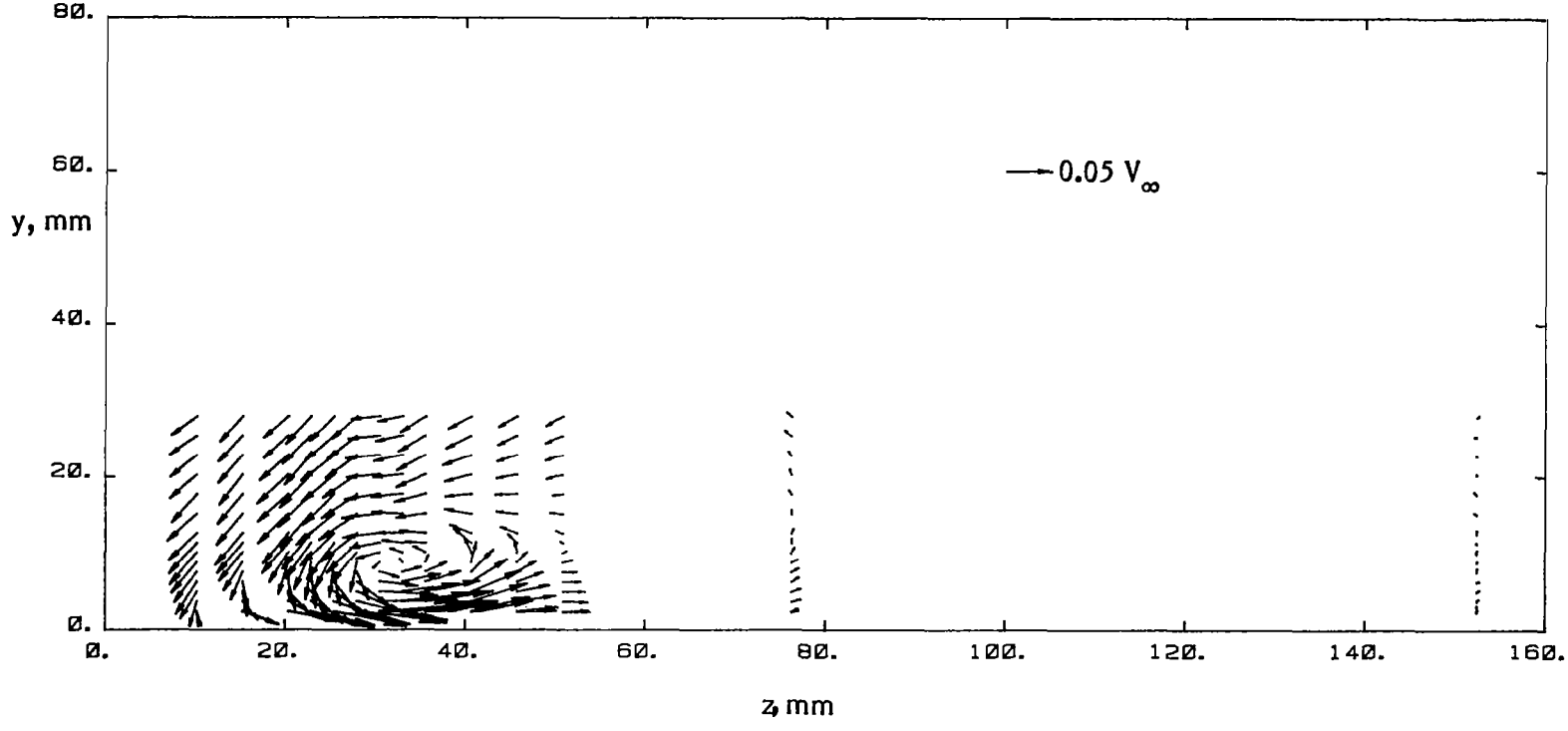

(a) x = 165 mm.

Figure 15. - Vector plot of secondary flow in the juncture.

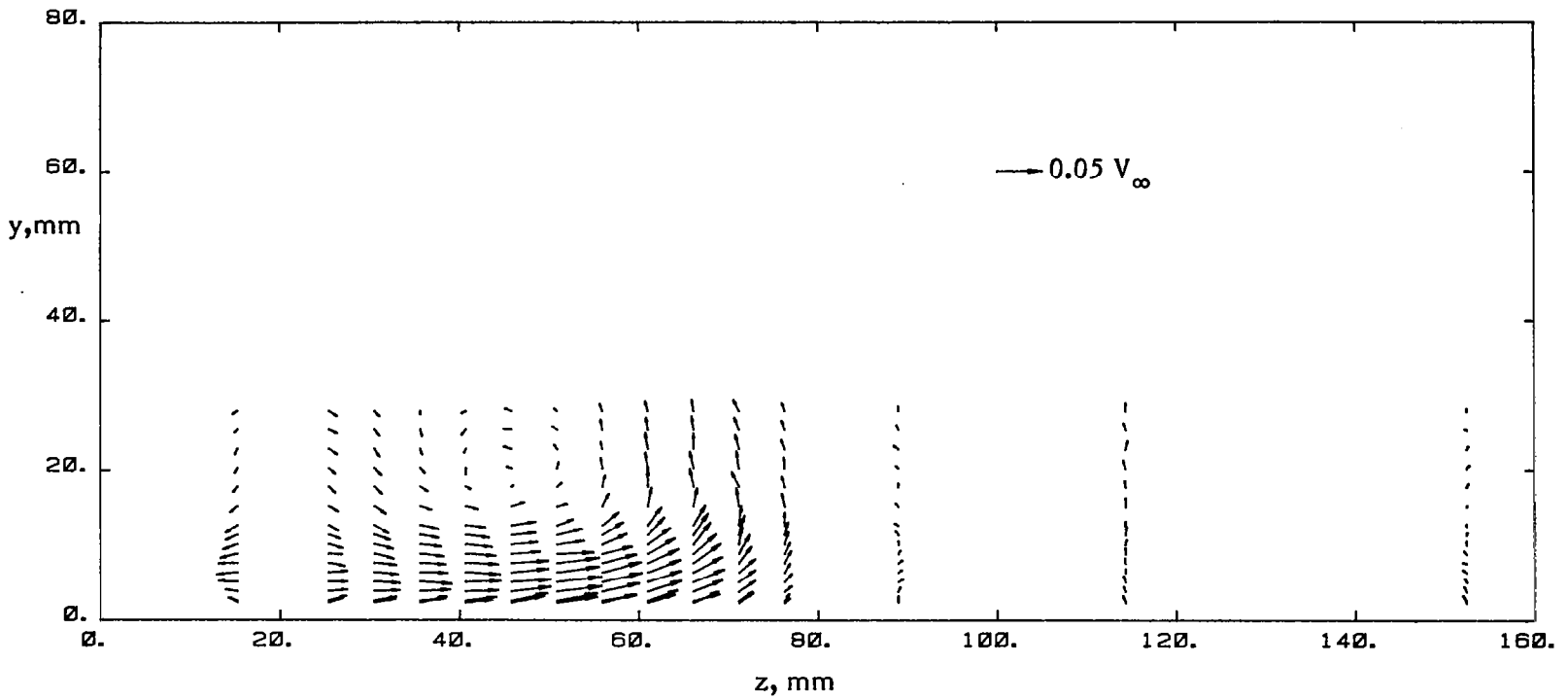

(b) x = 902 mm.

Figure 15. - Concluded .

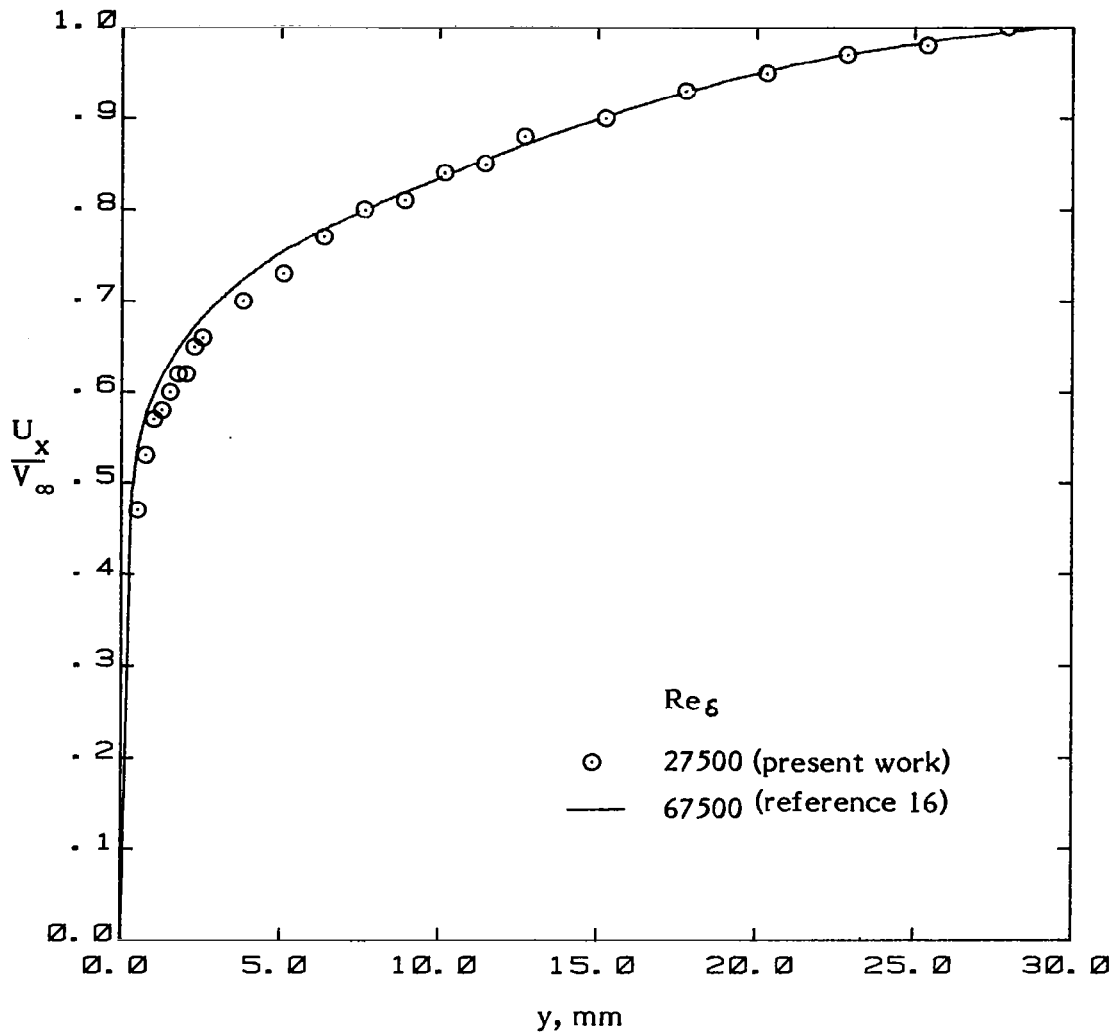

(a) Mean Velocity U_x.

Figure 16. - Profiles at z station furthest from body (z=152 mm , x =165mm).

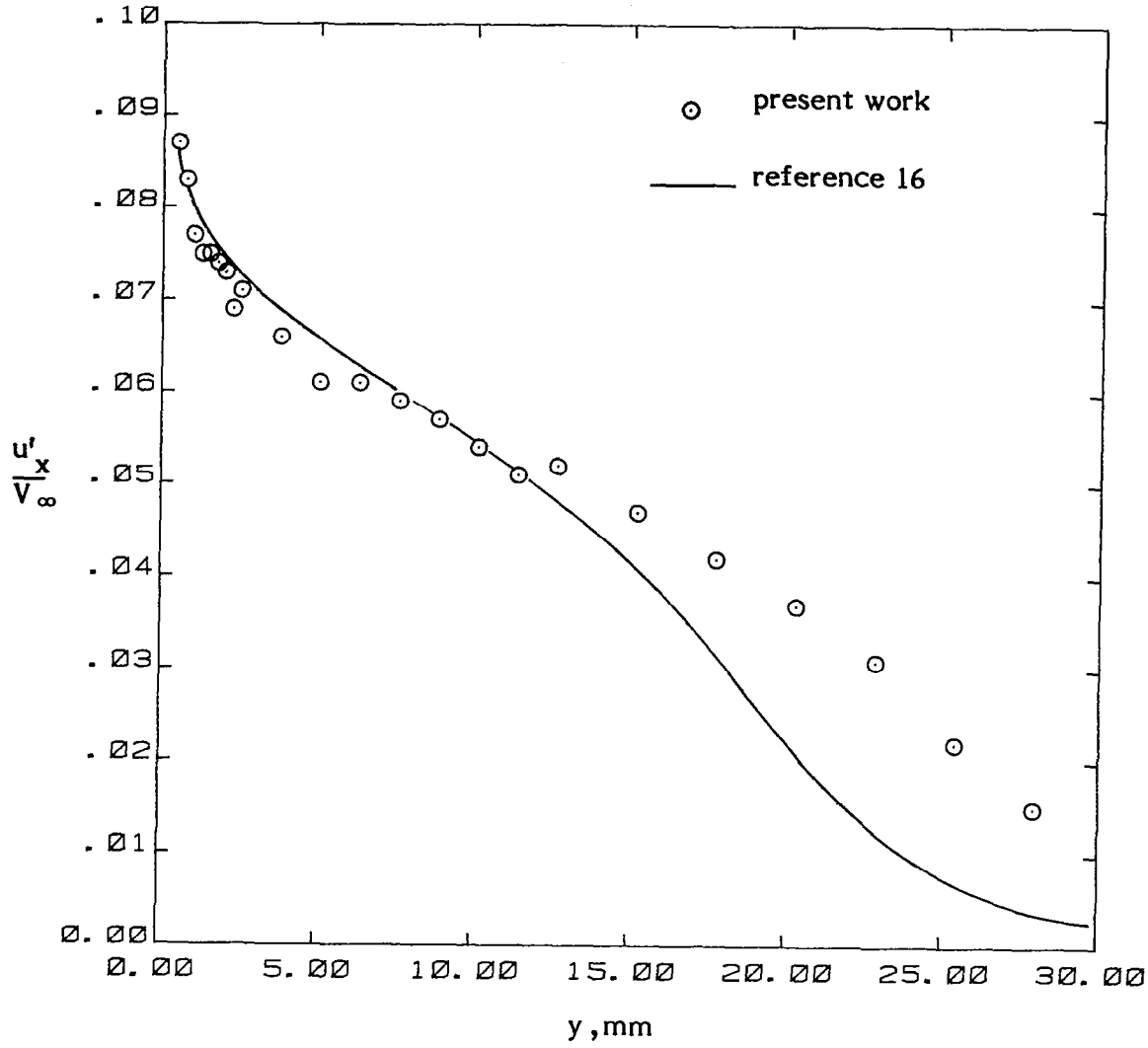

(b) Turbulent normal stress u'_x.

Figure 16. - Continued.

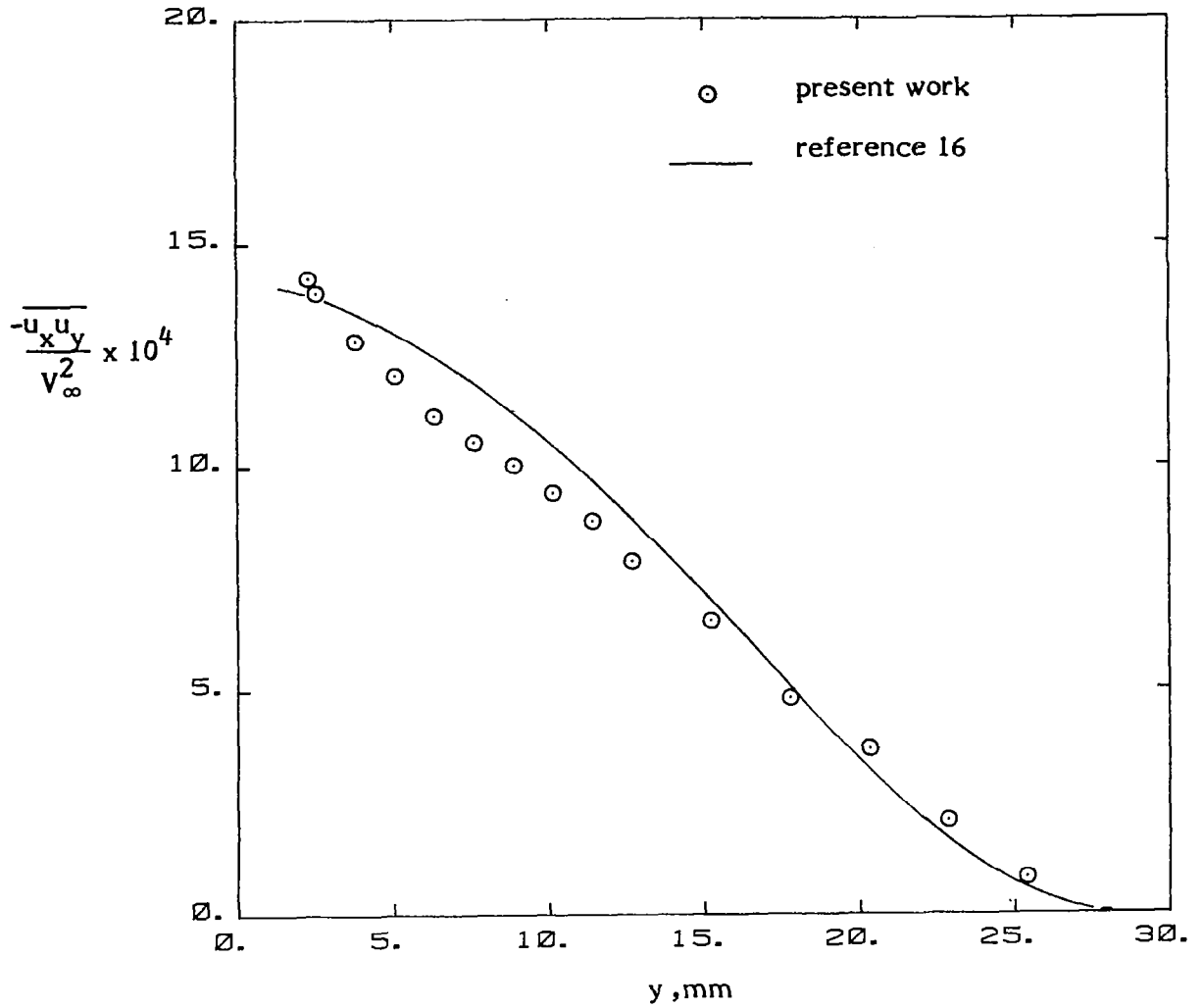

(c) Turbulent shear stress $\overline{u_x u_y}$.

Figure 16. - Concluded.

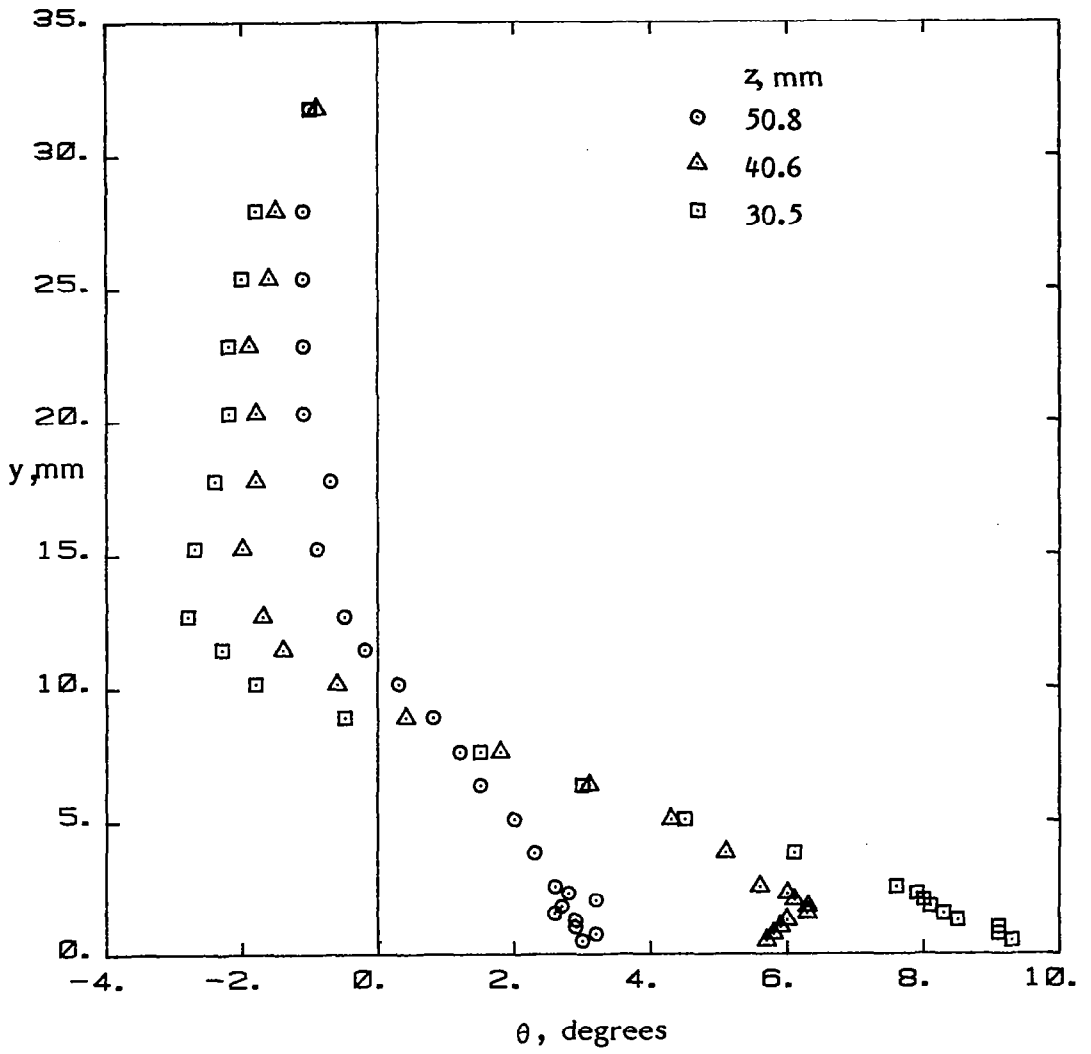

(a) x = 165 mm.

Figure 17. - Variation of local mean flow direction in the juncture.

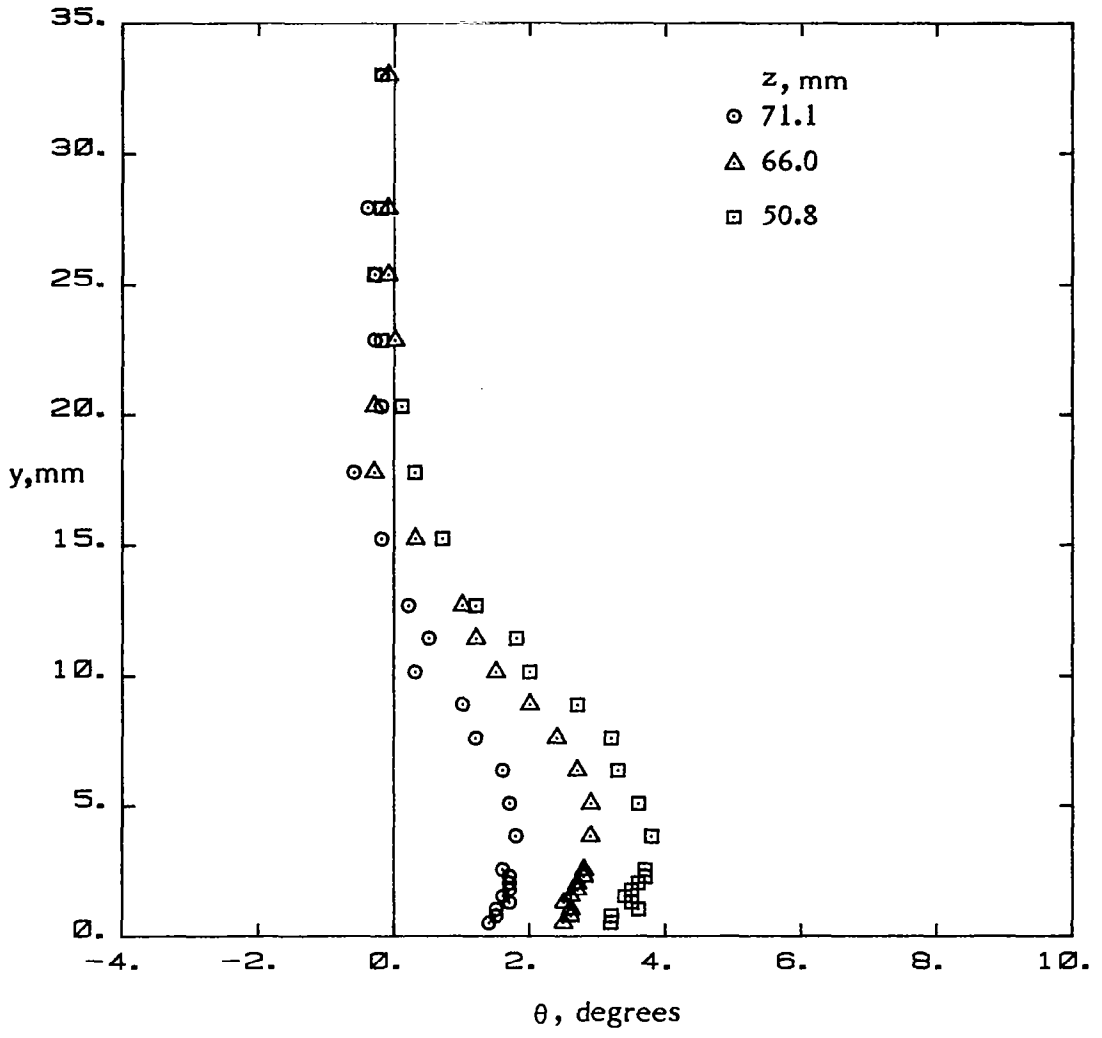

(b) x = 902 mm.

Figure 17. - Concluded.

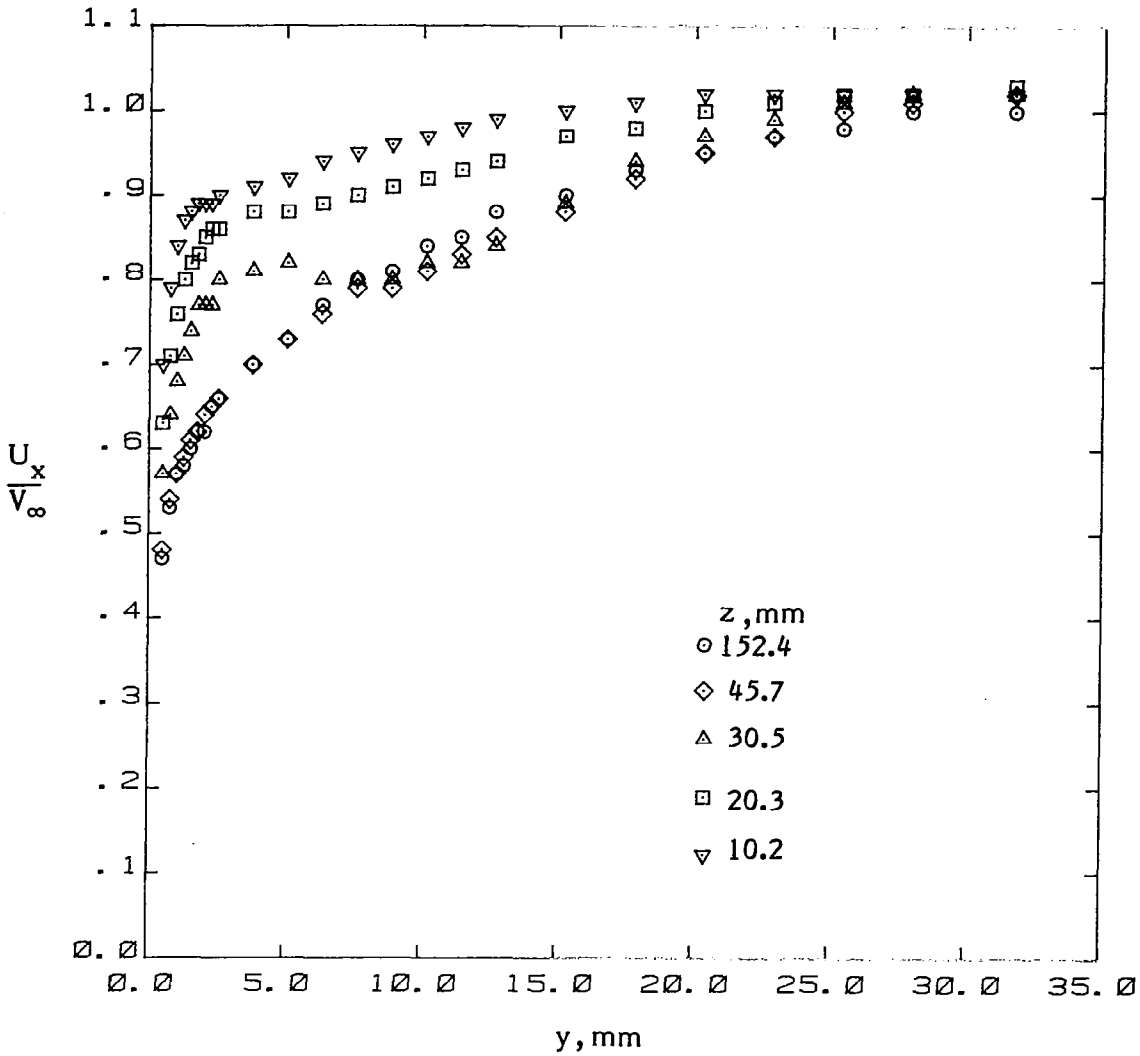

(a) Mean velocity U_x.

Figure 18. - Mean velocities and turbulence stresses in the juncture (x = 165 mm).

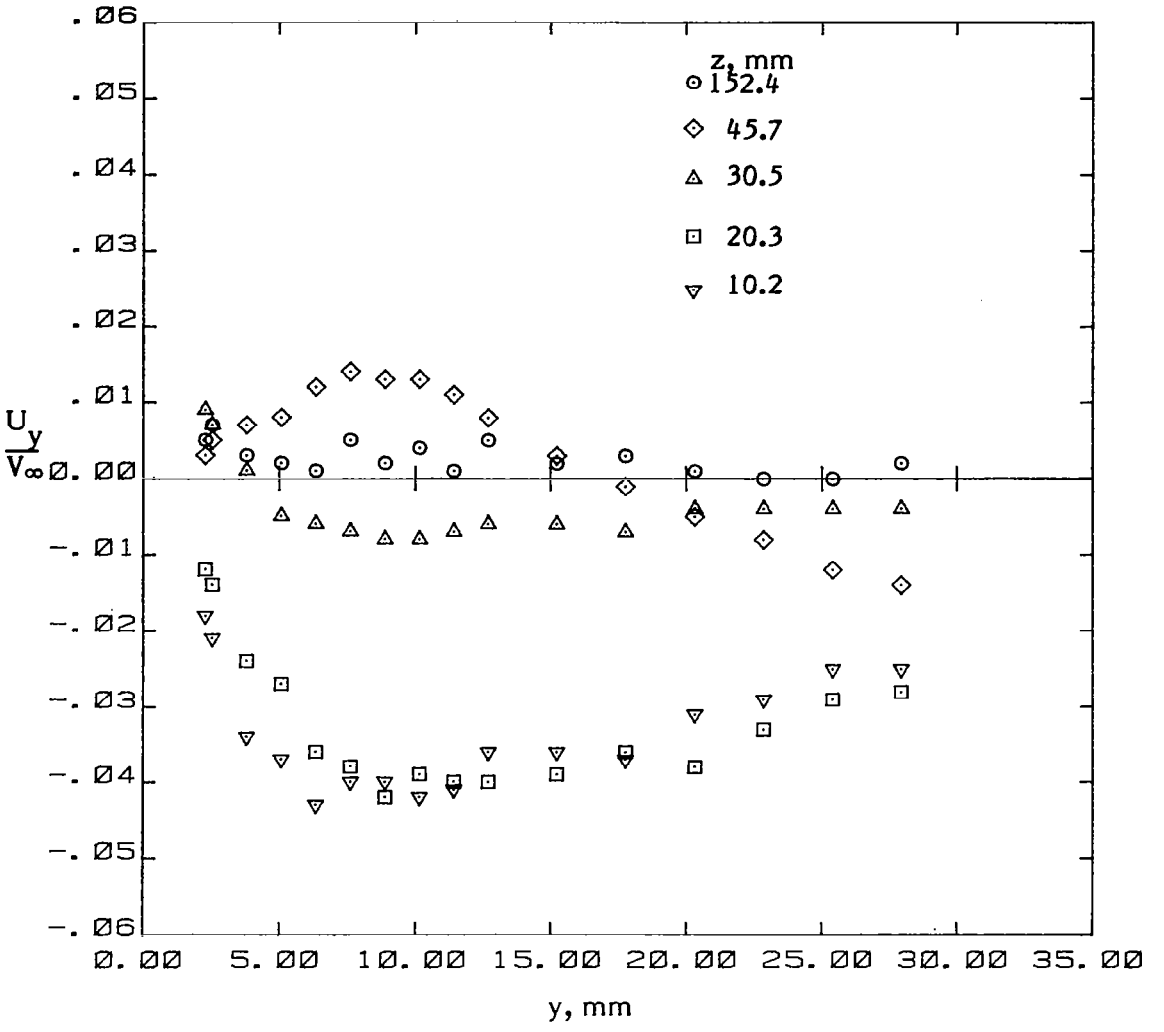

(b) Mean velocity U_y.

Figure 18. - Continued.

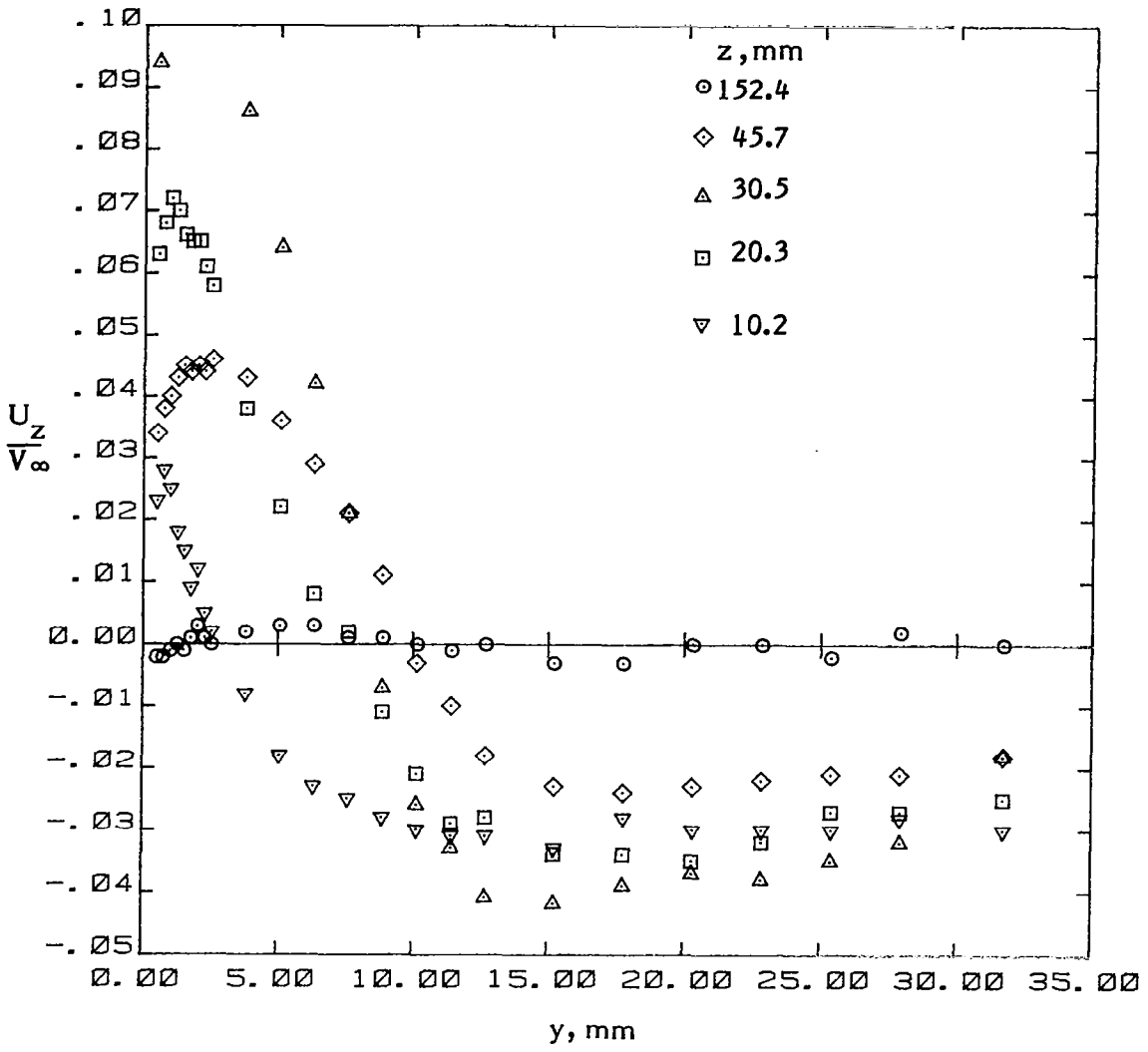

(c) Mean velocity U_z.

Figure 18. - Continued.

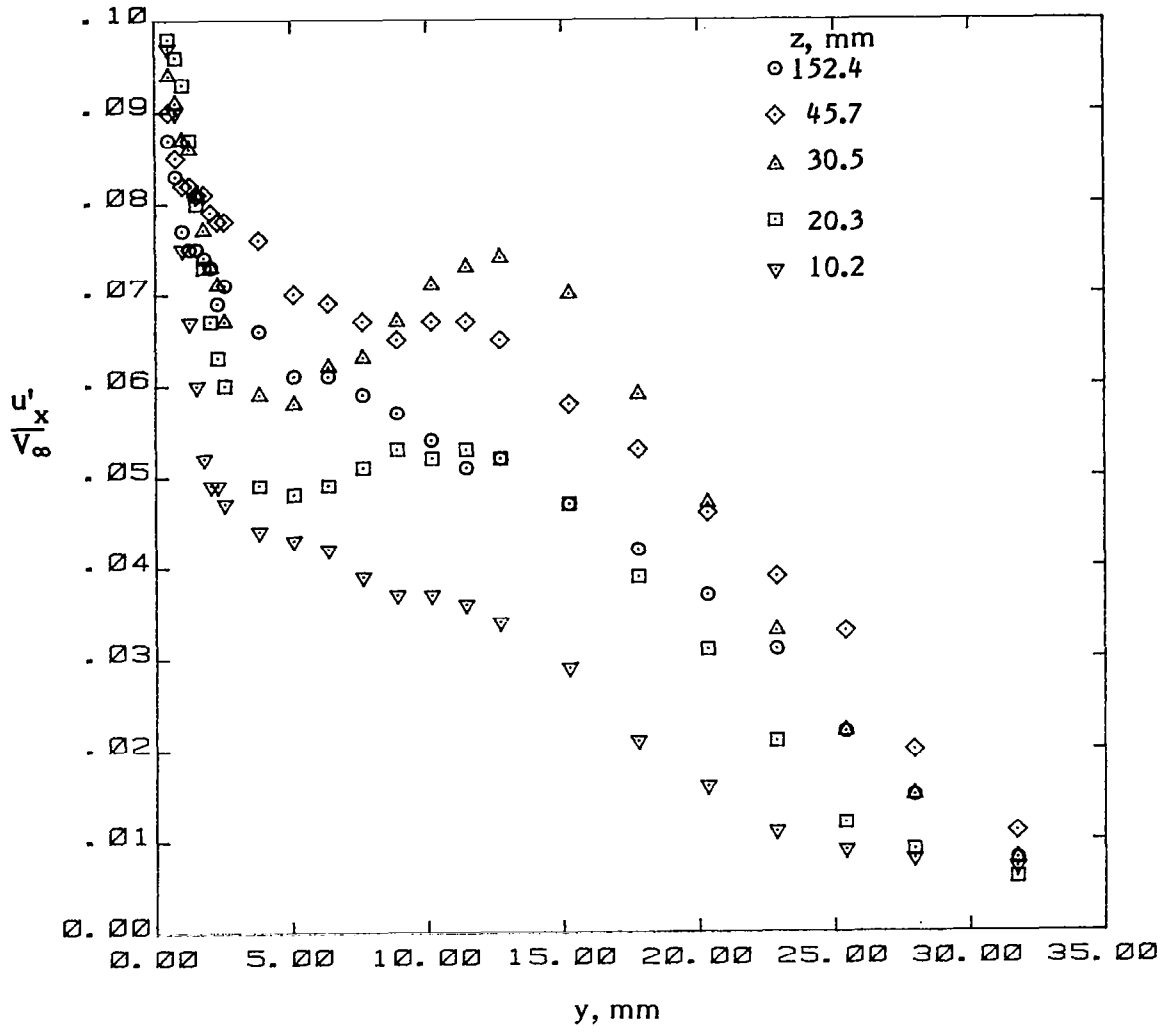

(d) Turbulent normal stress u'_x.

Figure 18. - Continued.

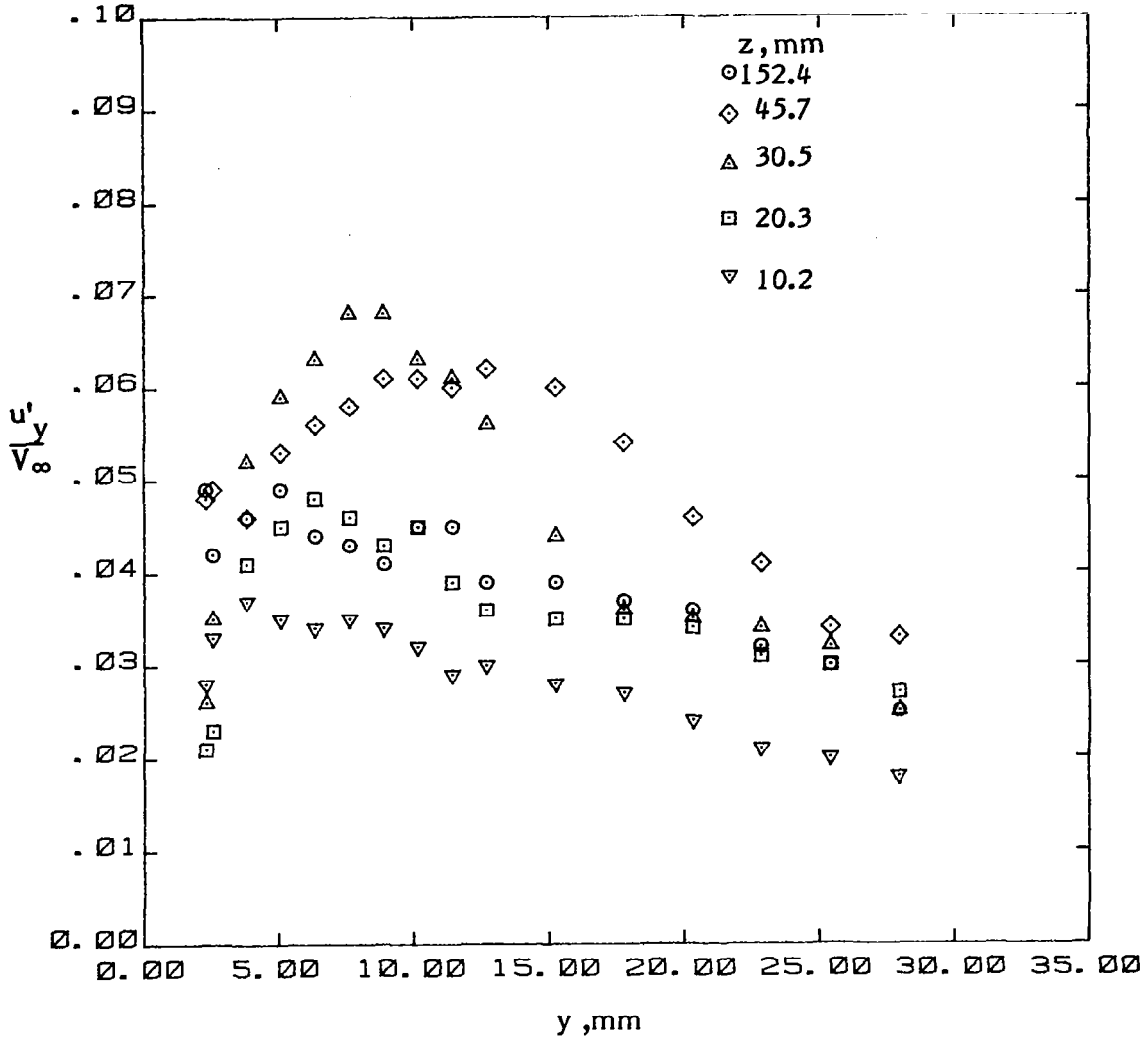

(e) Turbulent normal stress u'_y.

Figure 18. - Continued .

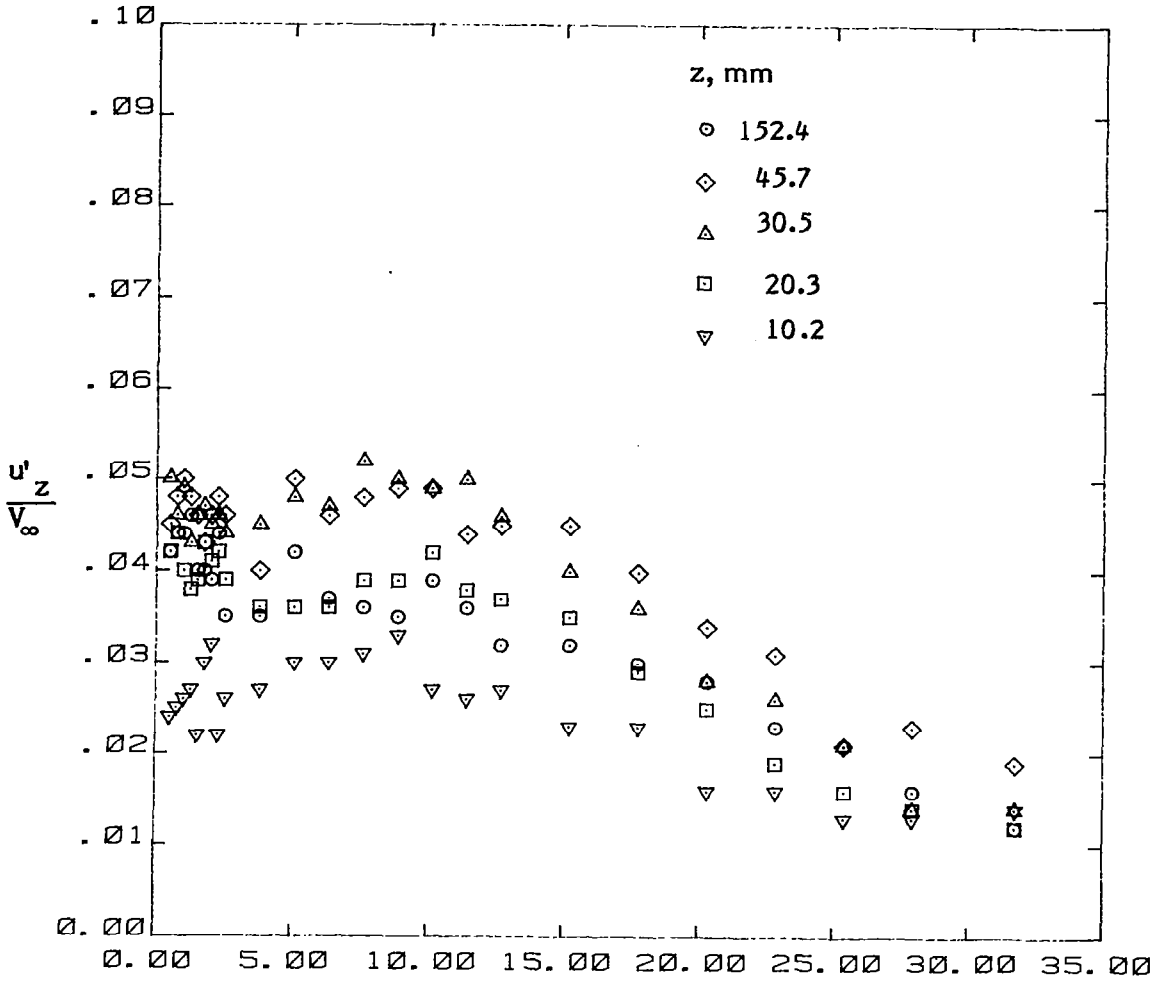

(f) Turbulent normal stress u'_z.

Figure 18. - Continued.

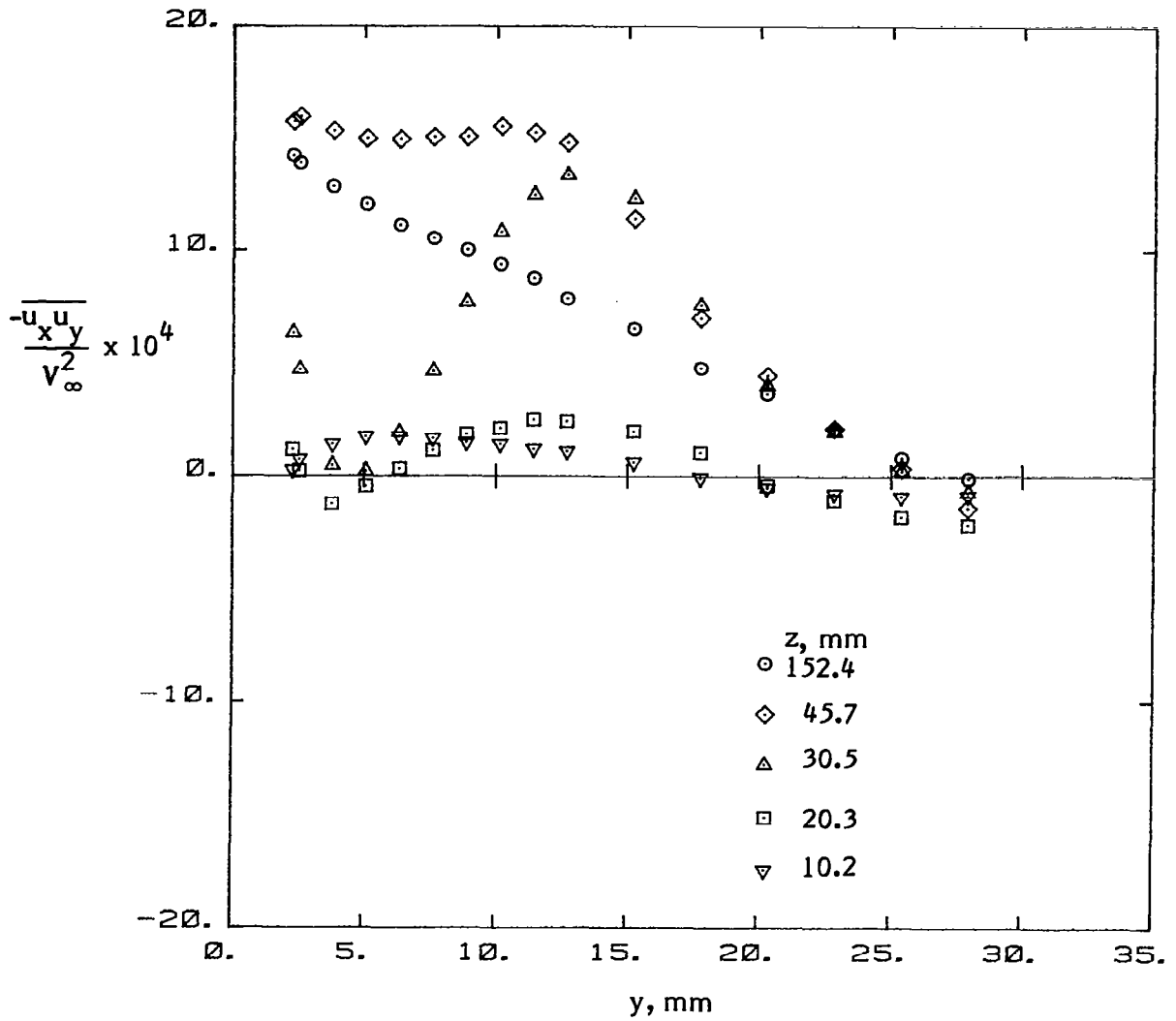

(g) Turbulent shear stress $\overline{u_x u_y}$.

Figure 18. - Continued.

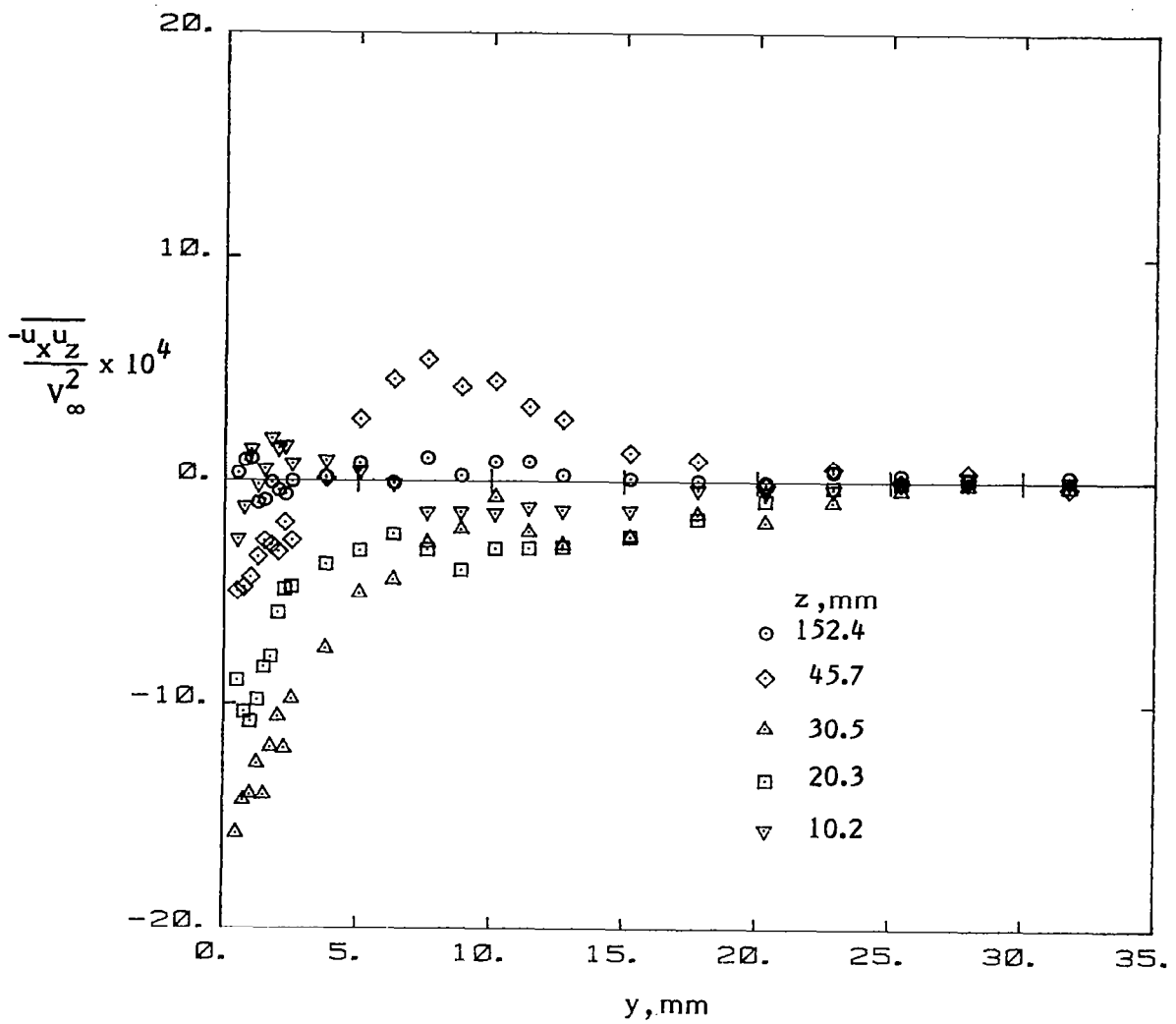

(h) Turbulent shear stress $\overline{u_x u_z}$.

Figure 18. - Continued.

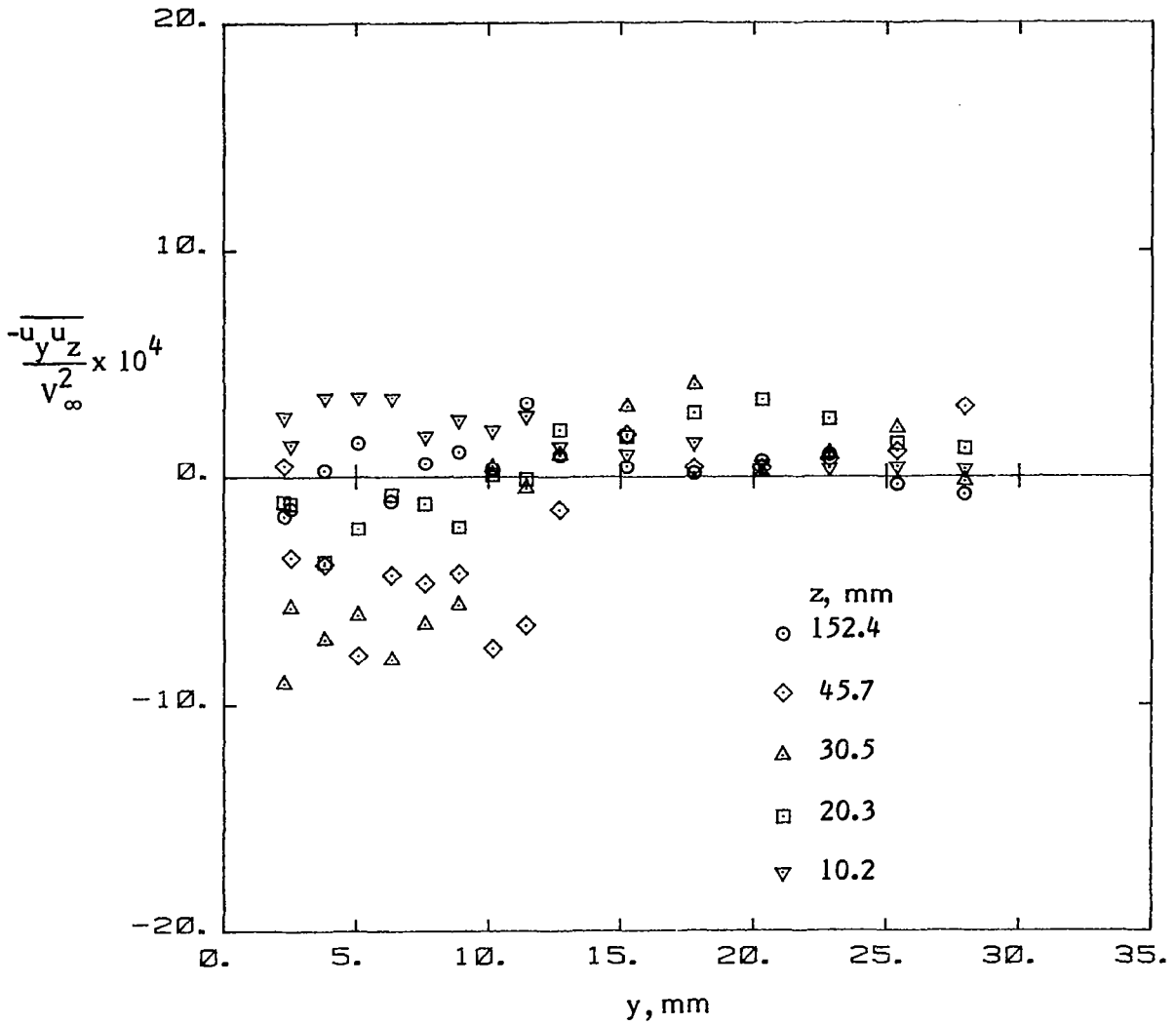

(i) Turbulent shear stress $\overline{u_y u_z}$.

Figure 18. - Concluded.

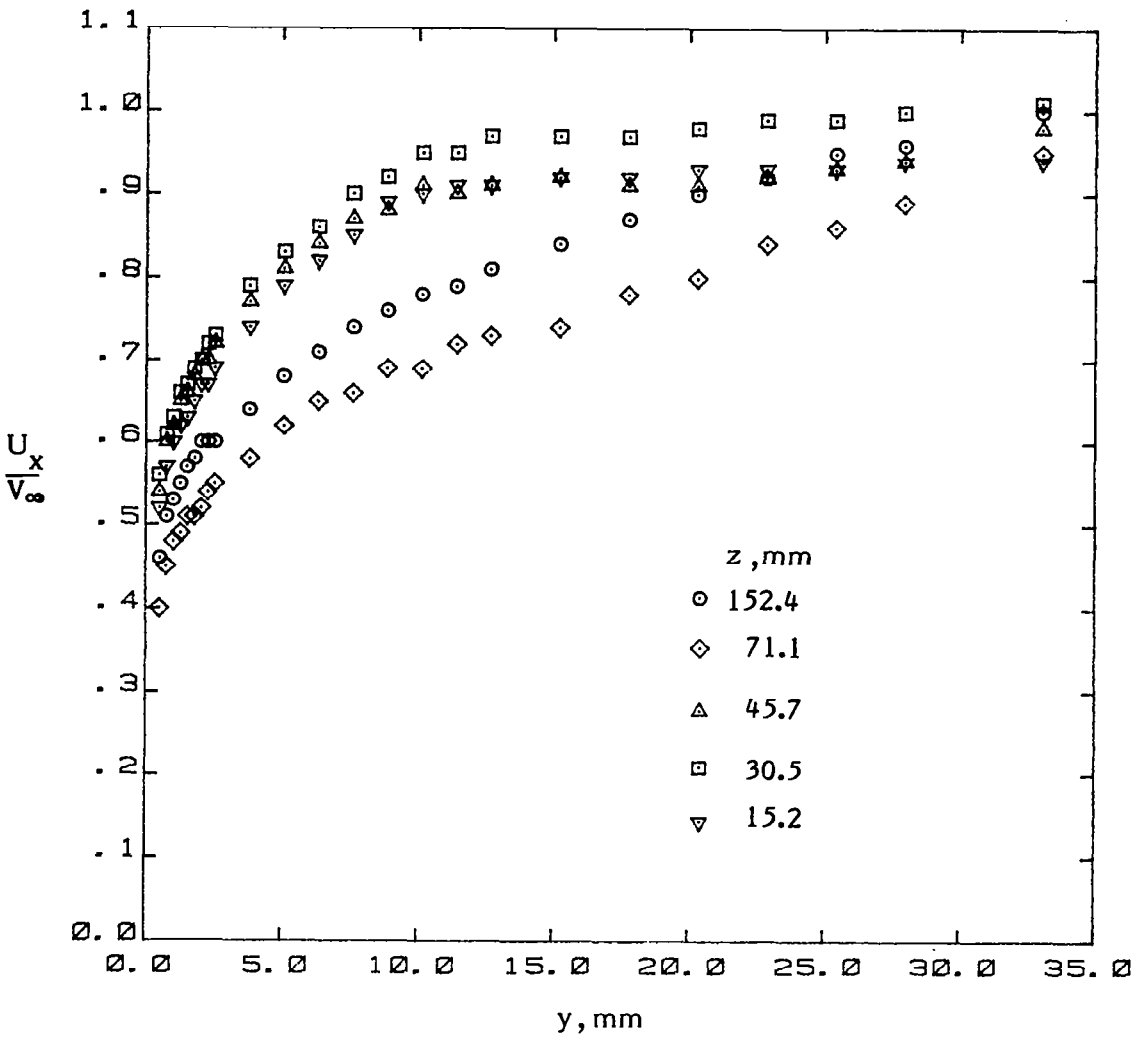

(a) Mean velocity U_x.

Figure 19. - Mean velocities and turbulence stresses in the juncture (x = 902 mm).

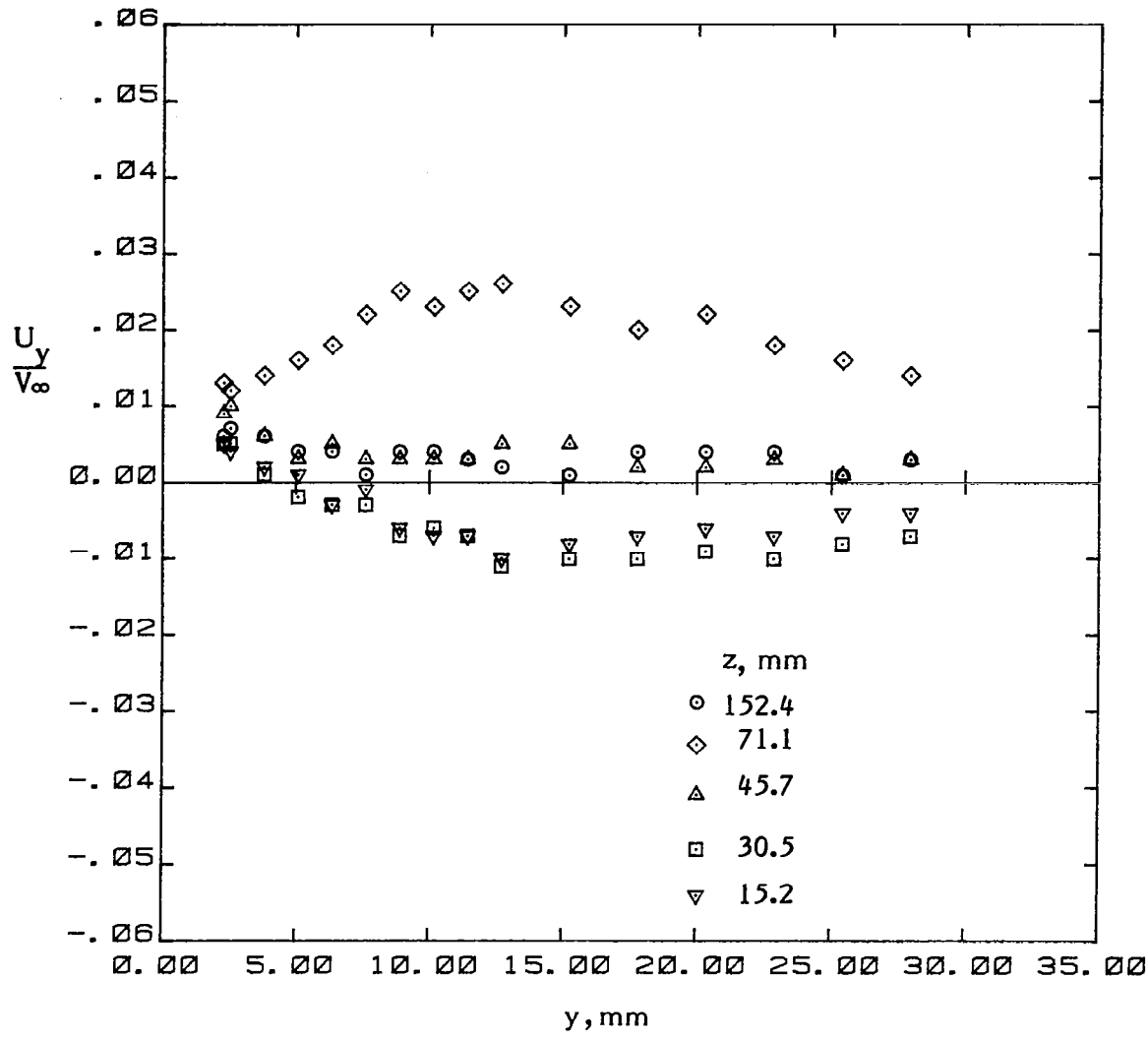

(b) Mean velocity U_y.

Figure 19. - Continued.

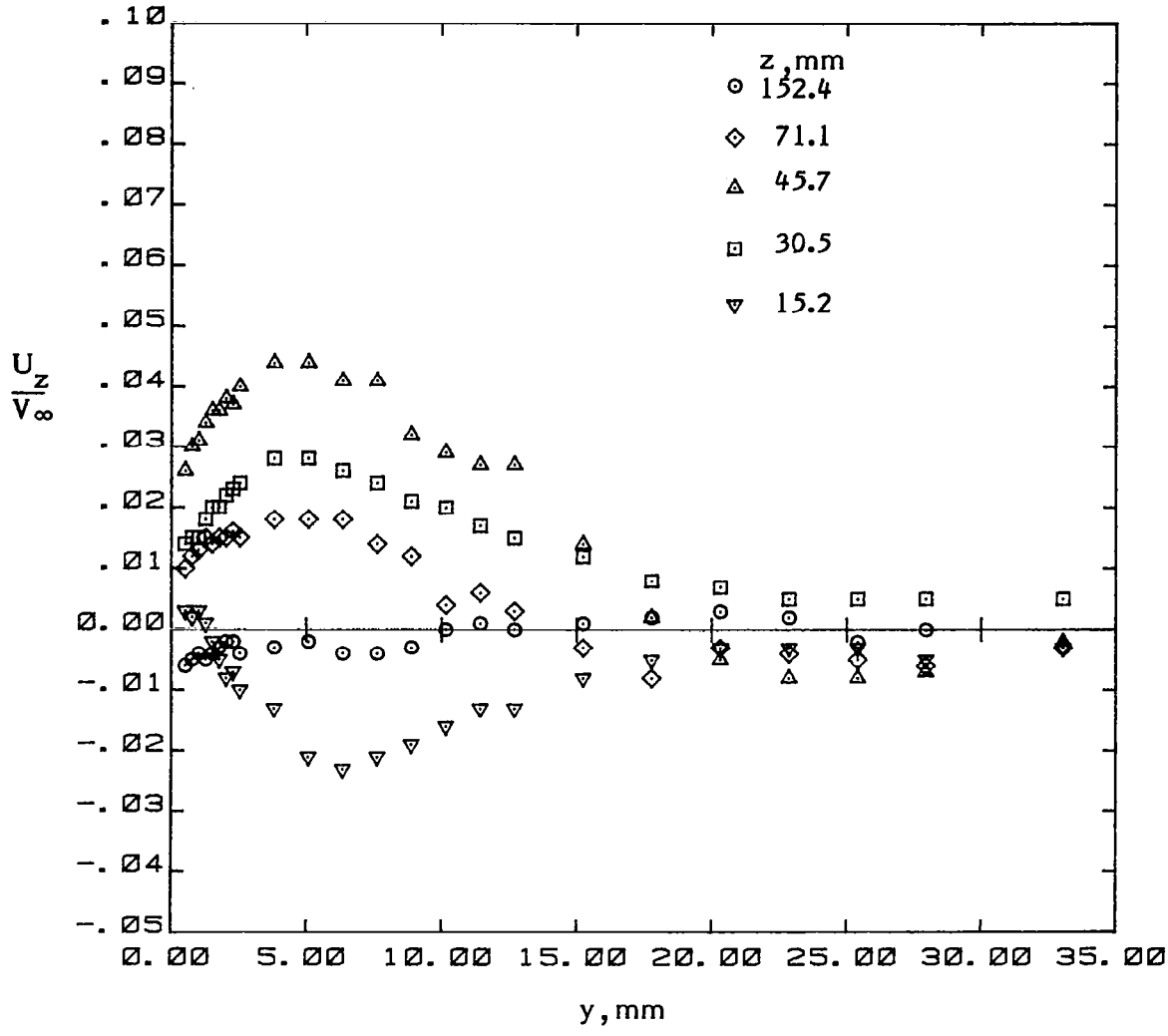

(c) Mean velocity U_z.

Figure 19. - Continued.

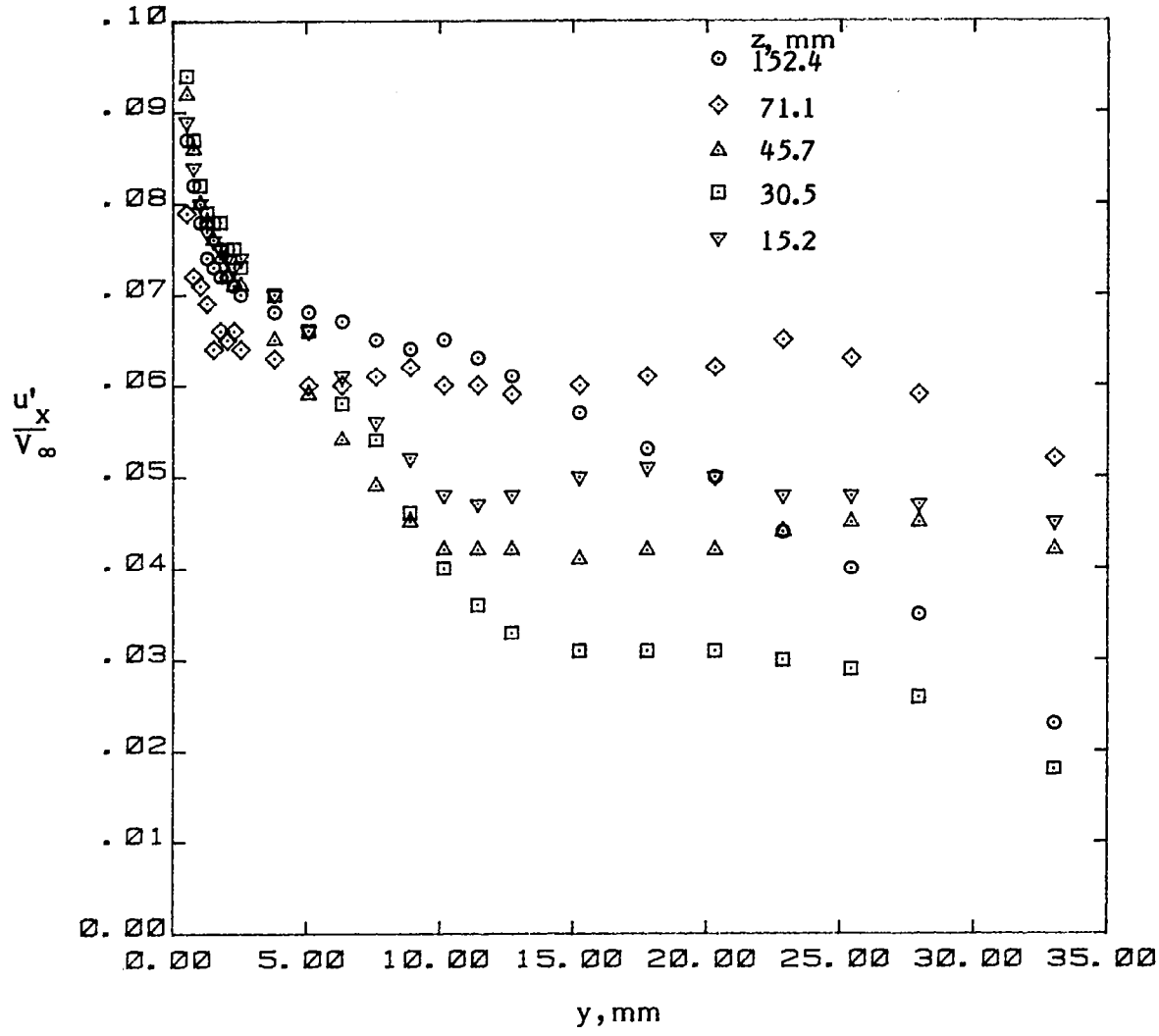

(d) Turbulent normal stress u'_x.

Figure 19. - Continued.

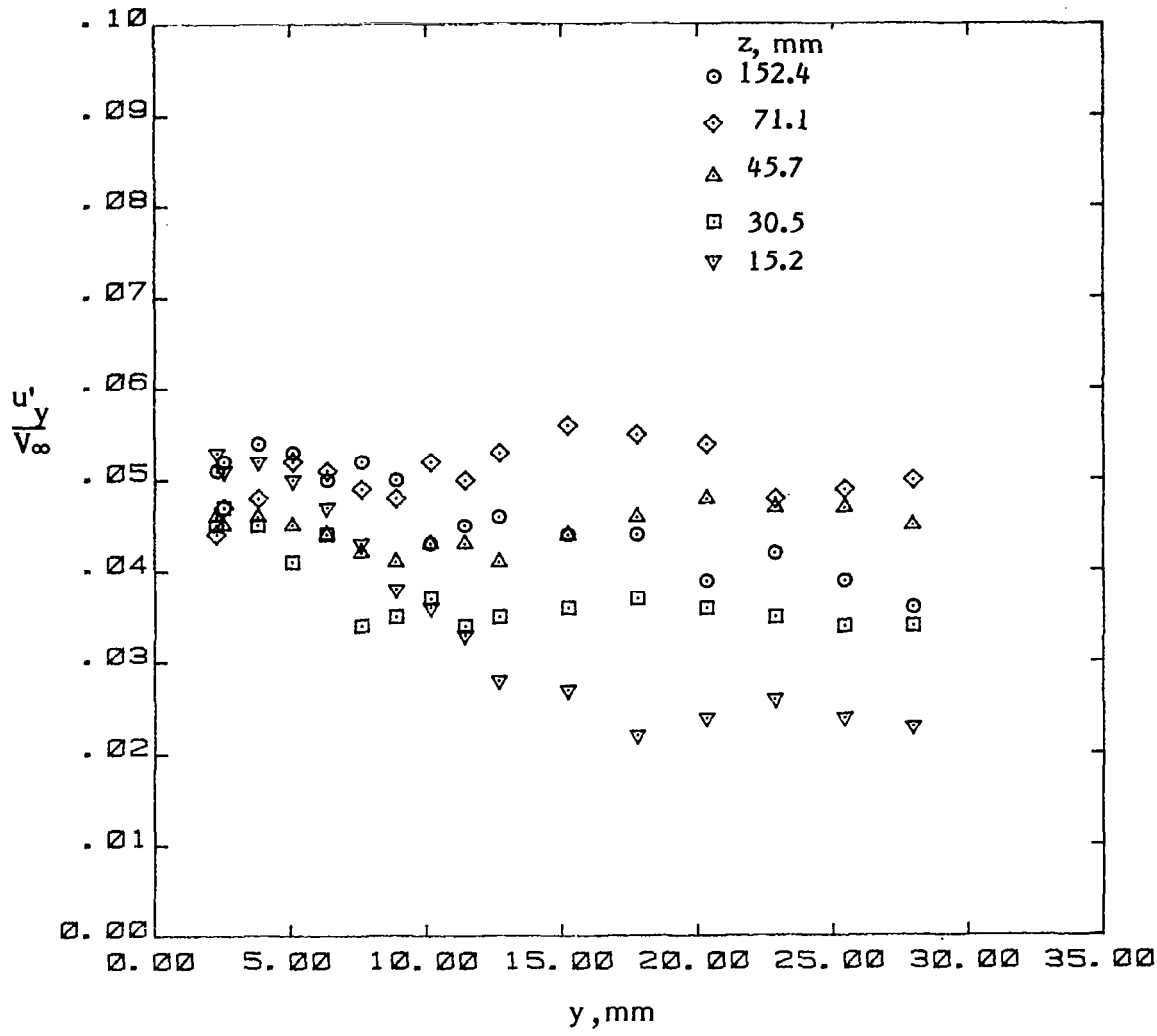

(e) Turbulent normal stress u'_y.

Figure 19. - Continued.

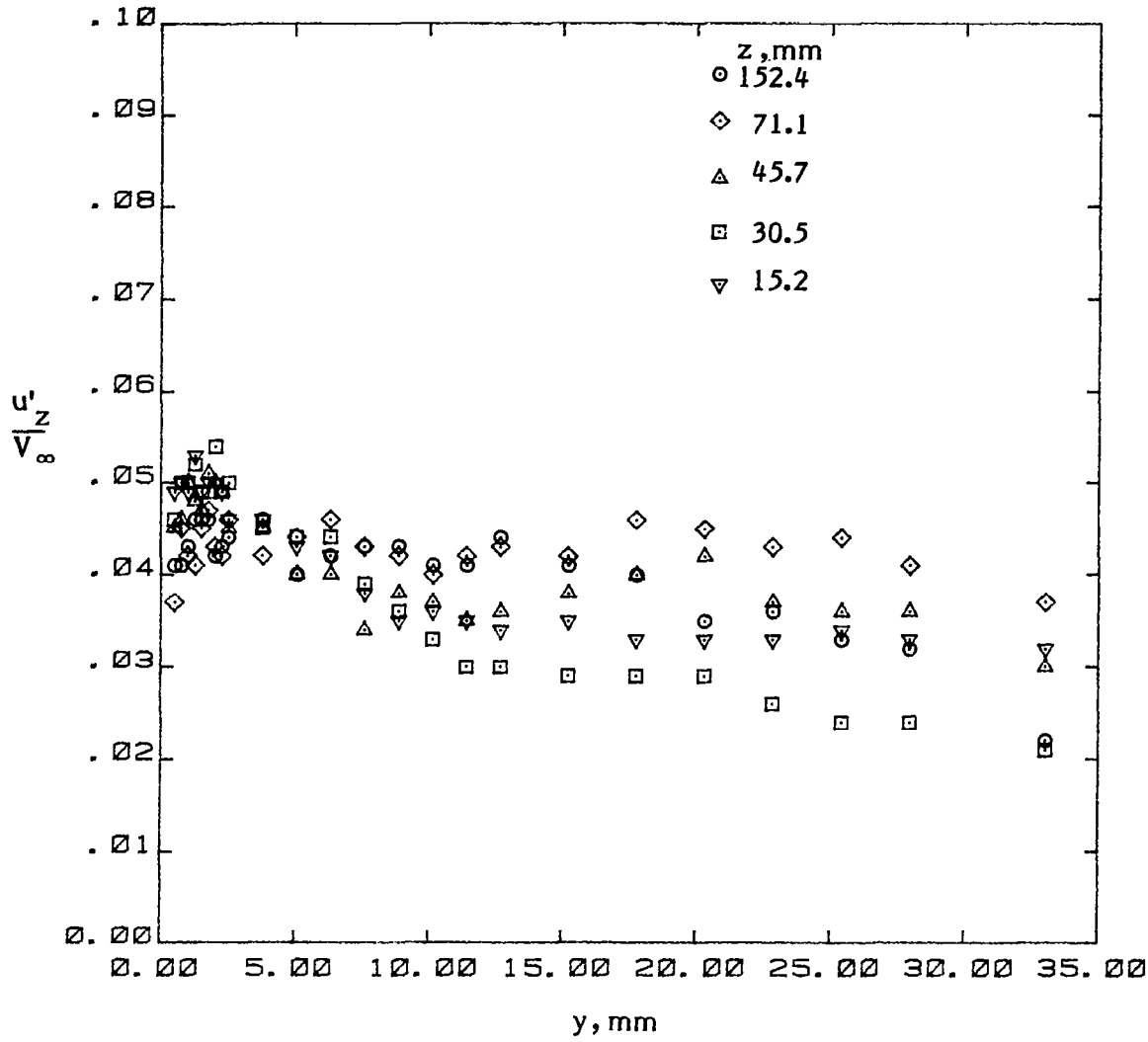

(f) Turbulent normal stress u'_z.

Figure 19. - Continued.

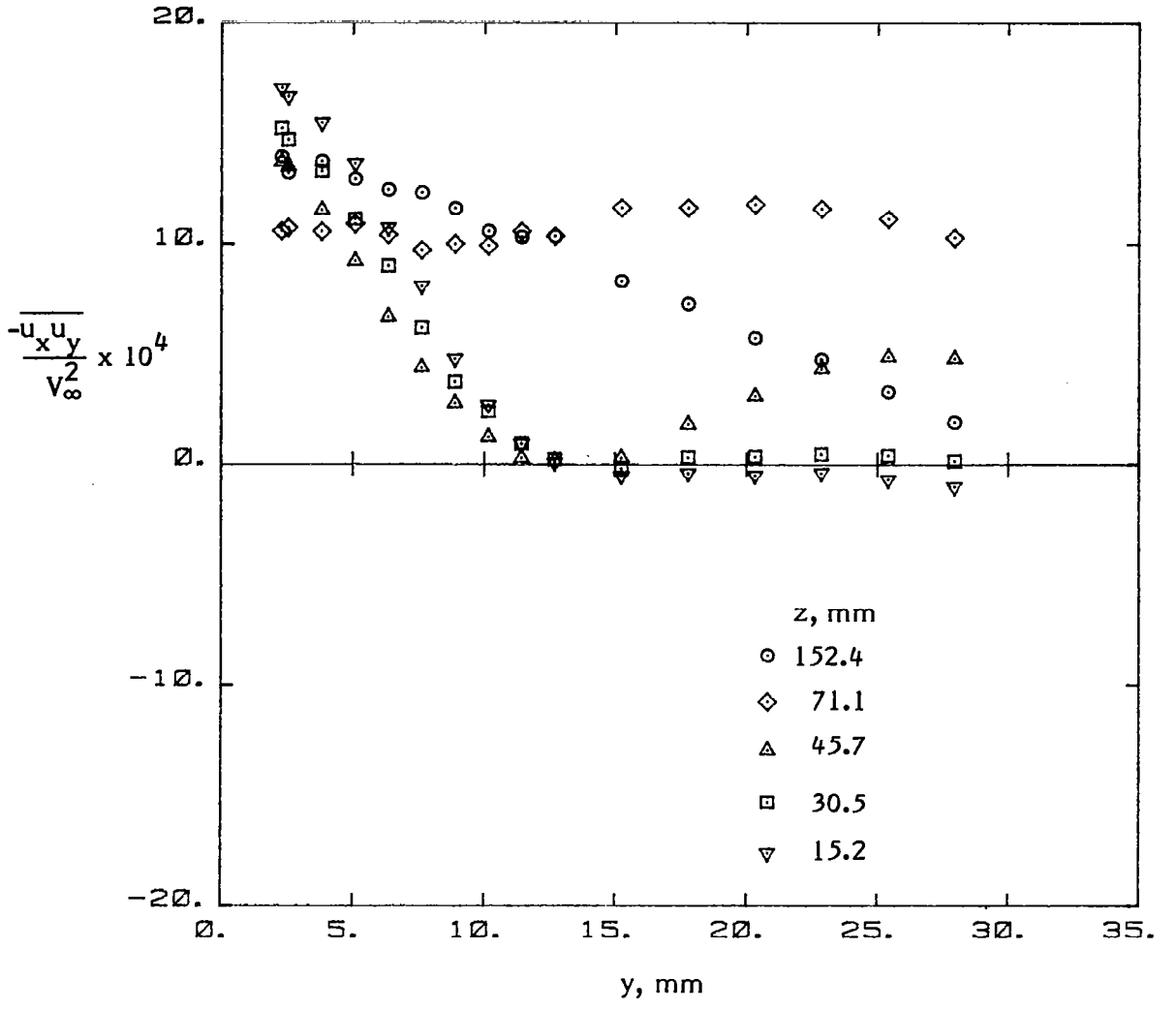

(g) Turbulent shear stress $\overline{u_x u_y}$.

Figure 19. - Continued.

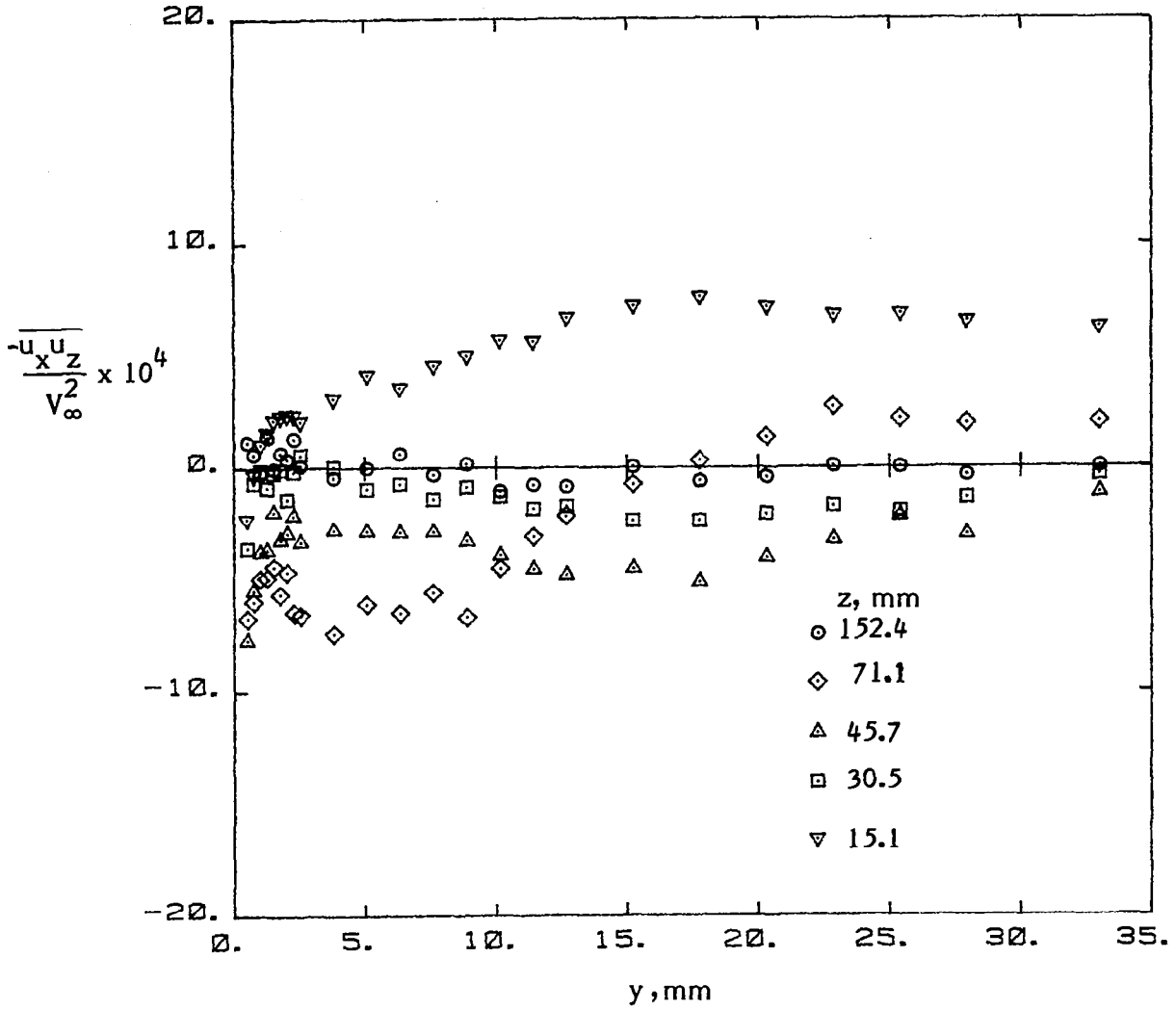

(h) Turbulent shear stress $\overline{u_x u_z}$.

Figure 19. - Continued.

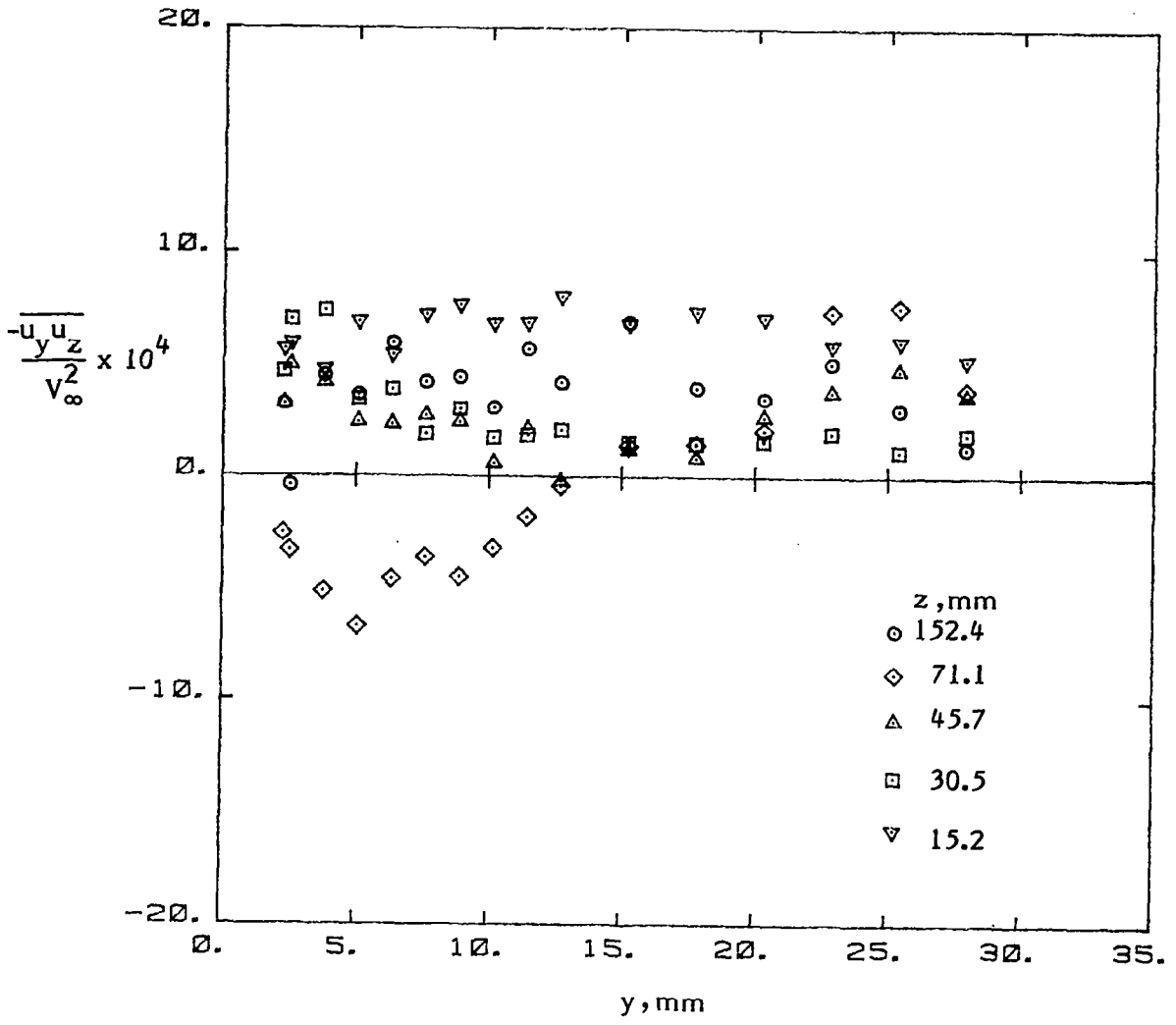

(i) Turbulent shear stress $\overline{u_y u_z}$.

Figure 19. - Concluded.

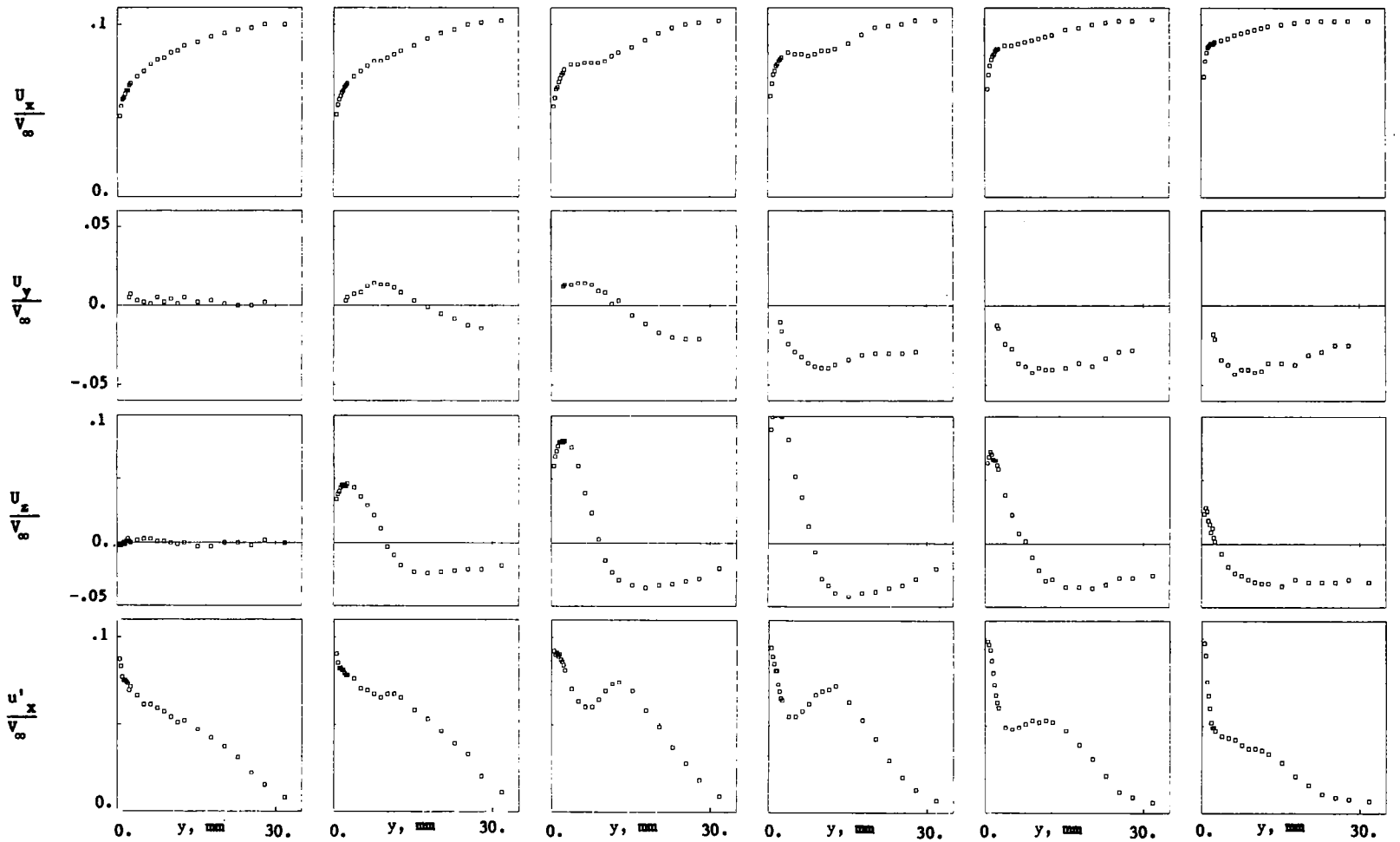

Figure 20. - Mean velocities and turbulence stresses in the juncture (x = 165 mm).

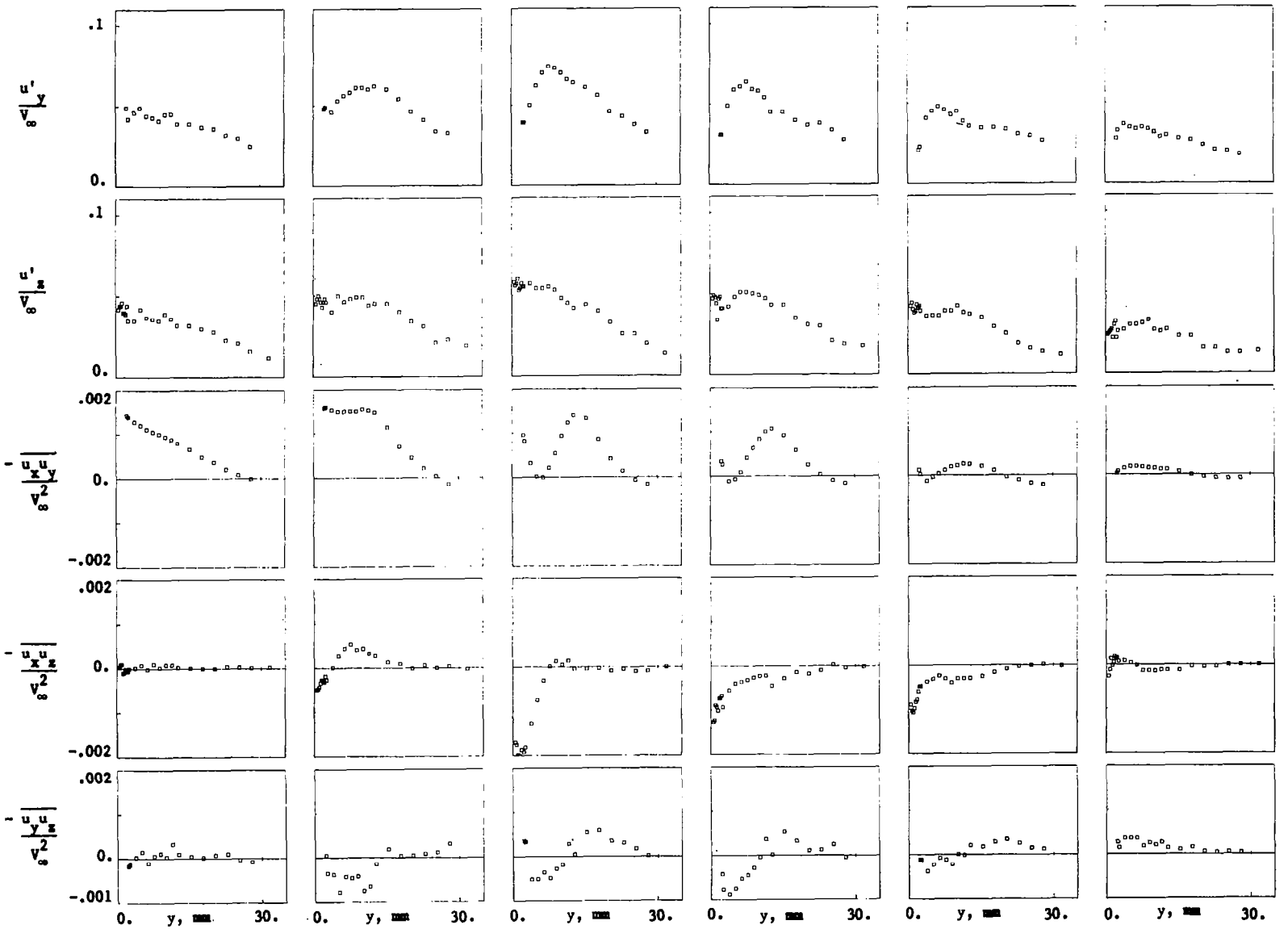

Figure 20. - Concluded.

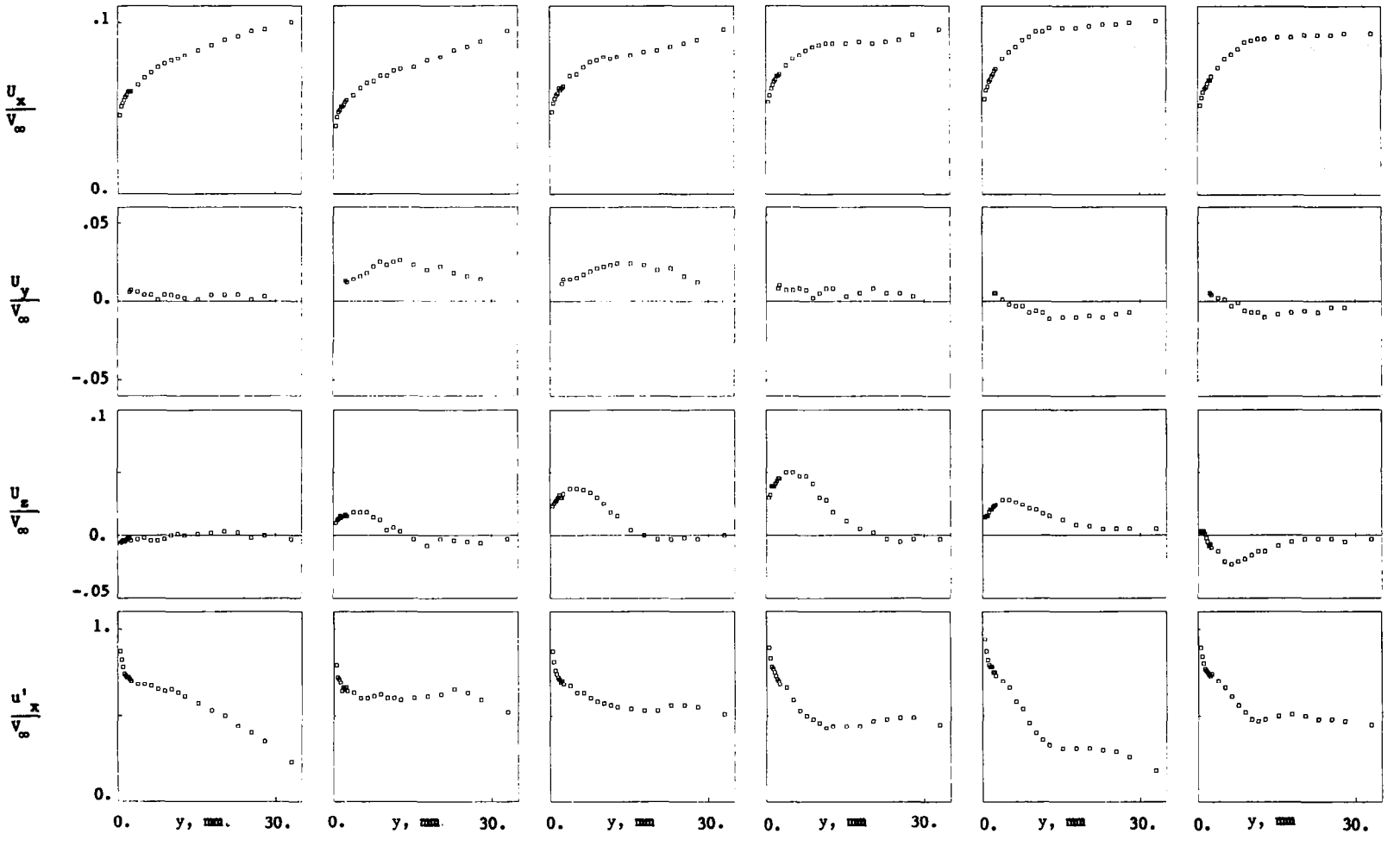

Figure 21. - Mean velocities and turbulence stresses in the juncture (x = 902 mm).

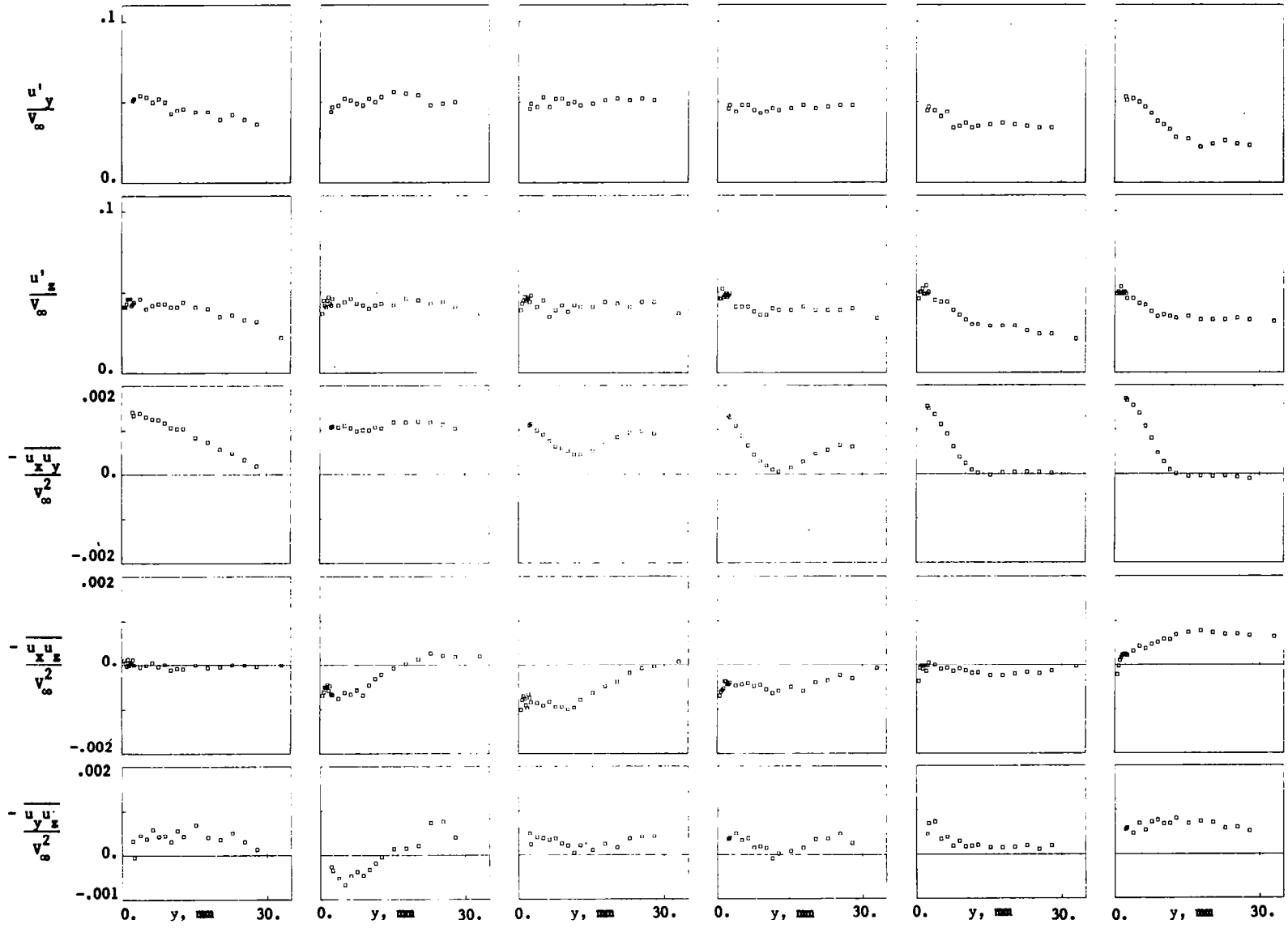

Figure 21. - Concluded.

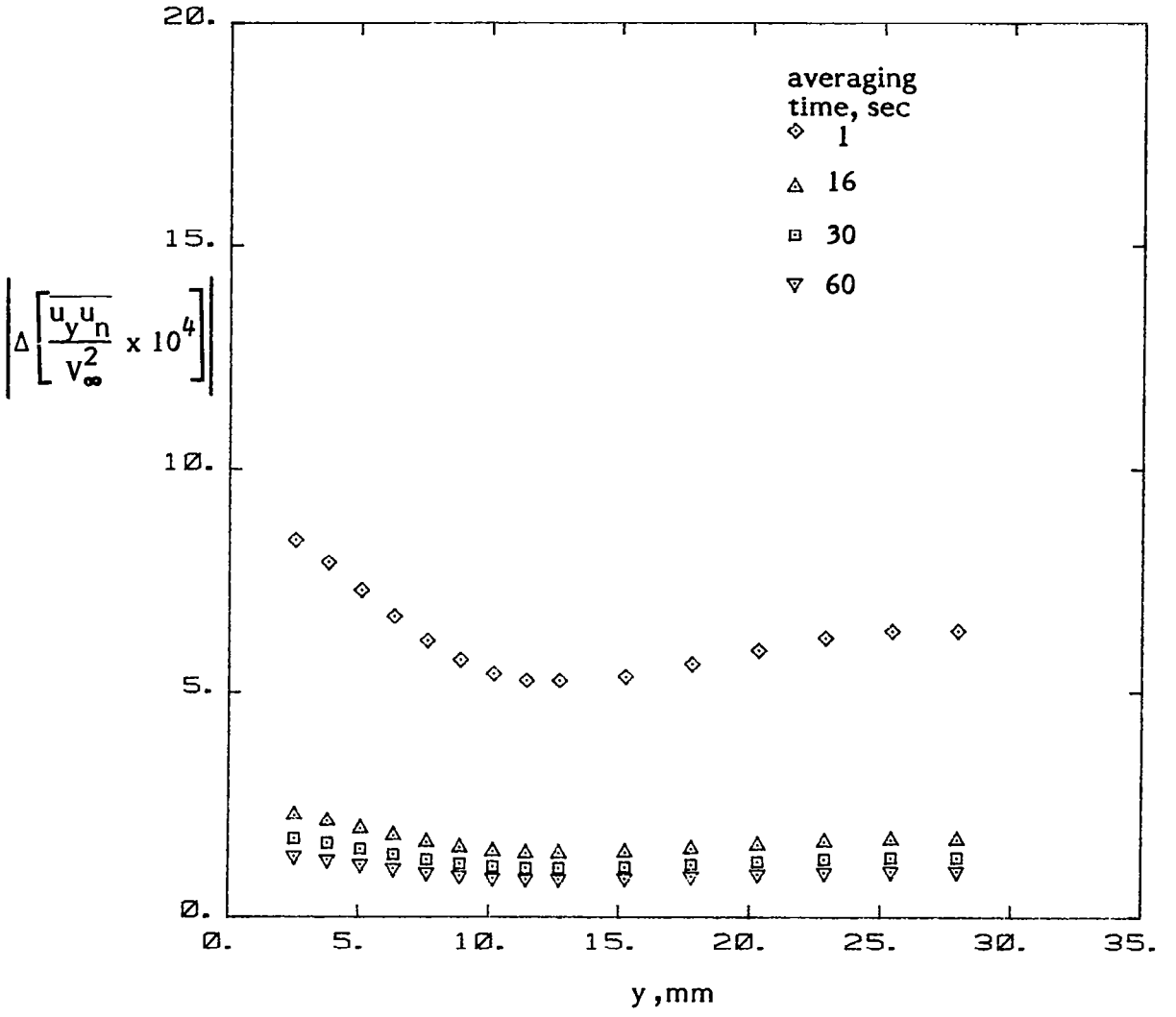

Figure 22. - Uncertainty in turbulent shear stress $\overline{u_y u_n}$ for different averaging times (appendix A).

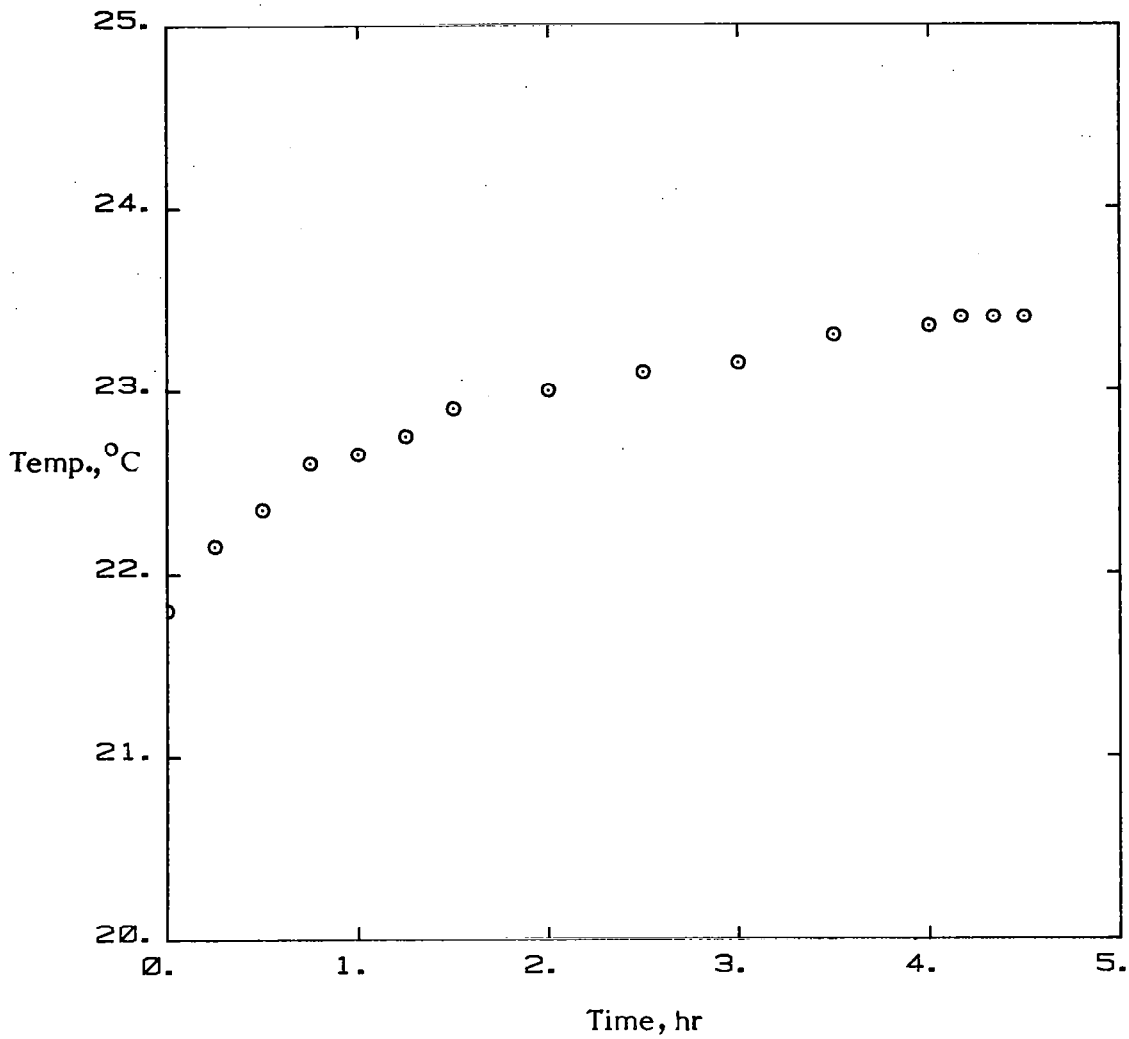

Figure 23. - Typical variation of flow temperature with time (appendix B).

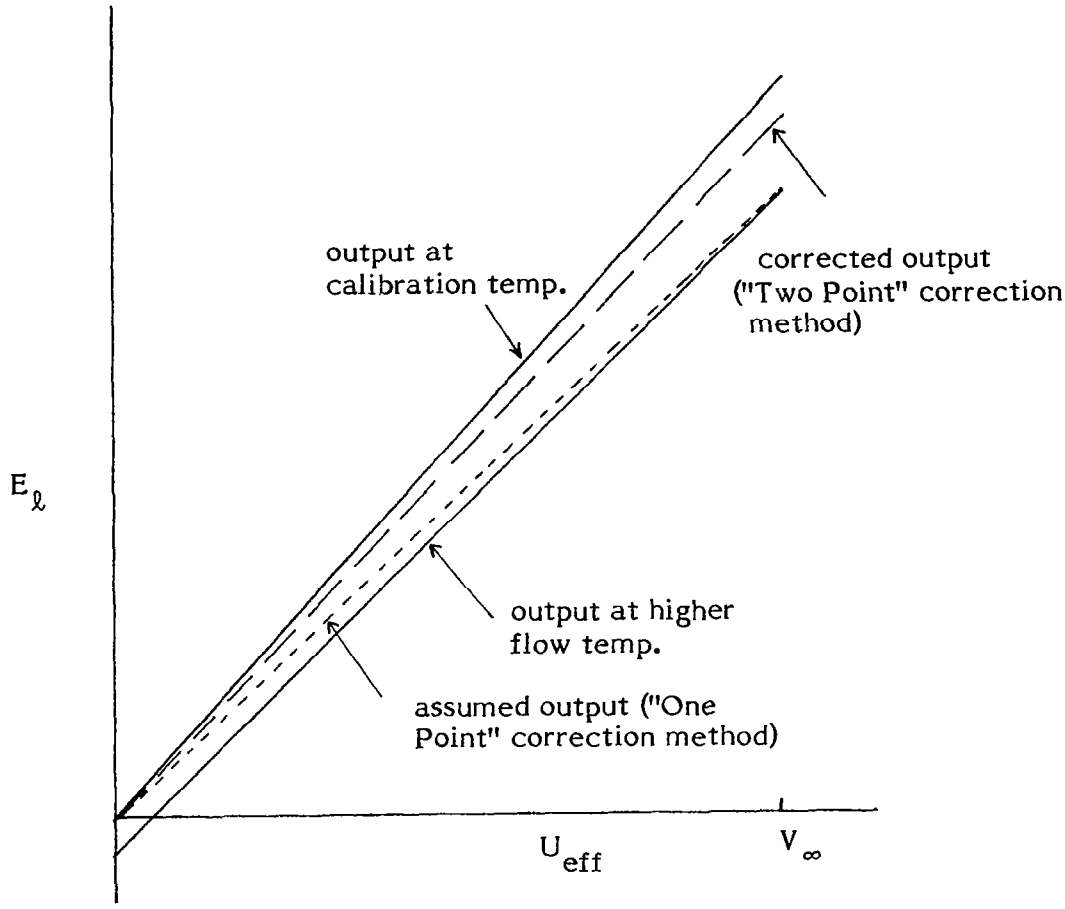

Figure 24. - Effect of flow temperature variations on the linearized output curve (appendix B).

1. Report No.	2. Government Accession No.	3. Recipient's Catalog No.
NASA CR-3605		

4. Title and Subtitle	5. Report Date
MEAN VELOCITIES AND REYNOLDS STRESSES IN A JUNCTURE FLOW	August 1982
	6. Performing Organization Code
7. Author(s)	8. Performing Organization Report No.
H. McMahon, J. Hubbartt, and L. Kubendran	
	10. Work Unit No.
9. Performing Organization Name and Address	
Georgia Institute of Technology 225 North Avenue, N.W. Atlanta, Georgia 30332	11. Contract or Grant No. NAG1-40
	13. Type of Report and Period Covered Contractor report
12. Sponsoring Agency Name and Address	
National Aeronautics and Space Administration Washington, DC 20546	14. Sponsoring Agency Code

15. Supplementary Notes

Langley Technical Monitor: James Scheiman
Final Report

16. Abstract

Values of three mean velocity components and six turbulence stresses measured in a juncture flow are presented and discussed.

The juncture flow is generated by a constant thickness body, having an elliptical leading edge, which is mounted perpendicular to a large flat plate along which a turbulent boundary layer is growing. The measurements were carried out at two streamwise stations in the juncture and were made using two single-sensor hot-wire probes.

The secondary flow in the juncture results in a considerable distortion in the mean velocity profiles. The secondary flow also transports turbulence in the juncture flow and has a large effect on the turbulence stresses.

From visual inspection of the results, there is considerable evidence of similarity between the turbulent shear stresses and the mean-flow strain rates. There is some evidence of similarity between the variations in the turbulent stress components.

17. Key Words (Suggested by Author(s))	18. Distribution Statement
Secondary Flow Turbulent Boundary Layer Reynolds Stress	Unclassified-Unlimited Subject Category 02

19. Security Classif. (of this report)	20. Security Classif. (of this page)	21. No. of Pages	22. Price
Unclassified	Unclassified	120	A06

For sale by the National Technical Information Service, Springfield, Virginia 22161

NASA-Langley, 1982